THE VORTEX LATTICE METHOD FOR THE ROTOR-VORTEX INTERACTION PROBLEM

by Raghuveera Padakannaya

1. Report No. CR-2421	2. Government Accession No.	3. Recipient's Catalog No.
4. Title and Subtitle THE VORTEX LATTICE METHOD FOR THE ROTOR-VORTEX INTERACTION PROBLEM		5. Report Date JULY 1974
		6. Performing Organization Code
7. Author(s) Raghuveera Padakannaya		8. Performing Organization Report No.
		10. Work Unit No.
9. Performing Organization Name and Address The Pennsylvania State University University Park, PA 16802		11. Contract or Grant No. NGR - 39 - 009 - 111
		13. Type of Report and Period Covered Contractor Report
12. Sponsoring Agency Name and Address National Aeronautics and Space Administration Washington, D.C. 20546		14. Sponsoring Agency Code

15. Supplementary Notes

Topical report

16. Abstract

This study is concerned with the rotor blade-vortex interaction problem and the resulting impulsive airloads which generate undesirable noise levels. A numerical lifting surface method to predict unsteady aerodynamic forces induced on a finite aspect ratio rectangular wing by a straight, free vortex placed at an arbitrary angle in a subsonic incompressible free stream is developed first. Using a rigid wake assumption, the wake vortices are assumed to move downsteam with the free steam velocity. Unsteady load distributions are obtained which compare favorably with the results of planar lifting surface theory.

The vortex lattice method has been extended to a single bladed rotor operating at high advance ratios and encountering a free vortex from a fixed wing upstream of the rotor. The predicted unsteady load distributions on the model rotor blade are generally in agreement with the experimental results.

This method has also been extended to full scale rotor flight cases in which vortex induced loads near the tip of a rotor blade were indicated. In both the model and the full scale rotor blade airload calculations a flat planar wake was assumed which is a good approximation at large advance ratios because the downwash is small in comparison to the free stream at large advance ratios. The large fluctuations in the measured airloads near the tip of the rotor blade on the advance side is predicted closely by the vortex lattice method.

17. Key Words (Suggested by Author(s)) Blade-vortex interaction Vortex lattice method Unsteady aerodynamics Rotor airloads	18. Distribution Statement Unclassified - Unlimited STAR Category: 01		
19. Security Classif. (of this report) Unclassified	20. Security Classif. (of this page) Unclassified	21. No. of Pages 141	22. Price* $4.75

Page Intentionally Left Blank

SUMMARY

This study is concerned with the rotor blade-vortex interaction problem and the resulting impulsive airloads which generate undesirable noise levels. First, a numerical lifting surface method is developed to predict unsteady aerodynamic forces induced on a finite aspect ratio rectangular wing by a straight, free vortex placed at an arbitrary angle in a subsonic incompressible free stream. Using a vortex lattice method unsteady airloads on the wing are obtained by starting the system from rest. Load distributions are obtained which compare favorably with the results of planar lifting surface theory.

The vortex lattice method is next extended to a single bladed rotor operating at high advance ratios and encountering a free vortex from a fixed wing upstream of the rotor. The predicted unsteady load distributions on the model rotor blade are generally in agreement with the experimental results.

Finally full scale rotor flight cases having vortex induced loads near the tip of a rotor blade were calculated. Assuming a flat planar wake the tip vortex from the preceding blade was placed at a specified height below the plane of the rotor. The large fluctuations in the measured airloads near the tip of the rotor blade on the advancing side are predicted closely by the vortex lattice method.

Using conformal transformation methods an exact analysis of the effects of thickness on the lift due to a two-dimensional wing-vortex interaction is presented.

Page intentionally left blank

TABLE OF CONTENTS

LIST OF FIGURES

NOMENCLATURE

a	Vortex core radius [radius where $v_i(r)$ is a maximum]
A	Aspect ratio = $(\text{span})^2/\text{area}$
b	Semi-chord or semi-span
c	Chord
C_ℓ	Section lift coefficient
C_L	Wing lift coefficient
d_o	Vortex core diameter
h	Blade-vortex or wing-vortex separation
ℓ_j, ℓ	Section lift
L	Lift per unit span
p	Perturbation pressure
p_∞	Pressure at infinity
r	Radial coordinate
R	Blade radius
S	Vt/b = distance traveled in semi-chords
t	Time
U	Velocity component in the disk plane
v_i	Induced velocity
V	Free stream velocity
w	Downwash or wake induced velocity
X	Chordwise coordinate of the wing
X_v	Horizontal distance of the vortex from the wing leading edge
y	Spanwise coordinate of the wing
z	Complex variable $x + iy$
Z	Distance between rotor axis and vortex axis

α Angle of attack

α_1 Shaft tilt angle, positive rearward

α_V Vortex induced angle of attack

$\beta_0, \beta_1, \beta_2$ Steady and first harmonic longitudinal and lateral blade flapping coefficients

γ Circulation

Γ Circulation strength of vortex

Γ_∞ Free vortex strength

δ Angle of intersection of the wing and the vortex

ϵ Distance defined in the Appendix A

θ Blade pitching angle

$\theta_0, \theta_1, \theta_2$ Coefficients in the harmonic series of blade pitching angle

μ Advance ratio = forward speed/tip speed

ξ, η Rectangular coordinates

ρ Air density

ϕ Velocity potential

$\phi(S)$ Wagner function

ψ Rotor azimuthal coordinate

ω Angular velocity of vortex

Ω Rotor rotational speed

Subscripts and Mathematical Terminology

f   Forward velocity

i,j   Number of chordwise and spanwise locations of control points

ℓ,m   Number of chordwise and spanwise locations of vortices

ℓ,u   Lower and upper surfaces

r   Resultant velocity

w   Component in the downwash direction

x   Velocity in the x-direction

Δ Indicates an increment, i.e. Δt is an increment in time

CHAPTER I

INTRODUCTION

The interaction of an aerodynamic surface with a vortex is of significance in the consideration of noise and blade stresses produced during helicopter operations. The airloads on a helicopter rotor blade can be strongly dependent on the interaction of the blade with its wake. The operating conditions of a helicopter rotor blade are such that its wake is not carried away by the free stream velocity as for a conventional wing, but rather spirals underneath the rotor disk and relatively small distances result between the tip vortex of one blade and the subsequent blade, especially on the advancing side. The wake of a helicopter rotor in forward flight consists of shed and trailed vorticity in a distorted, skewed helix behind each blade of the rotor. The edges of these sheets of vorticity roll up to form highly concentrated tip vortices. The bound circulation of a rotary wing is highly concentrated at the tip, so the rolling up is accomplished within a short distance from the tip and the tip vortex formed is very strong. The bound circulation goes to zero gradually at the root so that the vortex there will be weak. Regions where the blade passes close to tip vortices, its own and those from other blades are numerous, and are important because of their strong induced velocities at the blade which cause rapid fluctuations in the blade loads. This rotor blade-vortex interaction is one of the mechanisms postulated in the literature as the cause of blade slap, the term used for the sharp cracking sound associated with helicopter rotors.

The purpose of this study was to determine the unsteady spanwise load distribution on a helicopter rotor blade as it interacts with a vortex. The application of conventional lifting surface theory to the calculation of airloads on rotor blades is prohibited by the extensive calculations involved. Hence an approximate lifting surface theory like the vortex lattice method which is flexible and involves less calculations was considered.

The simpler problem of the wing-vortex interaction was considered first. The wing was replaced by a lattice of vortices and a wake consisting of shed and trailing vortex lines starting from the trailing edge of the wing. The shed vortices move downstream with the free stream velocity. The wing-vortex interaction problem was modeled by placing a vortex in the flow upstream of the wing. This vortex also moves downstream with the free stream velocity and is carried past the wing as time progresses.

In the rotor blade-vortex interaction problem, a particular blade-vortex interaction was considered first for which experimental data was available. This model consisted of a single bladed rotor operating at a high advance ratio and encountering a free vortex shed from a fixed upstream wing. A rigid flat wake was assumed in the computations. The free vortex was considered as a rigid infinitely long finite core vortex. The measured value of the free vortex strength was used in the computations.

Load distributions have been measured in flight on a full scale rotor which show that blade-vortex interaction can result in large blade load fluctuations. The vortex lattice method was extended to the full scale rotor flight cases for which vortex induced loads near the

2

tip of the rotor blade were indicated. The reference blade on which the load distribution was calculated was started from rest and a rolled up finite core tip vortex from the preceding blade was placed below this blade. The strengths of the tip vortex were calculated from the airloads measured in flight. Flight test values of the flapping angles were considered in the calculations. Blade pitch angles as well as the height of the tip vortex below the blade were adjusted to give agreement between the measured and predicted blade load values near the tip. As in the model rotor case a rigid flat wake was assumed.

CHAPTER II

PREVIOUS INVESTIGATIONS

Under certain flight conditions, a helicopter rotor blade intersects the trailing vortex system shed by other blades. Lehman (1) has shown from studies of the flow patterns of a model, two bladed helicopter rotor in a water tunnel that, in the low forward speed ranges, portions of the tip vortex shed at the front of the disc lie above the following rotor blade in such a manner that the following blade(s) can intersect one or more of the vortices. Vapor trail studies of Jenny, et al., (2) have also shown that the trailing vortex and the following blade can interact. This rotor blade-vortex interaction is one of the mechanisms postulated for blade slap, the term used for the sharp cracking sound associated with helicopter rotors.

At low forward speeds the blade slap is due to the rapid changes in angle of attack and subsequent lift change produced by blade-vortex interaction. At high forward speeds blade slap has been associated with the onset of compressibility effects on the advancing blade and the occurrence of local supersonic flow.

A considerable amount of research has been done recently on the effects of helicopter rotor blade-vortex interaction and wing-vortex interaction. Theoretical investigations have been carried out with various simplifying assumptions. Experimental investigations have included both model and full scale testing.

Simons (3) has solved the steady case of a three-dimensional wing in the presence of an infinite vortex at zero relative velocity. A lifting line was used to study the spanwise lift distribution on wings

in the vicinity of a line vortex normal to the span. A finite core
vortex was used when the vortex was close to the wing. Kfoury (4) has
applied vortex lattice method for the calculation of steady loads on
wings in the vicinity of infinite vortices. Jones and Rao (5) have
obtained an exact solution of a closed form based on lifting line theory
for the case of a wing of elliptic planform and a vortex located below
the mid-span of the wing. Analytical solutions of a series form were
also obtained for elliptic and rectangular wings when the vortex was
not located at mid-span.

Johnson (6) has applied planar lifting surface theory to the
unsteady model problem of the loads induced on an infinite aspect ratio
wing in a subsonic, compressible free stream and a straight, infinitely
long vortex at an arbitrary angle with the wing center line. The vortex
was placed in a plane parallel to the plane of the wing, at a distance,
h, below it and was convected past the blade by the free stream. The
distortion of the vortex by the flow field of the wing was not considered.
Linear lifting surface theory in the form of an integral equation between
the pressure and downwash at the wing surface was used to obtain the
solution to the model problem. The solution for the model problem was
applied to the calculation of aerodynamic loads induced on a rotor blade
by a nearby tip vortex. A comparison of the loads calculated for a
simplified vortex and blade configuration, using the lifting surface
solution and the usual lifting line theory indicated that the lifting
surface theory should be used for vortices closer than about five
chord lengths of the blade. Johnson (7) has compared the experimental
data and the vortex induced loads obtained from the application of
lifting surface theory to a single bladed rotor at high advance ratio

encountering a free vortex from a fixed upstream airfoil. Good correlation was indicated when the vortex was not close to the rotor hub. The lifting surface theory solution of Johnson (6) was also used in the calculations of helicopter rotor blade loads. Johnson (8) has also compared his lifting surface theory results with the experimental data obtained from flight measurements on a H-34 helicopter having a four-bladed rotor. Calculations, using rigid and nonrigid wake geometry, indicated that a good wake geometry model is necessary in order to predict accurate rotor airloads.

Surendraiah (9) and Padakannaya (10) have used a single bladed rotor, having a two inch chord and 12 inch radius, for the experimental investigation of blade-vortex interaction. The rotor was operated at high advance ratios in the proximity of a tip vortex generated by a fixed wing upstream of the rotor. The rotor was rigidly mounted at a zero collective pitch without flapping or lagging. The loads due to the interaction were obtained using chordwise pressure sensors mounted at different spanwise locations. Data were taken for rotor plane positions above and below the vortex axis and for different intersection angles. Two values of rotor RPMs and vortex strengths were used.

Pruyn and Alexander (11) have indicated that rotor wake effects are dominated by large disturbances caused by blade tip vortices. The proximity of the tip vortices to the blade was reflected by large pressure fluctuations on the blade. Section pressures were considerably different from those of a two-dimensional airfoil over extended areas of the rotor disc, apparently due to combined effects of compressibility and disturbances from tip vortex interference. The local Mach number

can reach the critical Mach number, especially near the tip of the advancing side, which can separate the boundary layer, thereby causing a change in chordwise pressure distribution. It was also found that the effect of the tip vortex was large when the angle between the vortex and the blade was small.

Scheiman (12) and Scheiman and Ludi (13) have tabulated both representative and critical helicopter rotor blade airloads measured in flight using pressure transducers on a rotor blade. A comparison of the measured loads with the loads predicted by elementary uniform inflow theory indicated a predominant influence of the intersection of the blade with the trailing vortex from the preceding blade. Large perturbations in the blade section loading as a function of azimuth angle were shown to occur near the intersection of the blade with the preceding blade tip vortex. The influence of the trailing vortices produced harmonic blade loadings of all orders with large higher harmonics. It was also observed that blade-vortex interaction decreases with an increase in forward speed. Landgrebe and Bellinger (14) have carried out an analytical investigation to evaluate quantitative applications of available model rotor tip vortex patterns from a water tunnel. This quantitative wake geometry information is required for use in the theoretical analyses for computing the instantaneous rotor flow field and associated blade airloads. Theoretical results indicated that, for forward flight conditions, the primary parameters influencing wake geometry for a given blade design are the number of blades, rotor advance ratio, thrust coefficient and tip path angle. Theoretical results also indicated that tip vortex geometry for moderate to high flight speeds ($\mu > 0.15$) is insensitive to parameters which influence the

7

azimuthal variation of blade airloading such as blade flexibility, cyclic pitch, Reynolds number and Mach number. When a tip vortex lies close to a rotor blade, the airloads are very sensitive to small changes in vortex position and hence a very accurate experimental determination or theoretical prediction of the tip vortex position is desired.

Kantha, et al., (15) have qualitatively studied the inverse problem of the influence of the changes in the convective velocity induced by the pressure field around a lifting surface on the structure of a vortex. The influence of a lifting surface on the vortex core was investigated by a qualitative examination of the interaction region of the tip vortex with a wing. Photographs of the flow patterns in the regions of interest indicated the qualitative responses of the vortex core. Flow patterns of the region of interaction between the flow field of a lifting surface and the vortex core showed that the vortex either bends following the streamline shape until it intercepts the wake where it is dispersed or the core may be sliced into two smaller vortices when the vortex hits the leading edge of the airfoil. The solution of this problem is required for a better understanding of blade-vortex interaction problems. Also a systematic quantitative investigation of this type should indicate the range of validity of the usual method of treating the modification in the loading on lifting surfaces in the proximity of vortices by assuming that the vortex itself remains intact.

Very recently Scully (16) has developed computer programs for the calculation of helicopter rotor tip vortex geometry in hover and forward flight and for the calculation of helicopter rotor harmonic airloads in forward flight. Lifting line theory was used for the airload calculations except when the tip vortex passes close to the blade. For close

blade-vortex interactions the approximations developed by Johnson (6) using lifting surface theory was used. Experimental tip vortex geometry data and the results of the wake geometry program were generally in agreement although there were local differences. The hovering tip vortex geometry agreed qualitatively with experiment. Comparisons of the rigid wake airloads and distorted wake airloads with measured airloads indicated that distorted wake airloads are much worse than the rigid wake airloads except at some local areas. It has been suggested by Scully (16) that to improve on the rigid wake results, distorted tip vortex geometry will have to be used along with a careful treatment of blade-vortex interaction effects.

CHAPTER III

VORTEX LATTICE METHOD FOR WING-VORTEX INTERACTION PROBLEM

3.1 Development of Unsteady Computational Model

The purpose of this study was to develop analytical techniques for predicting the unsteady load distribution on a helicopter rotor blade as it interacts with a vortex. Prior to investigating the load distribution on a rotor blade, the simpler problem of a numerical lifting surface analysis of a finite wing with a vortex passing over the wing was considered. As there is a large variation in the downwash induced by the interacting vortex along the spanwise and chordwise directions over the rotor blade, lifting surface methods are necessary for predicting unsteady load distributions.

The two basic classes of lifting surface theories are the kernal function technique and the finite element method. In the kernel function technique, the singular integral equation for the pressure difference across a lifting surface is to be solved assuming a series approximation for the pressure difference and using the expressions for the kernel function for a lifting surface given in the literature. Finite element methods like the vortex lattice and the doublet lattice methods are achieving wide acceptance because of their simplicity, accuracy and versatility. The extension of the vortex lattice method to the oscillatory case has been called in the literature the doublet lattice method. In the doublet lattice method, Albano and Rodden (17) have used steady horseshoe vortices and oscillatory acceleration potential doublets along the bound vortex to model a lifting surface.

This method reduces to the vortex lattice method in steady flow. In the vortex lattice method the only singularities used are the horseshoe vortices.

Two-dimensional analyses by James (18) and later by DeYoung (19) have shown the vortex lattice method to be accurate, and have proven its convergence. Comparison of the results with experimental data and theoretical solutions based on other approaches have proven the value of the vortex lattice method for three-dimensional cases though mathematical justification of the lattice method for three-dimensional cases has not yet been investigated.

In the unsteady wing-vortex interaction problem the wake consists of shed and trailing vortices with strengths proportional to the time and spanwise rates of change respectively of the bound vorticity. Hence the strengths of the shed vortex elements deposited in the wake at any time are made equal to the change in strength (between two time steps) of the corresponding bound vortex elements. The strengths of the trailing vortex elements in the wake are made equal to the change in strength of adjacent bound vortex elements.

In the analysis to follow the shed and trailing vortices are assumed to lie in the plane of the wing and to move downstream with the free stream velocity. In reality the wake rolls up under its own influence and the influence of the bound vortices. Djojodihardjo and Widnall (20) have shown in the case of an impulsively started airfoil problem that even for an angle of incidence of 0.3 radians, the indicial circulations associated with three wake configurations, namely, a free stream directed wake, a straight wake tangent to the limiting streamline at the trailing edge and a field-induced deforming wake (or free wake)

11

with rolled up starting vortex, differ only within four percent at a distance of about 1.25 semi-chords behind the airfoil. As the distance increases, the indicial circulation for the field-induced deformed wake approached that of the free stream directed wake. Giesing (21) has compared a deforming wake result to the Wagner function, which is the time history of normalized circulatory lift due to a step change in angle of attack, and showed that the free wake slightly retards the lift.

The wing is assumed to be of negligible thickness. Giesing (21) has also compared the Wagner function for a symmetrical 8.4 percent thick airfoil and a symmetrical 25.5 percent thick airfoil at a small angle of attack so that nonlinearities due to wake deformation do not enter the calculations. The effect of thickness was to retard the lift build up and hence a thick airfoil takes longer time to reach a given value of lift. Similar effects of thickness were found on the Küssner function which is the function used to describe the lift acting on a flat plate entering into a vertical gust. It has also been shown that the general effects of thickness on Theodorsen's function which is the function used to find lift on a flat plate executing simple harmonic pitching and heaving motions, is to reduce the lift for all frequencies and to increase the phase lag between the quasi-steady and total circulation. Using conformal transformation methods an exact analysis of the effect of thickness on the lift due to a two-dimensional wing-vortex interaction is presented in Appendix A. The results presented in Appendix A show the effect of thickness on the magnitude of lift due to wing-vortex interaction. The lift is calculated based on the

12

instantaneous angle of attack. As expected, the magnitude of the lift increases with thickness.

The effect of the bound and the wake vortices on the path of the interacting vortex is neglected. The viscous effects are neglected and thus the strengths of the wake vortex elements do not change with time.

3.1.1 Analysis

Bernoulli's equation extended to unsteady flow gives the pressure difference on the upper and lower surfaces of an airfoil in $z = 0$ plane as

$$\Delta P(x,y,t) = \rho V(2\Delta V) + \rho \frac{\partial}{\partial t} (\phi_u - \phi_\ell)$$

The velocity potential, in terms of the distributed vorticity, is

$$\phi_u - \phi_\ell = \int_0^x \gamma dx$$

and the circulation around a differential element of a vortex sheet is

$$2\Delta V \, dx = \gamma dx$$

$$\therefore \Delta P(x,y,t) = \rho V \gamma(x,y,t) + \rho \frac{\partial}{\partial t} [\int_0^x \gamma(\xi,y,t) \, d\xi]$$

The lift per unit span is the integral of the chordwise pressure

$$\ell(y,t) = \int_0^{c(y)} \Delta P(x,y,t) \, dx$$

$$= \rho V \int_0^{c(y)} \gamma(x,y,t) \, dx + \rho \int_0^{c(y)} [\frac{\partial}{\partial t} \int_0^x \gamma(\xi,y,t) \, d\xi] \, dx$$

13

The above expression for the unsteady lift is composed of two parts, one of which is due to the time rate of change of circulation around the airfoil. The part which appears to be independent of time, is not the same lift that would be computed using steady state methods. The γ distribution is altered by the wake, and the time history of the unsteady motion must be known to compute the wake structure. The second term is not the added or apparent mass term used in classical theories. Apparent masses are characteristically independent of the past history of the motion and are noncirculatory in nature.

During vortex interaction, a wing experiences a resultant velocity different from that of the free stream due to the presence of the vortex. Since every point on the wing experiences a slightly different horizontal component of the resultant velocity, V_x, the lift is given by

$$\ell(y,t) = \rho \int_0^c V_x \, \gamma(x,y,t) \, dx + \rho \int_0^c [\frac{\partial}{\partial t} \int_0^x \gamma(\xi,y,t) \, d\xi] \, dx$$

The solution to $\gamma(x,y,t)$ is determined from the boundary condition that the resultant flow be tangent to the surface or that the normal component of the velocity relative to the surface be zero. The trailing edge condition is that the circulation shed into the wake at any spanwise station equals the change in bound circulation at that spanwise station.

The method used to determine the bound vorticity distribution satisfying the flow boundary condition and the conservation of circulation is the vortex lattice method. In this method both the spanwise and the chordwise loadings are made stepwise discontinuous. The wing is sub-divided chordwise and spanwise into a number of panels. The loading on

14

a given panel is assumed concentrated at the quarter-chord of the panel with the chordwise vortices extending to the trailing edge of the wing. The velocity induced by these vortices is calculated at a finite number of control points located at the three-quarter-chord of the panel and is made to satisfy the boundary condition that the resultant flow be tangent to the surface. This placement of vortices and control points where the boundary condition is satisfied is an extension of the Weissinger lifting line approximation. The Kutta condition is automatically satisfied by placing the last control point downstream of the last vortex. James (18) also has shown conclusively that the choice of one-quarter-chord and three-quarter-chord points for the vortices and the control points respectively is both optimum and mandatory for the solution of any vorticity distribution in the steady two-dimensional problem. By satisfying the boundary conditions at all the control points (equal to the number of unknown vortices) a system of simultaneous linear equations for the unknown vortex strengths is obtained. This system of equations can be written as

$$\sum_{\ell,m} \Gamma_{\ell m}(t + \Delta t) \, A_{ij}(\ell,m) = V_{ij}(t + \Delta t) + v_{w_{ij}}(t + \Delta t)$$

where i,j = the number of control points in the chordwise and
           the spanwise directions respectively.

       ℓ,m = the number of vortices in the chordwise and spanwise
           directions respectively.

   $A_{ij}(\ell,m)$ = is the velocity induced at (i,j) by a bound vortex of
           unit strength at (ℓ,m).

15

V_{ij} = the component of the free stream velocity normal to the plane of the wing.

$v_{w_{ij}}$ = the component of the wake induced velocity normal to the plane of the wing.

$V_{ij}(t + \Delta t)$, the normal component of the free stream velocity is assumed known. $v_{w_{ij}}(t + \Delta t)$ must be calculated from the wake geometry that exists at time $(t + \Delta t)$.

The fundamental relation required for the determination of the induced velocities due to wake and wing vortices is the Biot-Savart law. From this relation, the velocity induced at any arbitrary point P in Figure 1 by a straight element of circulation strength, Γ, is

$$v_i = \frac{\Gamma}{4\pi} \int_A^B \frac{h}{r^3} \, ds$$

This induced velocity is directed normal to the plane formed by the vortex element and the point, P, and is in a direction consistent with the circulation sense.

Thus the induced velocity due to a vortex element AB in Figure 1 is

$$v_i = \Gamma(\cos \alpha + \cos \beta)/4\pi h$$

which reduces to

$$v_i = \Gamma/2\pi h \text{ for a vortex of infinite length.}$$

To avoid the mathematical singularity when the point P lies on the vortex a finite core for the vortex is to be introduced.

The computer model is started from rest to avoid prescribing the wake. Hence at time t there is no circulation on the wing. At time $(t + \Delta t)$ the wing increases its angle of attack while shed and trailing
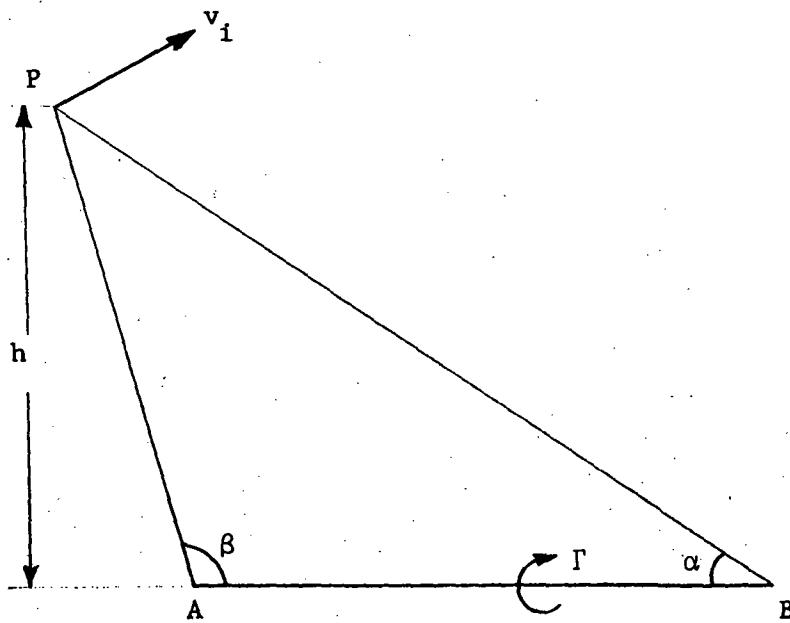
$$v_i\Big|_P = \frac{\Gamma}{4\pi h} \ (\cos \alpha + \cos \beta)$$

Figure 1. Biot-Savart Law.

filaments of unknown strength, but with known positions, are deposited in the wake. The shed vortex is formed at the trailing edge as time increment Δt approaches zero for the continuous case and each new wake vortex has a strength equal to the change in bound circulation. The wing is replaced by a lattice of vortices of unknown strength. The total downwash at the control points on the wing where the boundary condition of zero normal velocity is satisfied, is obtained by summing the contribution of the vortex lattice, the contribution from the wake vortices, the velocity induced by the free vortex and the normal component of the free stream velocity. Satisfaction of the boundary condition at all of the control points results in a system of simultaneous equations for the unknown vortex strengths. The solution of these equations gives the strengths of the vortices that are shed immediately behind the wing. All vortex element and points not attached to the wing are then allowed to translate a distance of VΔt behind the wing where Δt is the time increment used in the calculations. In subsequent time steps only the vortices at and just behind the wing have unknown strengths, while those in the wake have known strengths. In this manner arrays of discrete shed and trailing vortices are generated immediately behind the wing with strengths corresponding to the vortex induced wing loads. The vortex shedding process continues until steady state conditions are reached, that is, the bound circulation does not change with time. Figure 2 shows the vortex shedding procedure.

Piziali (22) has presented results of computations for several values of the distance from the midchord of the airfoil to the first shed vortex in the case of oscillating airfoils. It was found that the
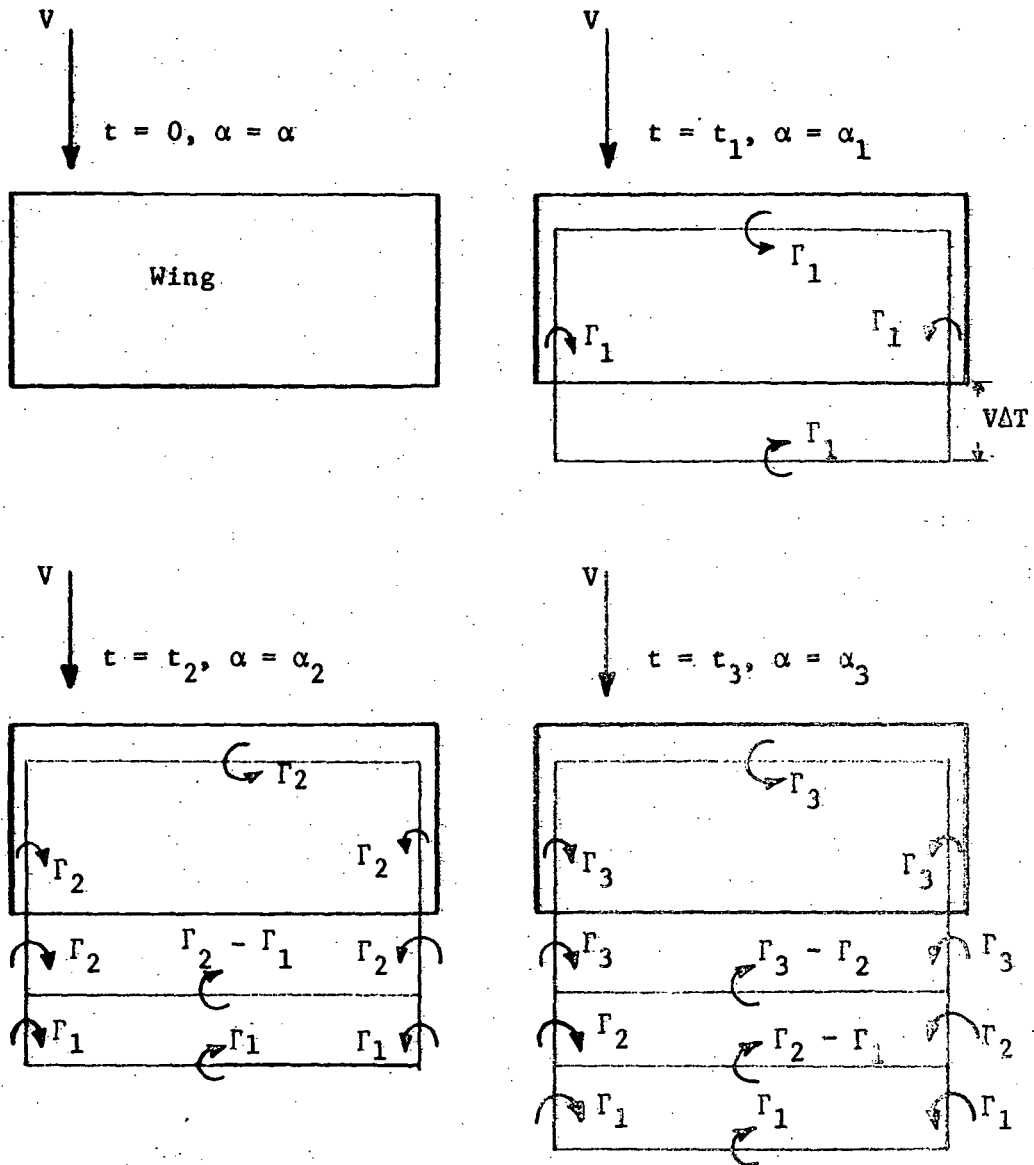
Figure 2. Unsteady Vortex Shedding.

computer results were much closer to classical results when the first shed vortex was at a distance of 30 percent of $V\Delta t$ from the trailing edge. The effect of this "wake advance" was also investigated by Piziali (22) in the HU-1A rotor blade load calculations at an advance ratio of 0.26 where the "wake advance" was changed from 0.0 to 0.7. It was found that "wake advance" had a relatively small effect, but in general, increasing the "wake advance" attenuated and shifted the phase of the airloads at higher harmonics. Hence in the present study instead of this artificial representation of the shed vortex wake, the first shed vortex is placed at a distance of $V\Delta t$ from the trailing edge.

Once the circulations Γ_{ij} at each section of the wing are known from the system of simultaneous equations, the lift at any spanwise station can be obtained from

$$\ell_j(y,t) = \rho V \sum_i \Gamma_{ij}(x,y,t) + \rho \int_0^c [\frac{\partial}{\partial t} \int_0^x \Gamma_{ij}(\xi,y,t)\, d\xi]\, dx$$

The IBM 360/67 digital computer at The Pennsylvania State University's computation center was used to obtain the numerical solution to the problem. The set of simultaneous equations for the unknown vortex strengths was solved by the Gauss elimination method. The coefficients of these simultaneous equations, and hence the strengths of the vortices, depend on the number of vortices and their locations in the chordwise and the spanwise directions. The vortex locations and the control point locations are handled as input data. This vortex lattice method permits an arbitrary number of vortices and their locations and at the same time maintains the correct number and locations of control points as the control points are located midway between the successive vortices.

20

The optimum number of vortices and their locations were selected on the basis of the required accuracy and the computation time and storage limitations. The present method of calculation required about 50 secs. of computer time for the vortex to travel a distance of about three chords. The nondimensional time step size, $V\Delta t/c$, was 0.15 and free stream velocity of 150 ft/sec. The computation time increased considerably with the decrease of time step size.

3.1.2 Results and Discussion

Before applying the unsteady numerical solution to wing interaction problems its validity was assessed by comparing the results to the Wagner function for the impulsive start problem. A wing having an aspect ratio of 1000 was considered as a good approximation to an infinite aspect ratio wing for which there is a theoretical solution due co Wagner. The circulatory part of lift which is time and wake dependent is the only part included in the Wagner function. Comparison of the results from the computation model and the Wagner function from reference 23 is presented in Figure 3. The comparison is good except initially where the apparent mass term, which is not included in the Wagner solution, is large. In the numerical solution the apparent mass term is included in the calculated unsteady lift. A comparison of the lift build up in the case of a rectangular wing of aspect ratio six subjected to a step change in angle of attack is shown in Figure 4. Ten spanwise and five chordwise vortices were considered for the lattice. The results of Jones (24) were based on simplified approximations for the growth of lift function corresponding to a sudden unit change of incidence. The comparison is good.
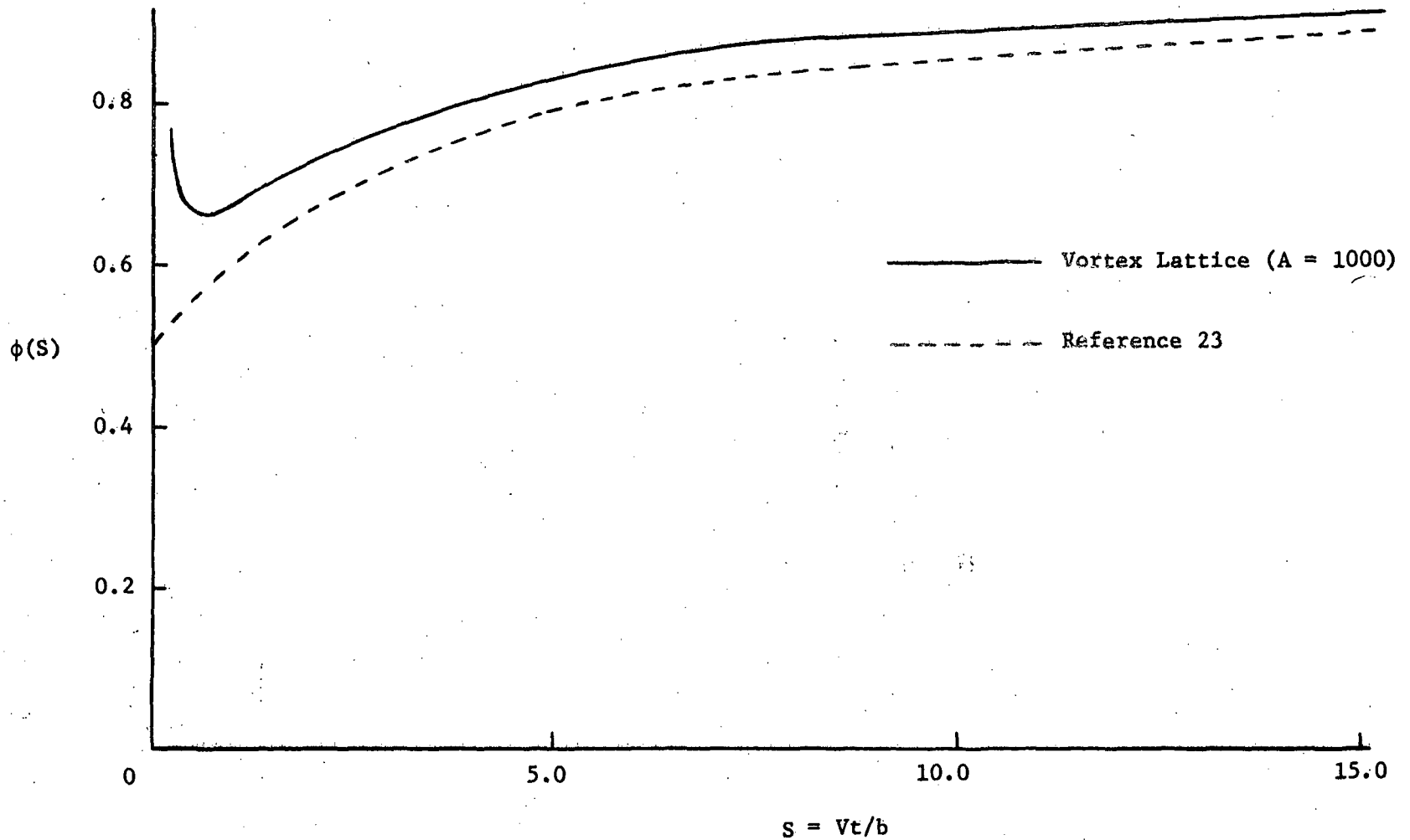
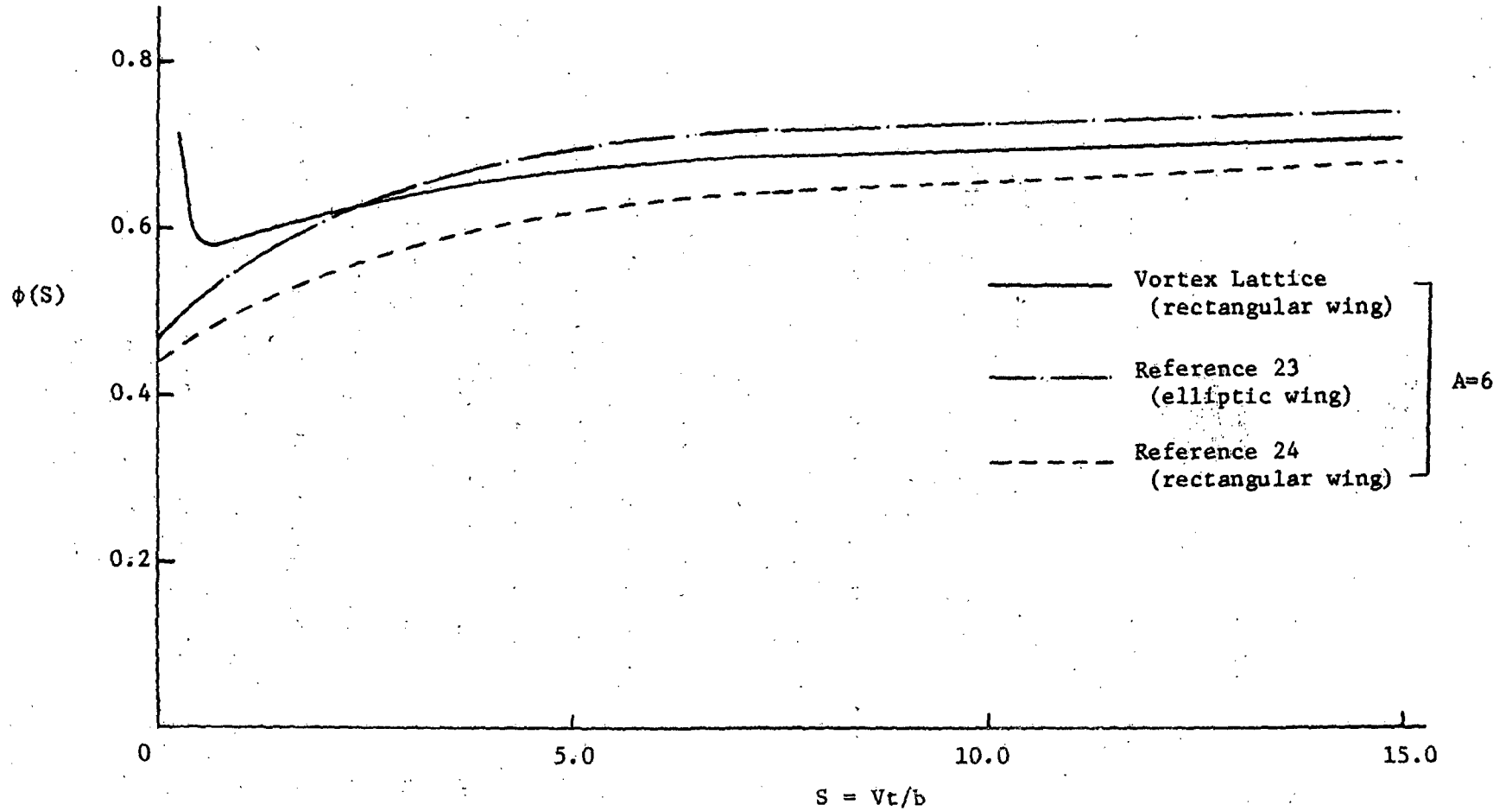Figure 3. Comparison of Numerical Solution to Wagner Function.

Figure 4. Development of Lift Following a Sudden Change in Angle of Attack.

The circulation strengths obtained by the lattice method depend on the location and the number of vortices along the span and the chord of a wing. Calculations were done with different locations of vortices and control points in the wing-vortex interaction problem. The effect on the circulation strengths of increasing the number of chordwise vortices is shown in Figure 5. As can be seen in this figure there is no significant improvement by increasing the number of chordwise vortices beyond five. As can be seen in Figure 6 there is no noticeable difference in the lift coefficient between the cases of ten and twenty spanwise vortices. Hence in most of the calculations ten spanwise and five chordwise vortices were considered as a compromise between the total number of vortices for sufficient accuracy and computer time and storage requirements.

The model used for the wing-vortex interaction problem was a finite aspect ratio wing in an incompressible free stream, and a straight, infinite vortex at an arbitrary angle δ with the wing as shown in Figure 7. Most of the calculations were done with an intersection angle of zero degrees. In the wing-vortex interaction problem the important parameters are the height, h, of the vortex above or below the wing, the wing chord, c, the free vortex strength, Γ_∞, the positive and the negative peak values of lift coefficient, the time interval between the peaks and the maximum difference of section lift coefficients. The starting position of the free vortex was chosen 1.5 chords ahead of the leading edge of the wing. The furthest distance possible is desired from a long wake generation standpoint but increasing distance increases the computation time and storage requirements.
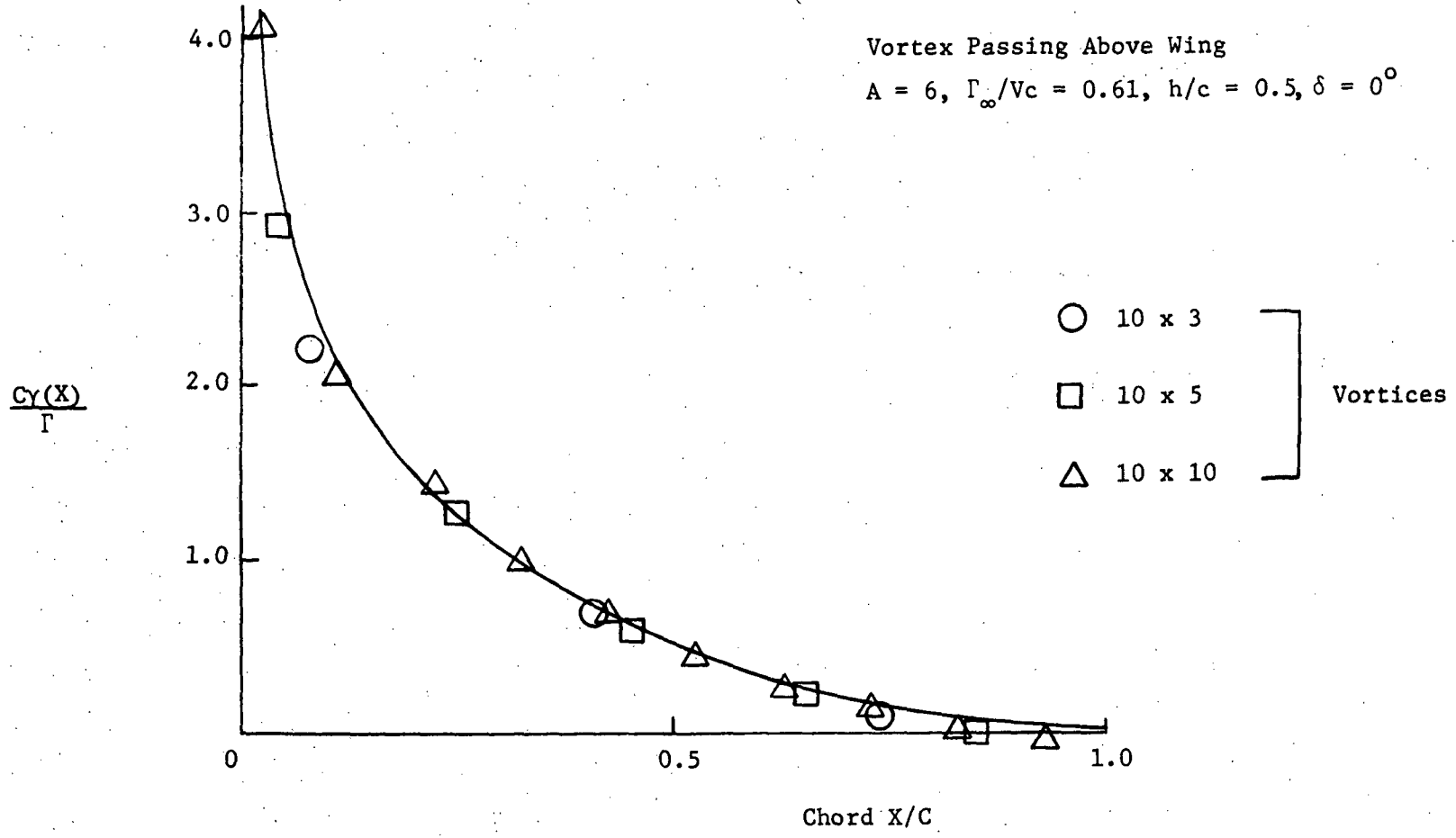
Figure 5. Chordwise Distribution of Circulation for $C_{\ell_{max}}$ at Center Section.
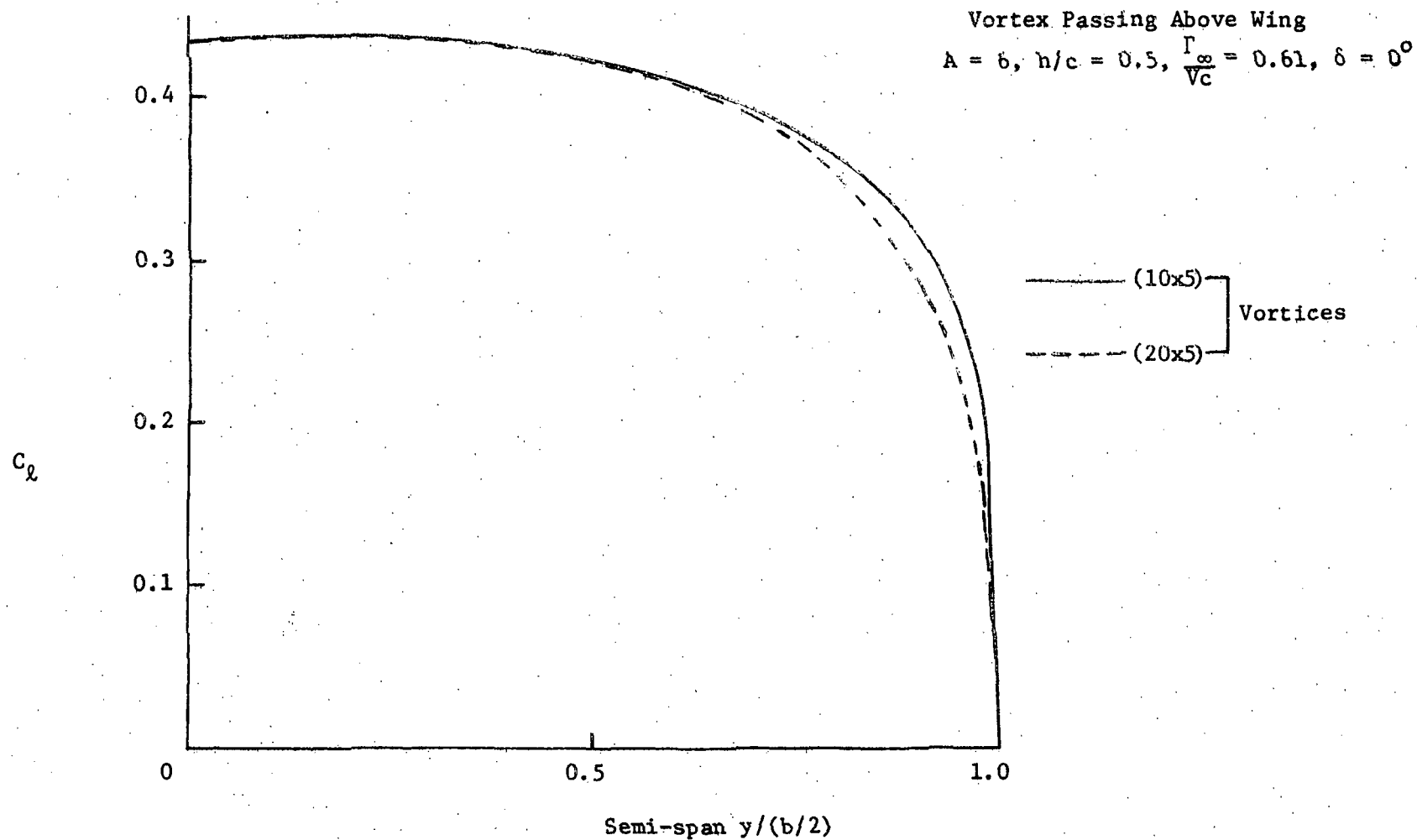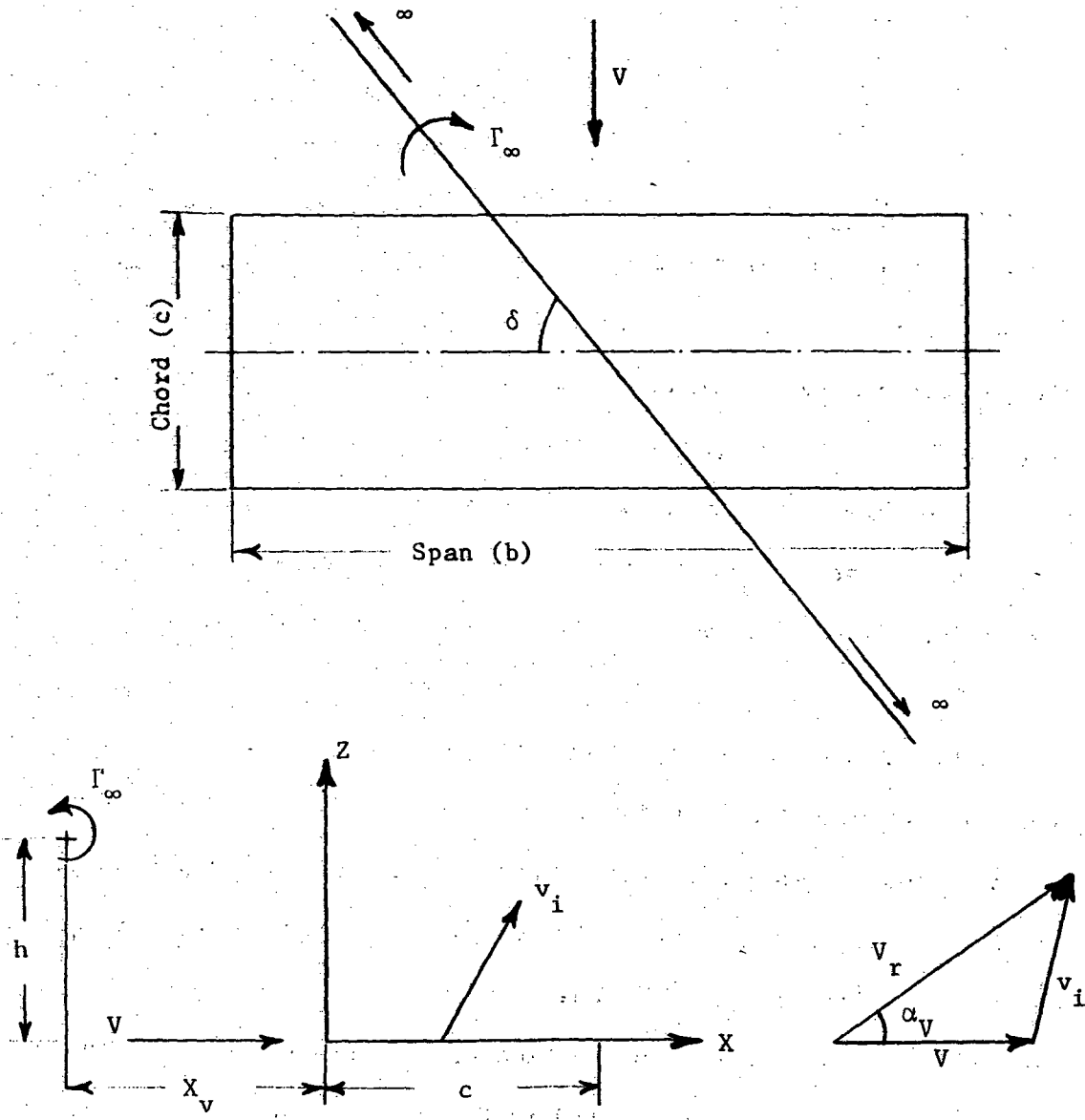
Figure 6. Spanwise Distribution of Lift Coefficient.

Figure 7. Wing-Vortex Interaction.

$\dfrac{X_v}{c} = 0$, Leading Edge (L.E.)

$\quad = 1$, Trailing Edge (T.E.)

α_V = Vortex Induced Angle of Attack

In the numerical calculations of lift due to wing-vortex interaction, it was observed that the time step size (Δt)has considerable influence on the peak lift coefficients, especially the negative peaks. Calculations were done with different values of nondimensional time step sizes $V\Delta t/c$. The variations of peak positive and negative wing lift coefficients and peak positive and negative midspan circulations with time steps are indicated respectively in Figures 8 and 9. A typical variation of wing lift coefficient with vortex location is shown in Figure 10 for different time steps. As the computation time increases with the decrease of time step size, most of the calculations were done with a nondimensional time step, $V\Delta t/c$, of 0.15.

Some of the results obtained by the present vortex lattice method are compared with the results of Johnson (6). Johnson (6) has obtained induced loads on an infinite aspect ratio wing due to a straight, infinite vortex using linear lifting surface theory. A comparison of tne two-dimensional values of peak circulation values and peak lift coefficients predicted by the lattice method and by the lifting surface theory are respectively presented in Figures 11 and 12. The circulation (Γ) and lift coefficient (C_ℓ) values for the lattice method are the values at the midspan of the wing which is a good approximation to two-dimensional values. As seen in these figures the comparison is good except at small values of (h/c). Decreasing the time step should decrease the peak values obtained by the lattice method and hence give better agreement with the results of Johnson (6). The effect of finite aspect ratio is shown in Figure 13 by comparing the present three-dimensional results with the two-dimensional results of Rudhman (25).

28
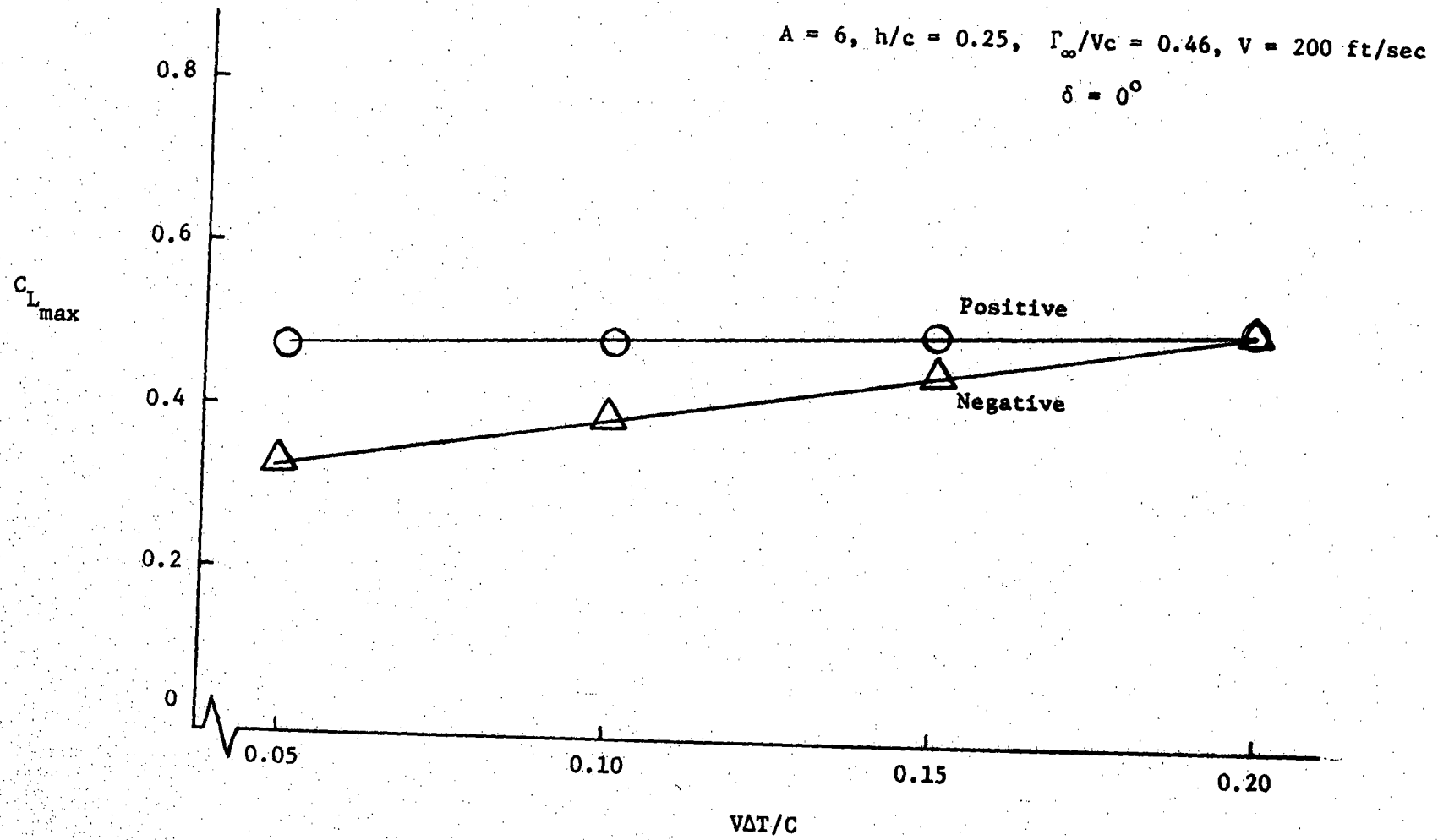
Figure 8. Effect of Time Step Size on Peak Wing Lift Coefficient.
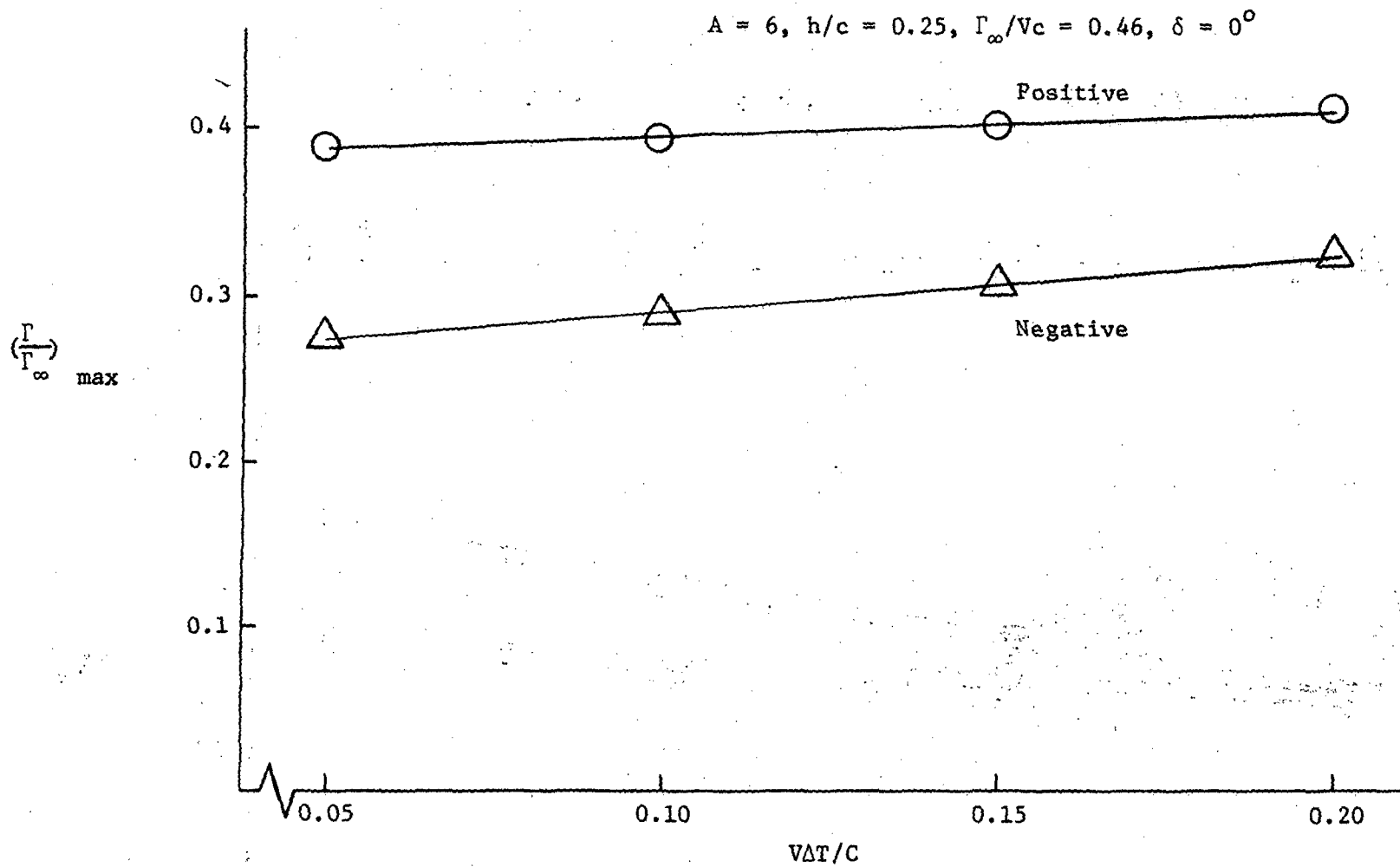
Figure 9. Effect of Time Step Size on Peak Circulation.

30
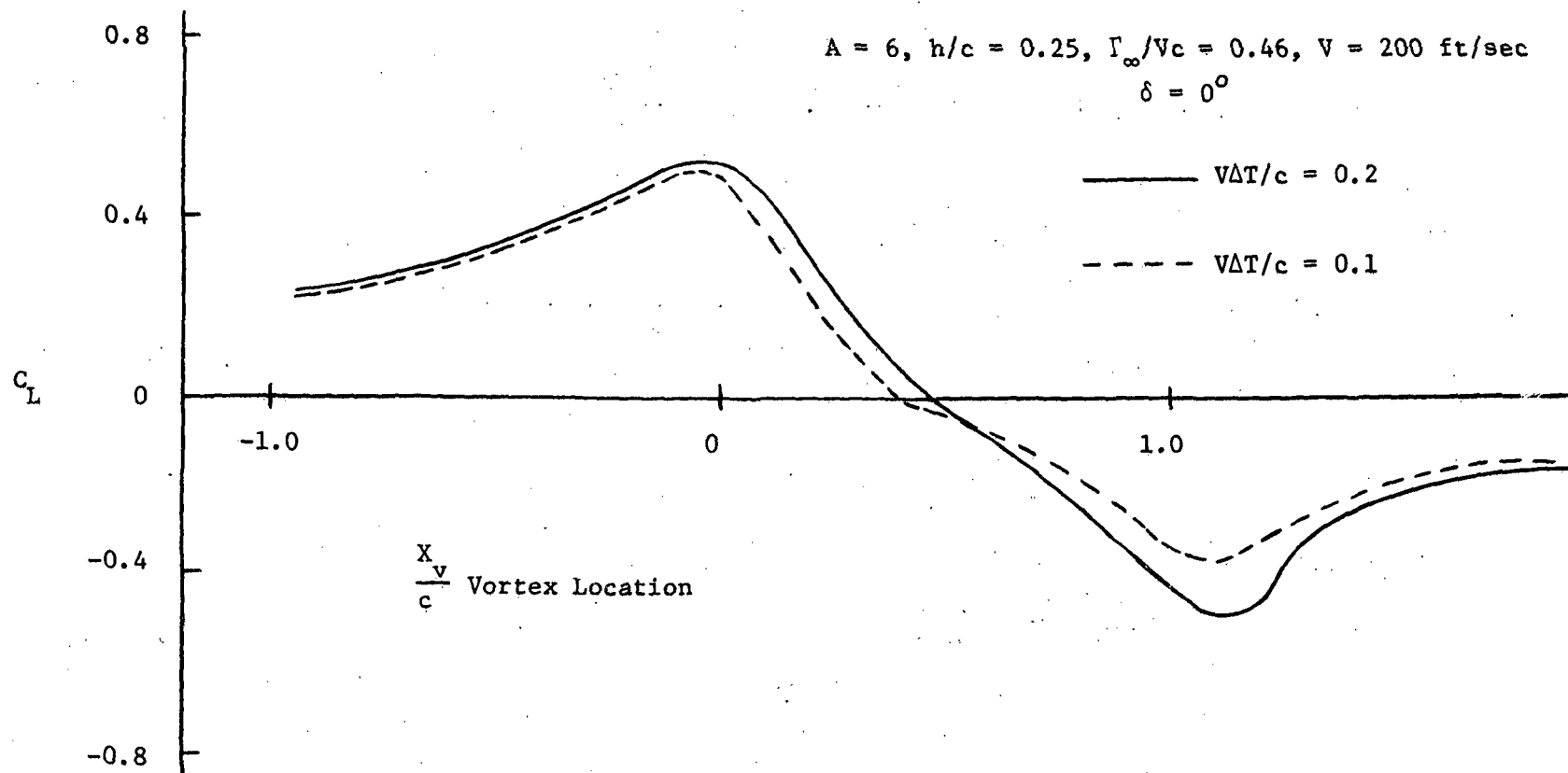
Figure 10. Variation of Wing Lift Coefficient with Vortex Location for Different Time Increments.

31
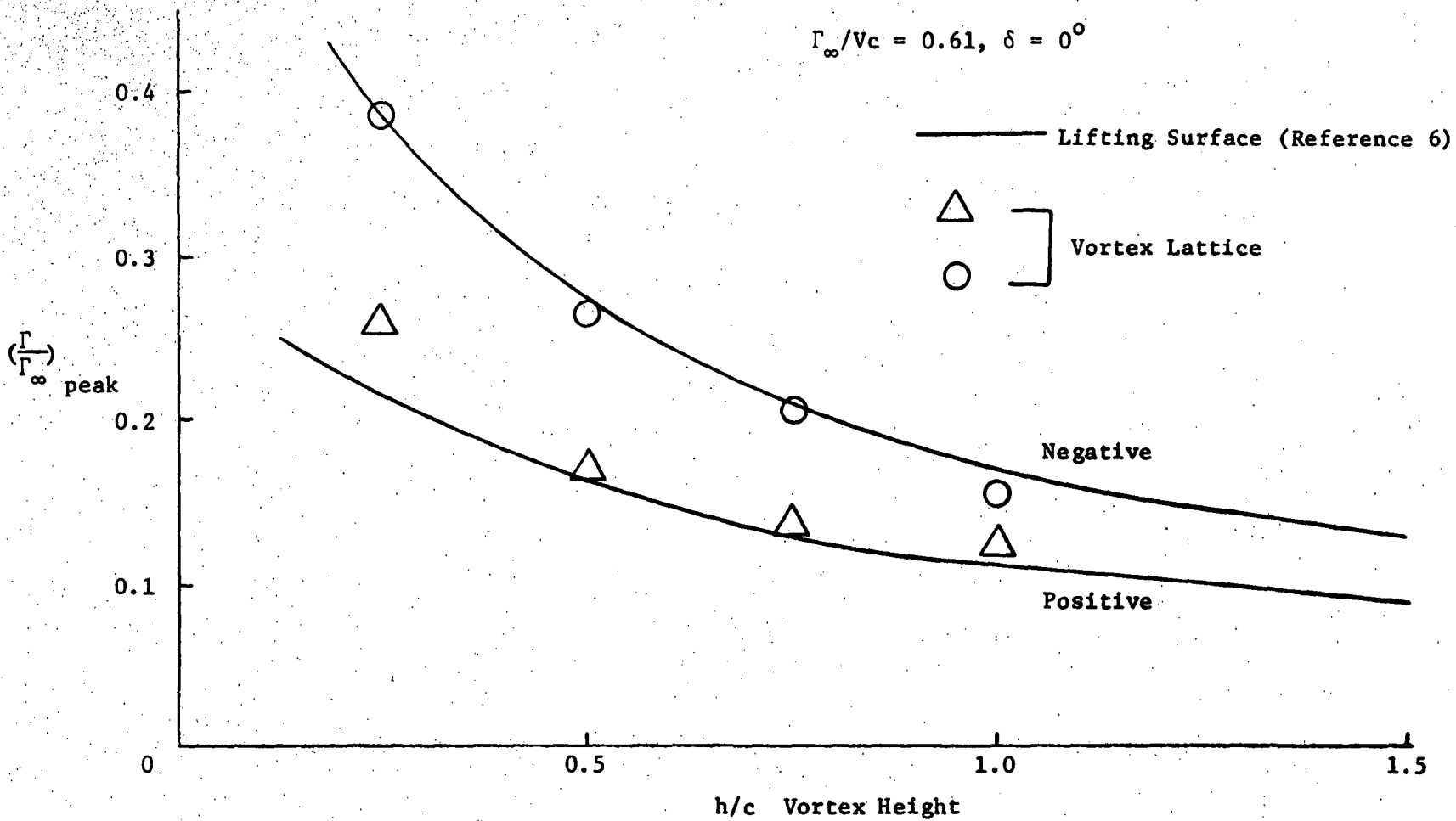
Figure 11. Variation of Peak Circulation with Vortex Height.
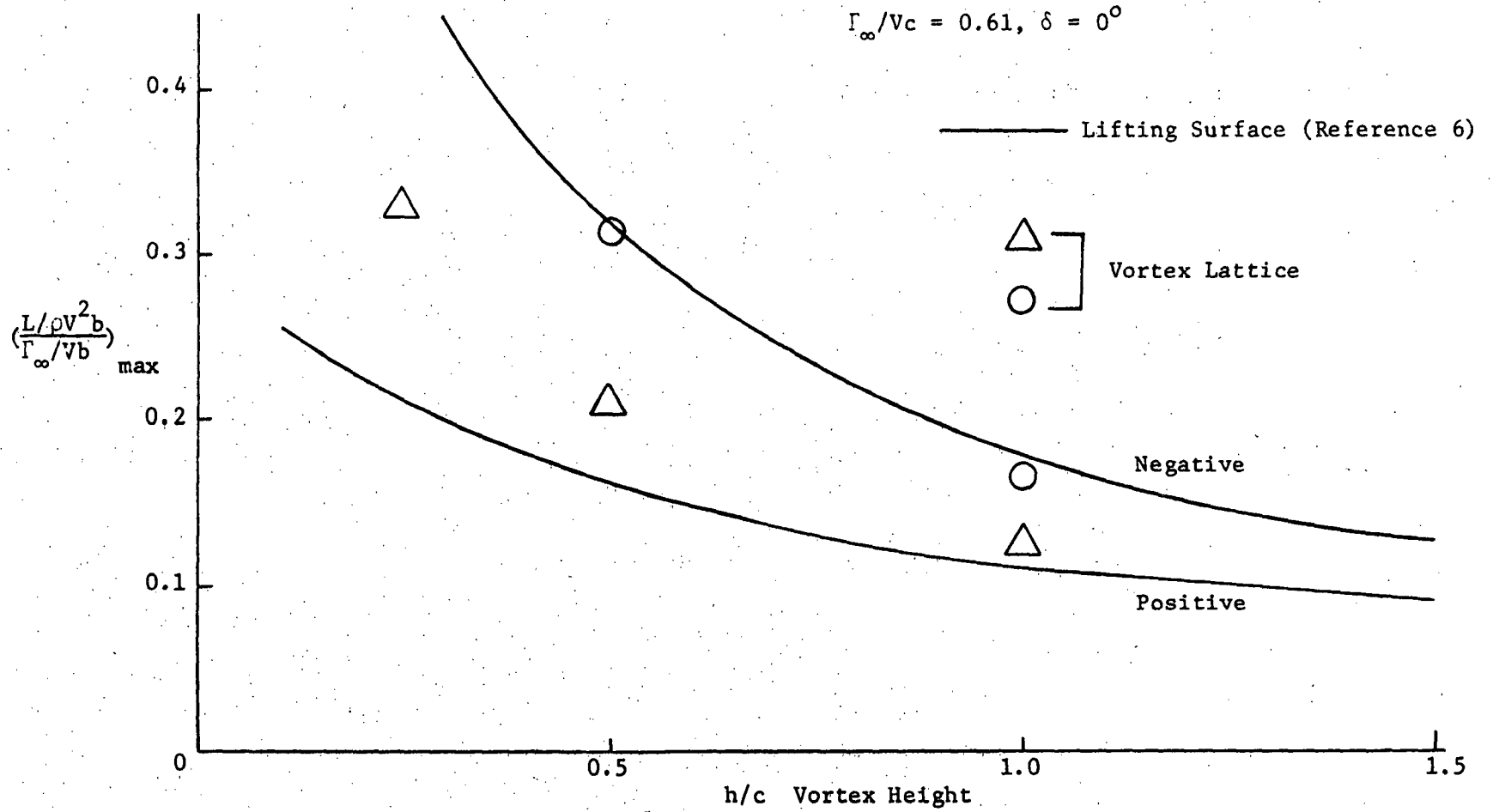
Figure 12. Variation of Peak Lift Coefficient with Vortex Height.

33
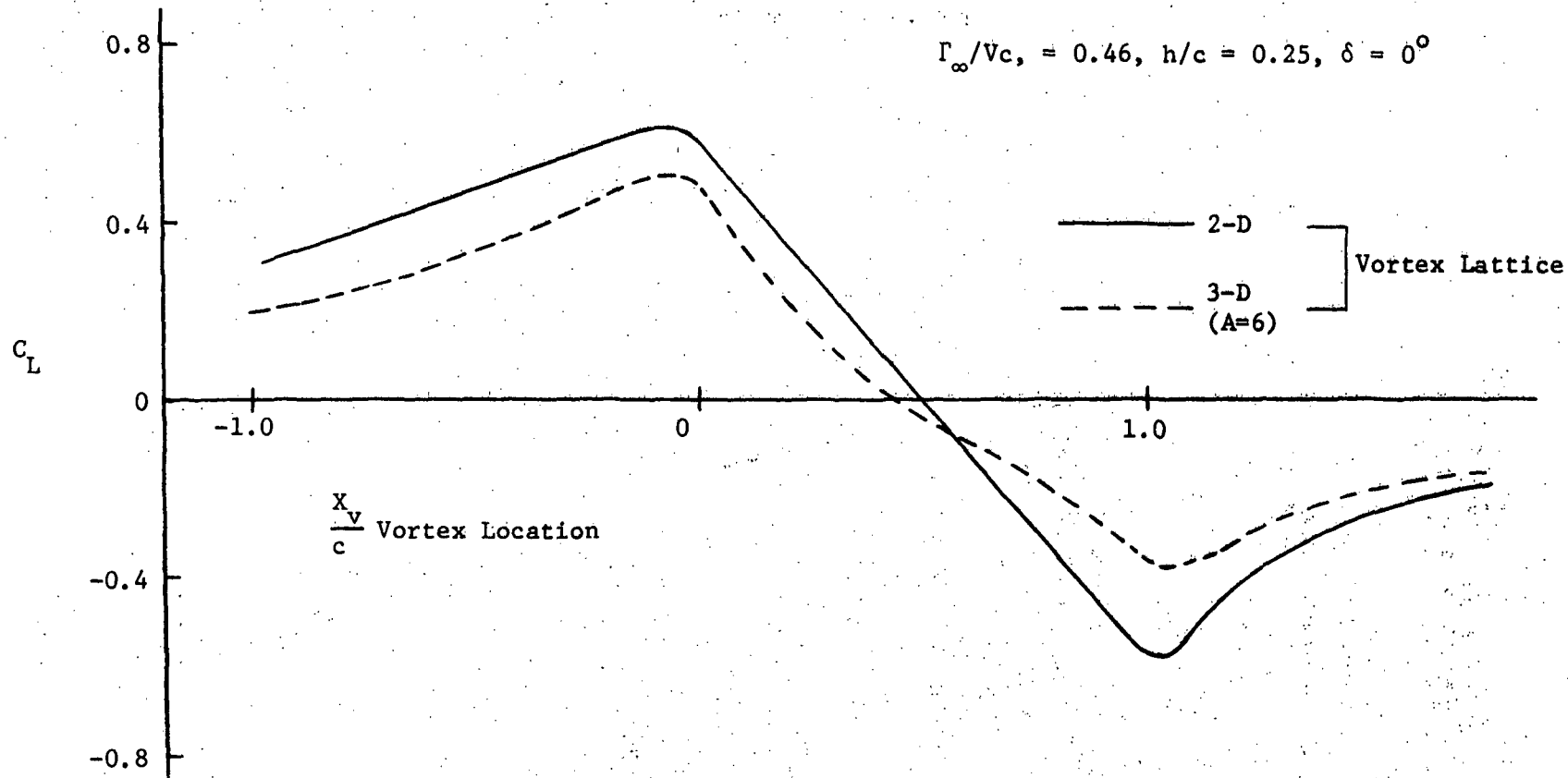
Figure 13. Variation of Lift Coefficient with Vortex Location for Two-Dimensional (2-D) and Finite (3-D) Wings.

34

Figure 14 shows the wing lift coefficient variation as the vortex

passes over the wing for two different (Γ_∞/Vc) values. Figure 15 shows

the lift coefficient variation as the vortex passes over the wing at

different heights. These figures indicate that lift coefficient

magnitudes increase with decreasing vortex heights, h, and also with

increasing values of (Γ_∞/Vc). Figure 16 shows a comparison of lift

coefficients for the same positive and negative vortex heights. As can

be seen in this figure, there is no significant difference in the lift

coefficients.

Figure 17 shows the effect of using quasi-steady and steady state

approximations in computing unsteady lift on the wing. In the quasi-

steady approximation the lift was computed including the unsteady term

but the contribution of the shed wake was neglected. In the steady

state approximation the lift was computed using the instantaneous

velocity and angle of attack. Both the positive and negative peak lift

coefficients computed using the quasi-steady approximation are well

above those predicted by the unsteady model as the wake which reduces

the induced loads was not included in this approximation.

Figure 18 shows the variation of lift coefficient with vortex

location for different aspect ratios. The reduction of peak lift

coefficient with decrease in aspect ratio does not correspond to the

reduction given by the aspect ratio correction factor as in the steady

case.

Figure 19 shows the variation of lift coefficient at a particular

spanwise station as a vortex passes over the wing at an angle $\delta = 90^{\circ}$.

As can be seen in this figure the peak lift coefficients increase with
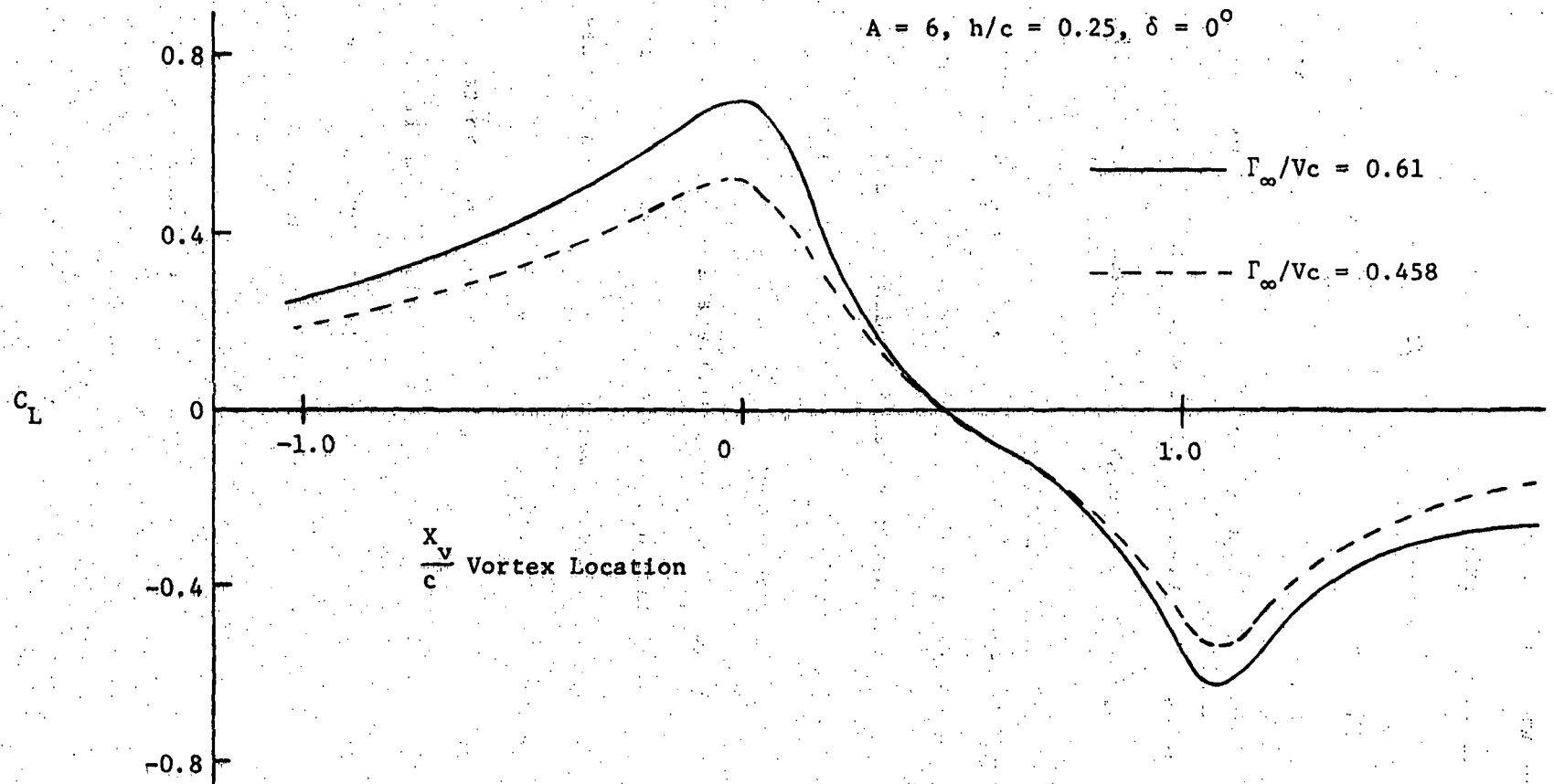
Figure 14. Variation of Lift Coefficient with Vortex Location for Different (Γ_∞/Vc).

36
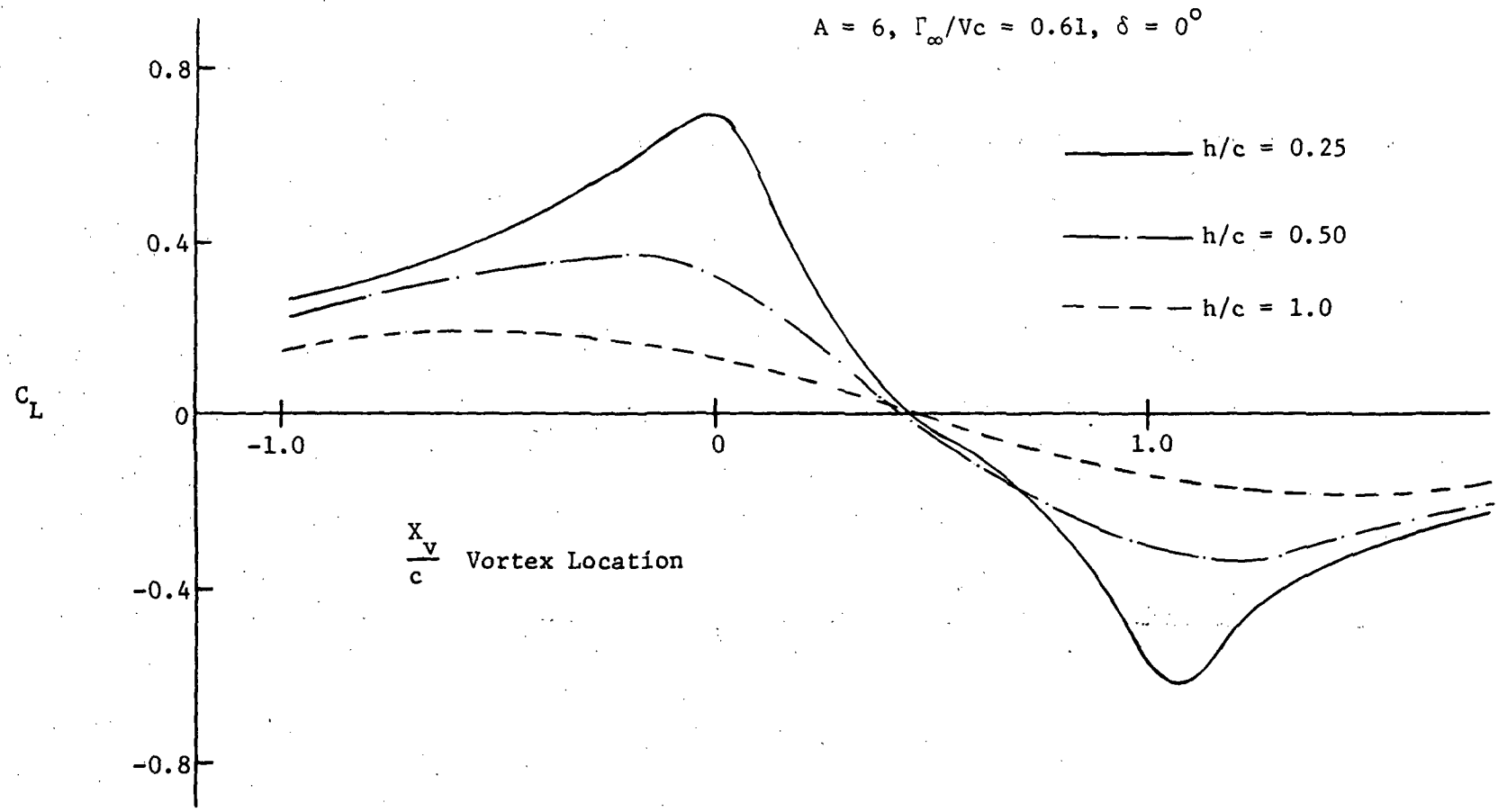
Figure 15. Variation of Lift Coefficient with Vortex Location for Different (h/c).
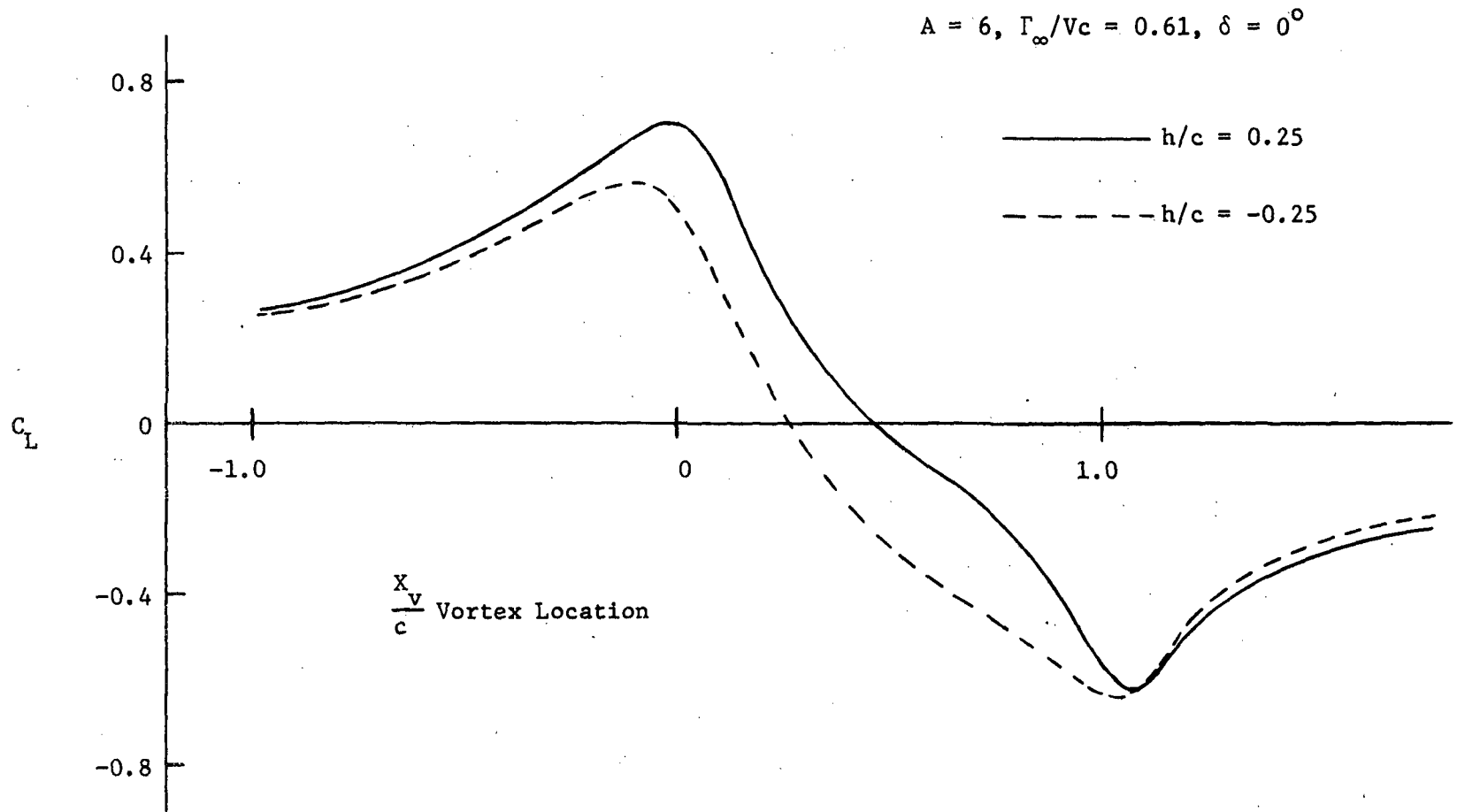
Figure 16. Variation of Lift Coefficient with Vortex Location for h/c = 0.25 and h/c = -0.25.

38
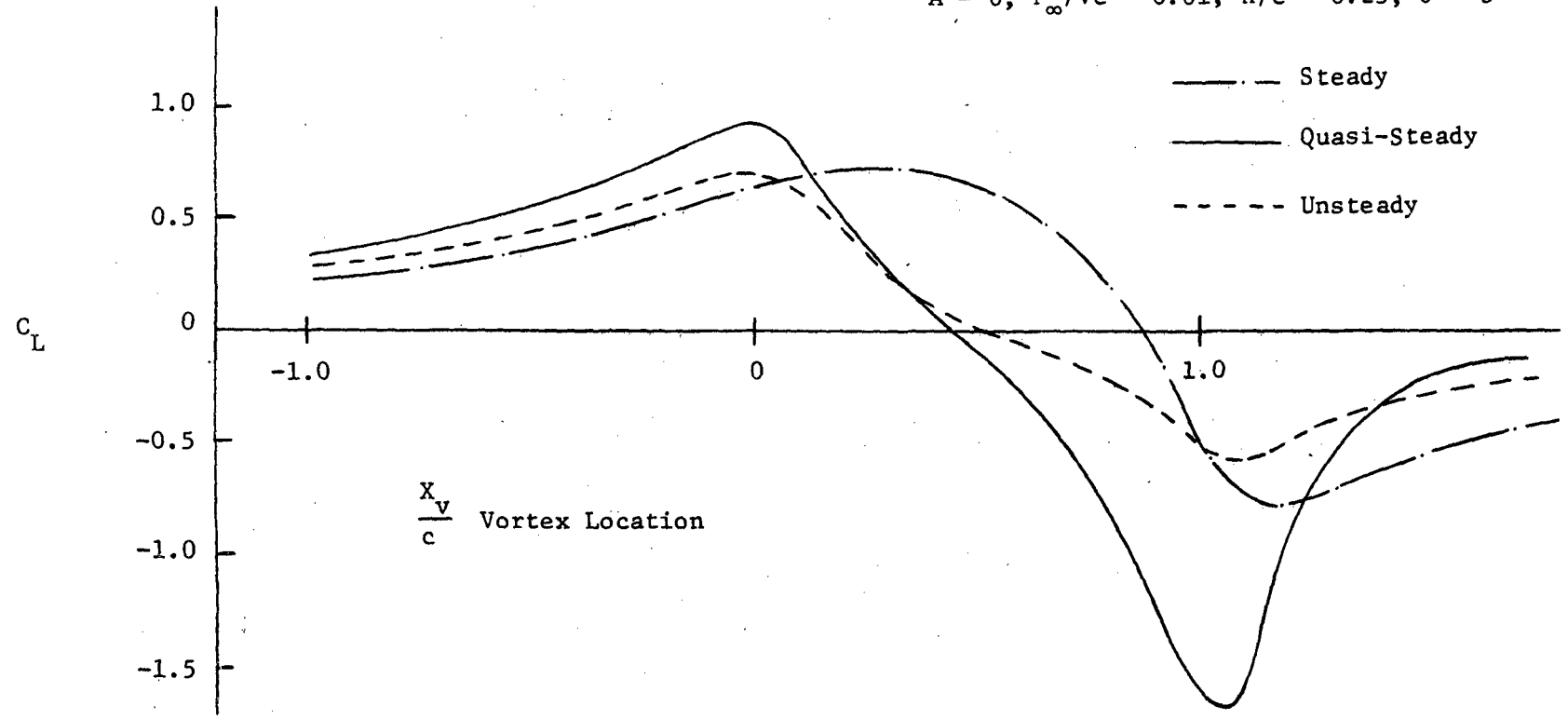
Figure 17. Effect of Steady and Quasi-Steady Assumptions on Lift Coefficient.

$A = 6$, $\Gamma_\infty/Vc = 0.61$, $h/c = 0.25$, $\delta = 0^\circ$

Steady

Quasi-Steady

Unsteady

C_L

$\dfrac{X_v}{c}$ Vortex Location

39
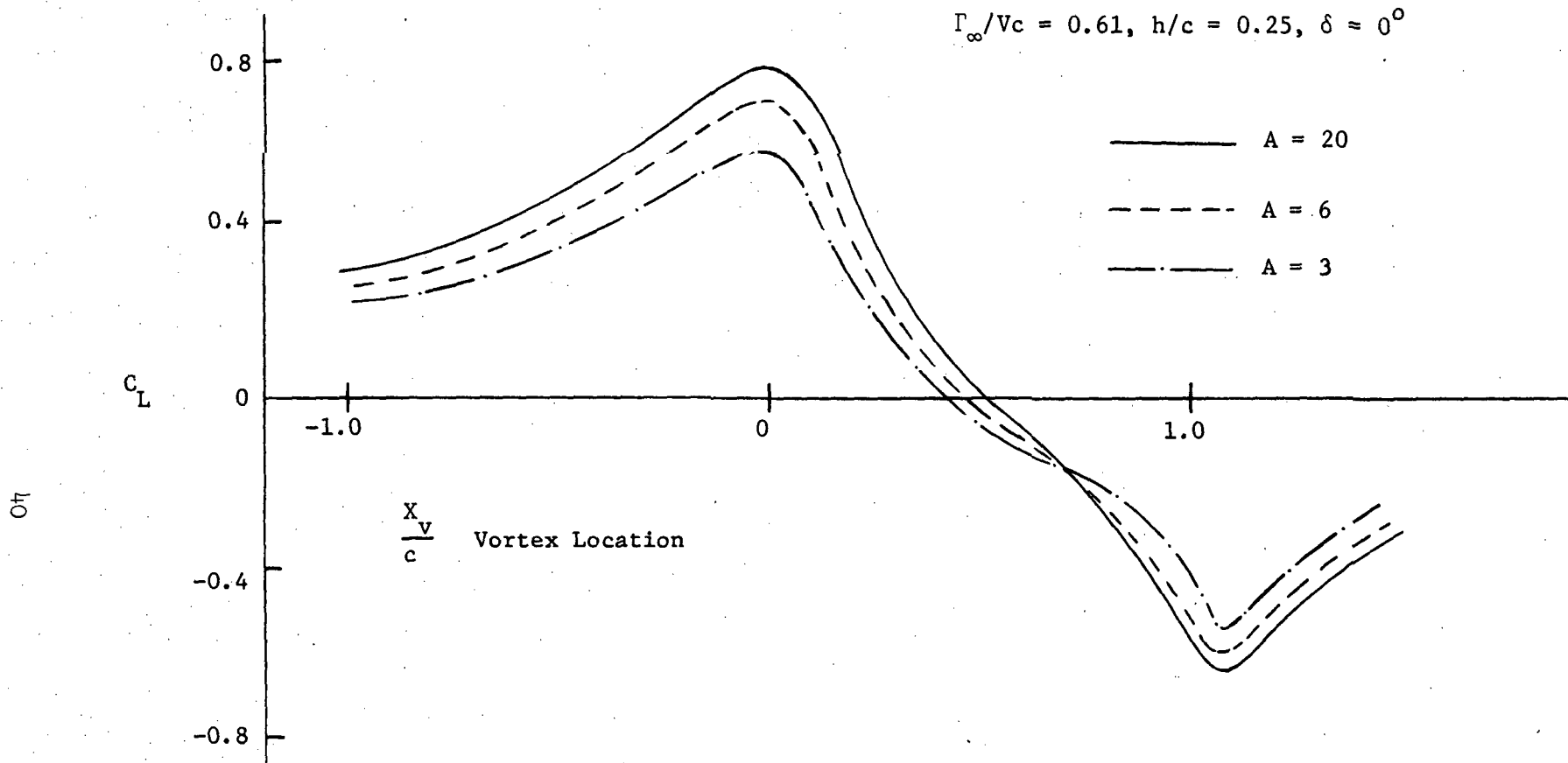
Figure 18.   Variation of Lift Coefficient with Vortex Location for Different Aspect Ratios(A).
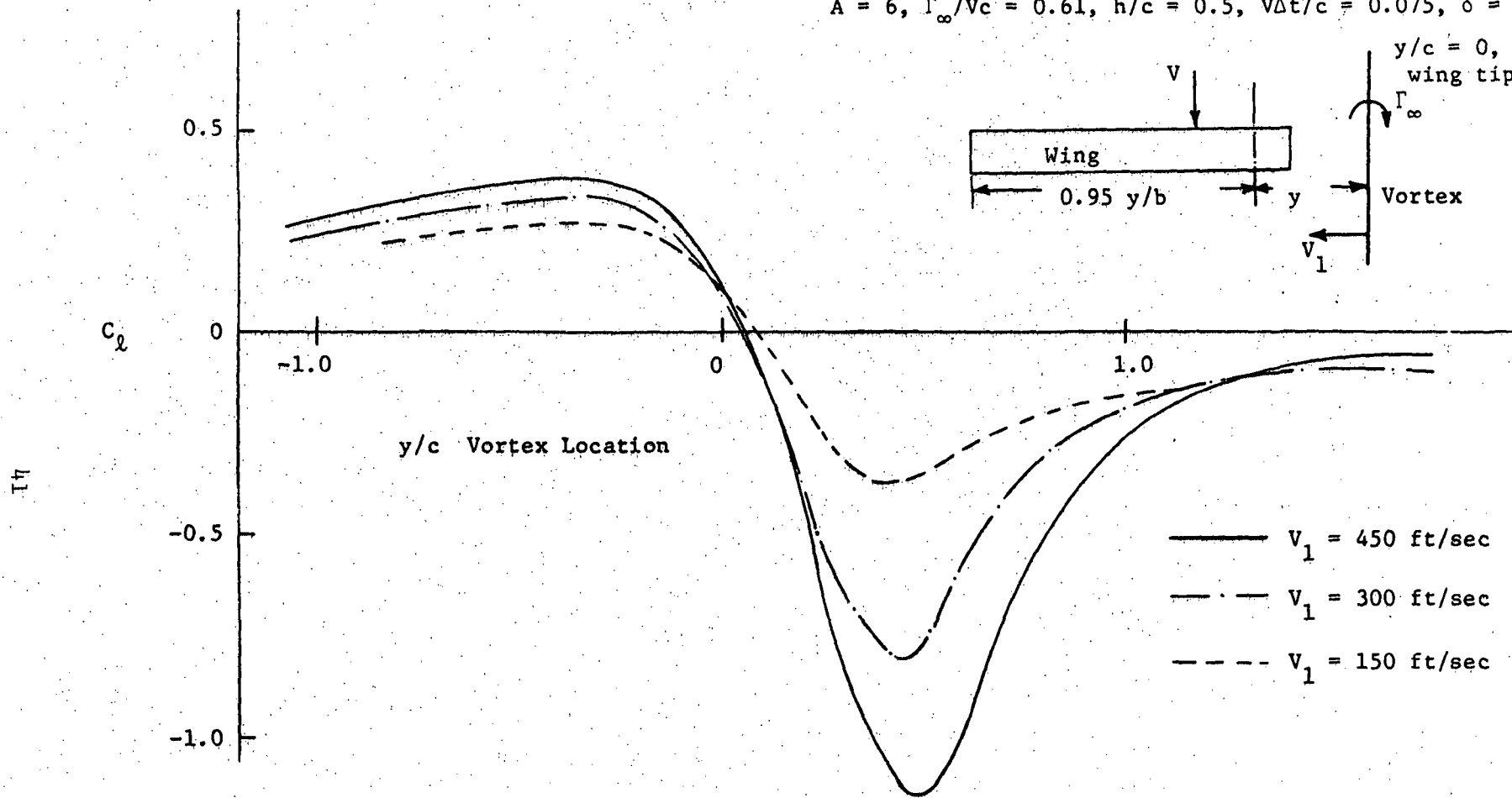
Figure 19. Variation of Lift Coefficient with Vortex Location at Spanwise Station y/b = 0.95.

increasing sweep rates. This case approximates helicopter rotors over a range of azimuth angles where the tip vortex sweeps across the span at approximately $\delta = 90^{\circ}$.

In this chapter the vortex lattice method has been applied to the relatively simple problem of planar wing-vortex interaction. Comparison of the results with those obtained by linear lifting surface theory has shown good agreement. With the confidence gained in the vortex lattice method by this comparison, the method is extended in the next chapter to the more complex geometry of the rotor-vortex interaction problem.

CHAPTER IV

APPLICATION OF VORTEX LATTICE METHOD
TO THE ROTOR-VORTEX INTERACTION PROBLEM

4.1 Model Rotor-Vortex Interaction Problem

4.1.1 The Model Rotor and Wake Configuration

The wake of a rotor blade is important because of the interference of the blade with its own wake and the wake of other blades. The wake of a helicopter rotor in forward flight consists of shed and trailed vorticity in a distorted, skewed helix behind each blade of the rotor. This vorticity which is trailed and shed in sheets rolls up to form tip and root vortices. Since the bound circulation of a rotor blade is highly concentrated at the tip the rolling up is accomplished within a short distance behind the rotor. Since the bound circulation at the root of the blade goes to zero gradually the root vortex is weak and hence can be neglected.

In the present study of rotor-vortex interaction problem, a simplified model for the rotor and its wake has been assumed. An approximate lifting surface method like the vortex lattice method is used in the calculations. The rotor blade is replaced by a lattice of vortices. As an approximation for the calculation of the downwash on the rotor due to its own wake, the wake is approximated by a net of finite strength, finite length straight line vortices, the trailing lines being along streamlines relative to the rotor blade and the shed vortices being shed parallel to the instantaneous position of the rotor blade. The azimuthal spacing in the vortex net is determined by the azimuth step size in the calculations while the spanwise spacing is

43

determined by the chosen number of spanwise vortices. The change in the wake geometry as the blade moves to the next azimuth station is calculated on the basis that a point in the wake moves with the velocity of the fluid at that point, due only to the blade motion; namely, $(V \sin \psi + \Omega r_j)$. In other words, it is not a "free-wake" treatment. At high forward velocities or large advance ratios the downwash becomes small in comparison to the free stream velocity and hence flat, planar wake is a good approximation for the large advance ratios considered in the calculations.

The more exact free wake model for use in the calculation of rotor airloads would be to represent rotor blades by lifting surfaces and blade wakes by vortex sheets. Calculation of wake geometry would involve the computation of the distortion and roll up of these vortex sheets due to their own induced velocities and those of lifting surfaces. This detailed wake model, however, is too complicated and time consuming for practical computations.

Experimental data is available from a model, single bladed rotor operating at an advance ratio and encountering a free vortex from a fixed wing upstream. The rotor was positioned at a zero incidence angle of the tip path plane with the free vortex from the wing lying in a plane parallel to the tip path plane. The rotor hub was positioned at a lateral distance Z from the vortex and a distance h below it. Rigid geometry is also assumed for the free vortex, i.e., the influence of blade loading on the geometry of the vortex is not considered in the calculations. The model rotor blade configuration used in the

computations is shown in Figure 20. A detailed description of this
model rotor and its instrumentation can be found in the report by
Surendraiah (9).

4.1.2 Effect of Vortex Core

In order to calculate the loads on the blade for small values of
blade-vortex separation, h, it is necessary to consider the viscous
core of the interacting free vortex. An approximation to the induced
velocity inside a vortex core is the Rankine model which assumes a
solid body rotation of the vortex core with an induced velocity at the
outer edge of the vortex core equal to the value given by the Biot-Savart
law at that point.

$$v_i(r) \Big|_{r=a} = \Gamma/2\pi a = \omega a$$

Thus,

$$\omega = \Gamma/2\pi a^2$$

where: ω = rotational velocity inside the core

        a = core radius

        Γ = strength of vortex

        v_i = induced velocity

Thus it is only necessary to check whether the point at which the
induced velocity must be determined is inside the core or not and apply
either the Biot-Savart relationship or the solid body rotation model.

For a vortex with a finite core McCormick, et al., (26) have
given an alternate expression for the induced velocity at any point,
namely,
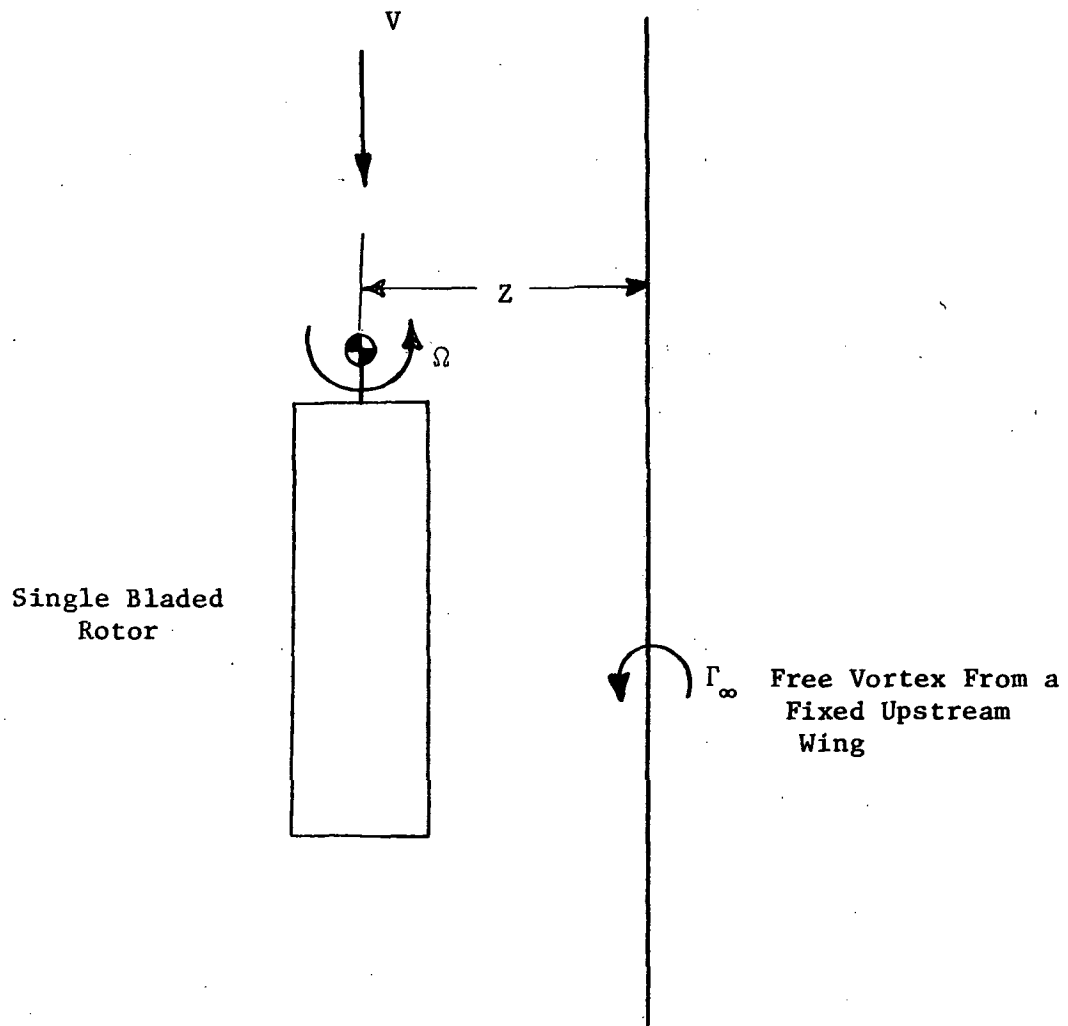
Figure 20.   Rotary Wing Configuration for the Vortex Lattice Method.

$$v_i(r) = v_i(a) \left(\frac{a}{r}\right) [1 + \ln(r/a)]$$

where $v_i(a)$ is the induced velocity at the core radius.

The logarithmic variation of induced velocity is higher than the Rankine model induced velocity. Both the logarithmic variation and the Rankine model were tried in the load calculations. The logarithmic variation overestimated the vortex induced loads. The Rankine model has been used in the calculation of vortex induced loads as these loads showed better agreement with experimental results.

4.1.3 Calculation Procedure

Figure 21 shows the blade coordinates used in the calculation of blade airloads. The wake geometry is calculated by starting the rotor blade from rest in a free stream. The blade is located at a specified azimuth (ψ = 0 degrees) without any wake vortices. The blade is then rotated through an azimuthal increment, $\Delta\psi$, and shed and trailing filaments are deposited in the wake. These are of unknown strength but with known positions. The blade is replaced by a lattice of vortices of unknown strength. Since the load on a rotor blade is highly concentrated near the tip, vortices near the tip are placed closer than the vortices near the root of the blade. Ten spanwise and three chord-wise vortices are considered in the lattice. The total downwash at the control points on the blade where the boundary condition of zero normal velocity is satisfied is obtained by summing the contribution of the vortex lattice, the contribution from the wake vortices, the velocity induced by the free vortex and the normal component of the free stream velocity. Satisfying the boundary condition at all the control points

47
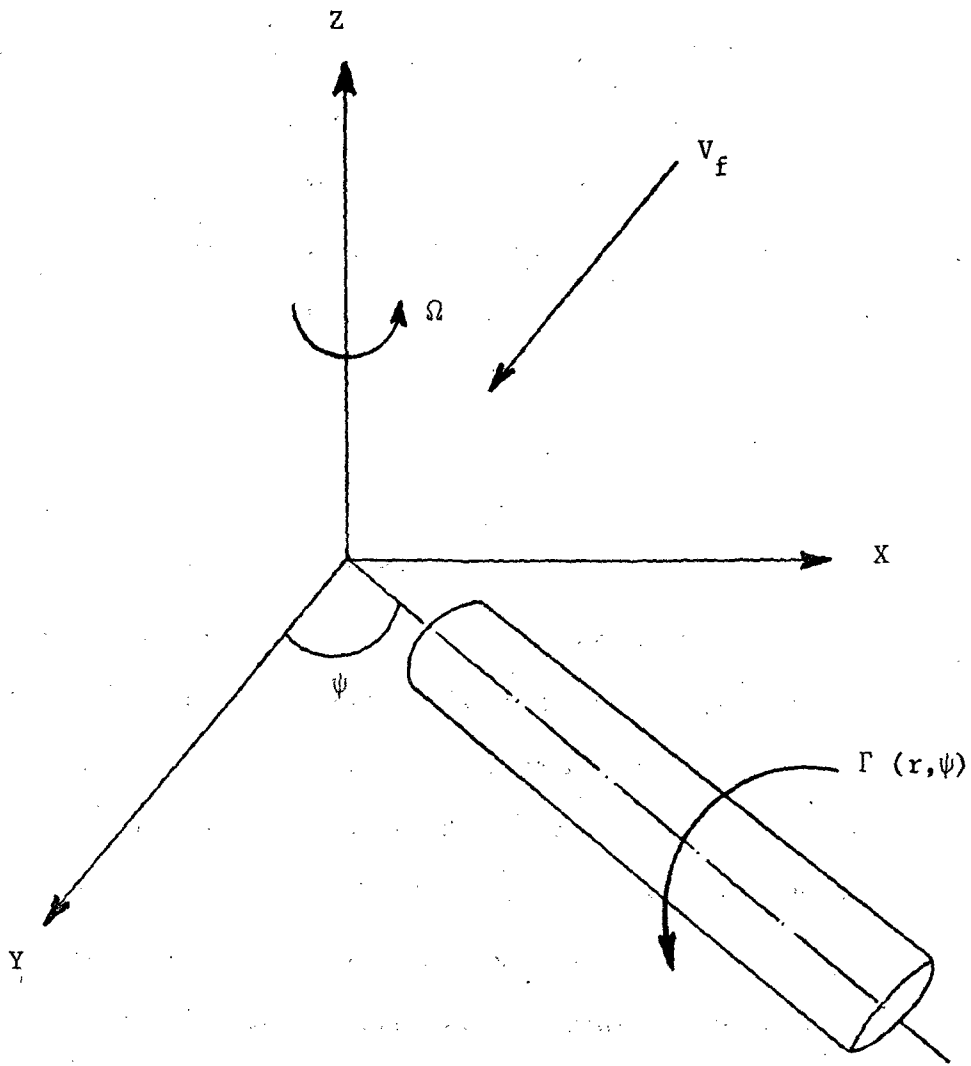
Figure 21. Blade Coordinates.

(equal in number to the number of unknown vortices on the rotor blade)
results in a system of simultaneous equations for the unknown vortex
strengths. Solving these equations gives the strengths of vortices that
are shed immediately behind the blade. All vortex element end points
not attached to the blade are then allowed to translate as the blade is
stepped forward for a time Δt (equal to $\Delta \psi / \Omega$) with velocity ($V \sin \psi$
$+ \Omega r$). This completes a typical first step in the calculation of the
wake and airloads induced by the free vortex.

In the subsequent steps only the vortices at and just behind the
blades have unknown strengths, while those in the wake have known
strengths. In this manner arrays of discrete shed and trailing vortices
are generated immediately behind the blade with strengths corresponding
to blade loads. Figure 22 shows the wake configuration behind a single
bladed rotor. Knowing the circulations at each section of the blade
from the solution of the simultaneous equations, the section lift can
be obtained from

$$\ell_j(y,t) = \rho U \sum_i \Gamma_{ij}(x,y,t) + \rho \int_0^c [\frac{\partial}{\partial t} \int_0^x \Gamma_{ij} (\xi,y,t) \, d\xi] \, dx$$

when $U = V \sin \psi + \Omega r_j$.

The section lift coefficient is based on the local velocity
relative to the blade

$$C_\ell = \frac{\ell_j}{\frac{1}{2}\rho U^2 c} \qquad \text{where } c = \text{chord of the blade}$$

The strength of the free vortex, the core diameter of the free vortex,
the blade dimensions and the rotational velocity of the blade are

V_f

Ω

Blade

$\Gamma(r_i,\psi_j)$ Bound Vortex

$\Gamma(r_{j+1},\psi_j)$

$-\Gamma(r_i,\psi_j)$

Trailing Vortex

Shed Vortex

$\Gamma(r_{i+1},\psi_j)$

$-\Gamma(r_{i+1},\psi_{j-1})$
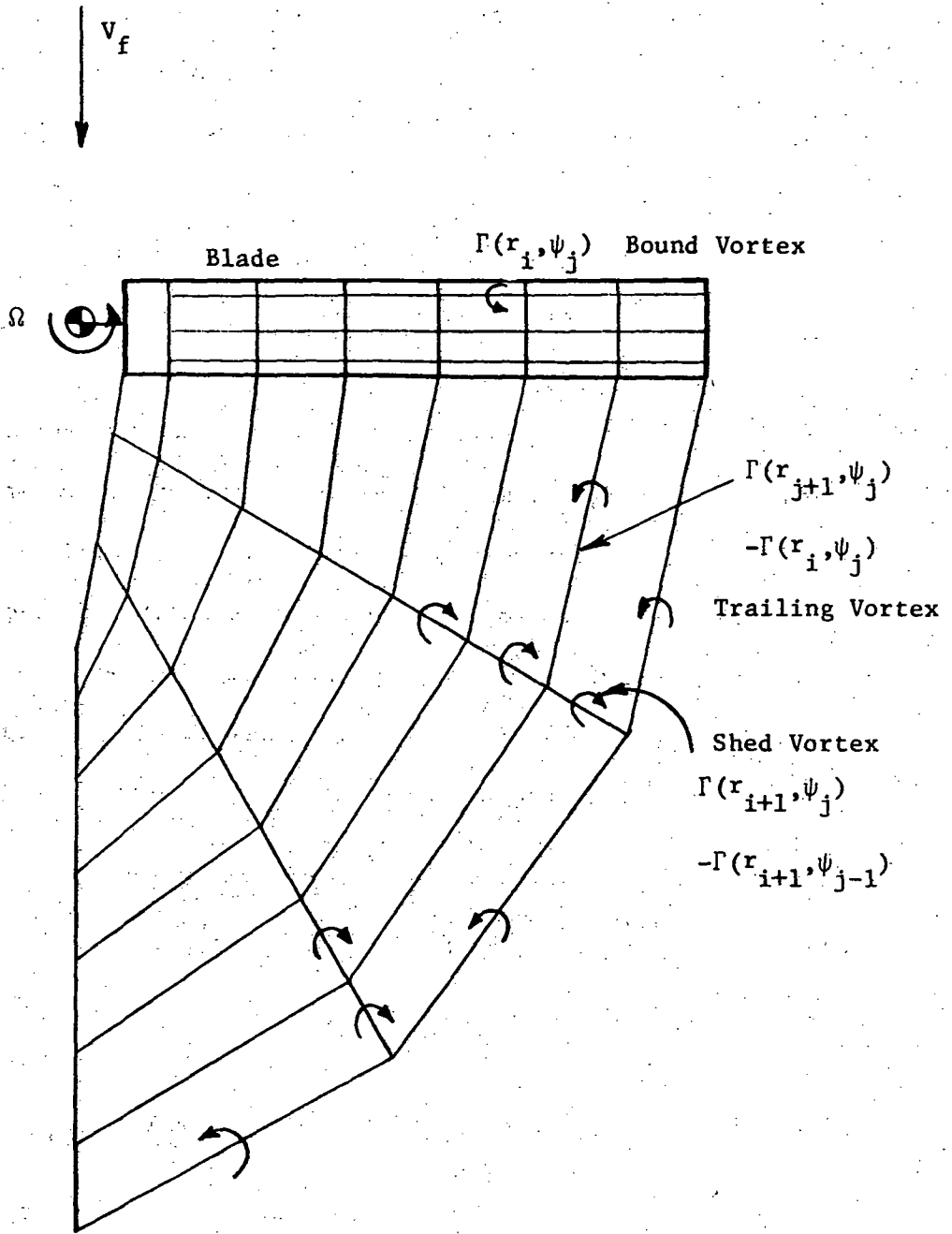
Figure 22. Example of Wake Configuration.

handled as input data. The time increment Δt is chosen to correspond to the finite change $\Delta \psi$ in the azimuth position of the blades

$$\Delta t = \Delta \psi / \Omega$$

where Ω is the rotor angular speed.

The IBM 360/67 digital computer was used to obtain the numerical solution to the problem. For the advance ratio of 0.7, the computer time required for an azimuth travel of about 60 degrees with an azimuth increment of five degrees was about 150 secs. The accuracy of the predicted load distribution depends very much on the azimuth increment and the number of vortices. It was found that an azimuth increment of about five degrees was necessary to predict the vortex induced loads.

4.1.4 Results and Discussion

The parameters describing the model rotor blade and the free vortex are given in Table 1. The azimuth increment $(\Delta \psi)$ in most of the calculations was five degrees. The values of the free vortex strength and the free vortex core radius in Table 1 are from experimental measurements of Surendraiah (9).

The results of the vortex lattice method are compared with the lifting surface theory results of Johnson (7) and also experimental results of Surendraiah (9) and Padakannaya (10). The lifting surface theory solution developed for a model wing-vortex interaction problem has been applied by Johnson (6) for the rotor-vortex interaction problem. Johnson (7) has presented the results of the application of the lifting surface theory for the single bladed rotor-vortex configuration. A typical variation of the section lift coefficient as

51

Table 1

Model Rotor Operating Parameters

Rotor Rotational Speed	Ω	= 1500 RPM and 2000 RPM
Forward Velocity	V	= 110 fps
Advance Ratio	μ	= 0.7 (Ω = 1500 RPM)
		= 0.526 (Ω = 2000 RPM)
Free Vortex Strength	Γ_{∞}	= 15.25 ft^2/sec
Blade Chord	c	= 0.167 ft
Blade Radius	R	= 1.0 ft
Free Vortex Core Radius	a	= 0.031 ft
Collective Pitch	θ	= 0 deg
Tip Path Inclination Angle	α_T	= 0 deg

the rotor blade cuts through the vortex is shown in Figure 23. As indicated in this figure the maximum section lift coefficient difference is the difference between the positive and the negative peak section lift coefficients. Figures 24a, 24b, and 25 show the comparison of the maximum section lift coefficient difference due to vortex interaction as predicted by the vortex lattice method and the lifting surface theory. These figures show the variation of the maximum section lift coefficient difference with rotor plane position (h/c) at the radial location r/R = 0.95. The section lift coefficient is based on the local relative velocity of the rotor blade. Good agreement is shown between the lifting surface results and those from the vortex lattice method. Padakannaya (10) has presented the measured spanwise loads due to vortex interaction. Comparisons of the measured and the predicted spanwise maximum lift difference distribution for the different rotor plane positions, h/c, and for various positions of shaft axis, Z/R, are shown in Figures 26a, 26b, 27 and 28. As can be seen in these figures the predicted results are higher than the experimental results with the difference between the two results increasing with decreasing values of Z/R. This discrepancy may be due to the effect on the measured results of increased interference between the vortex and the hub with its large spinner as Z/R decreases.

The spanwise variation of maximum section lift coefficient difference predicted by the vortex lattice method and the measured values are presented in Figures 29a, 29b, and 30, for the different rotor plane positions, h/c, and for different shaft axis positions, Z/R. The lift coefficients are based on local rotational velocities of the rotor blade to be consistent with the experimental results. As
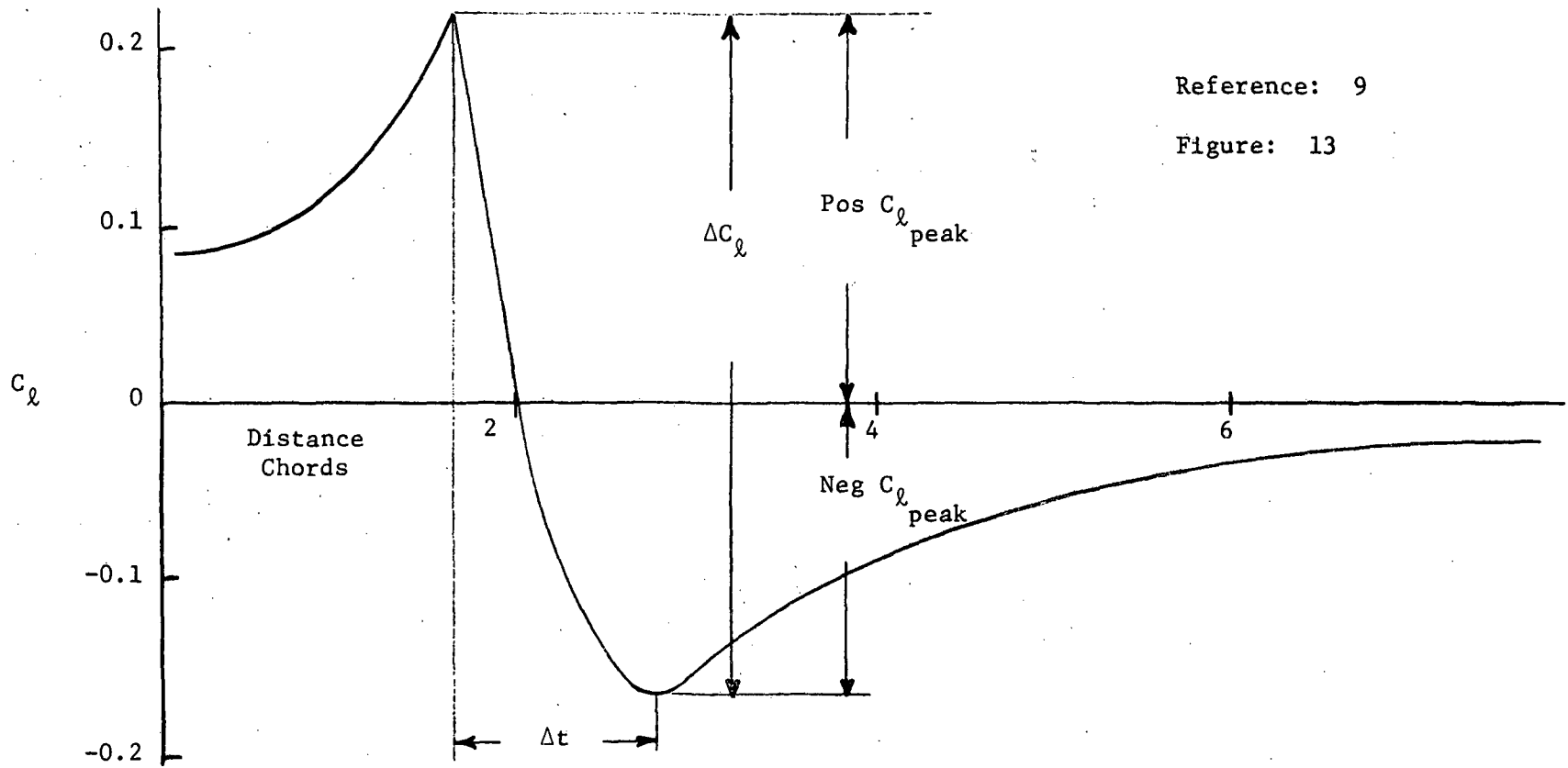
53

Figure 23.   Typical Section Lift Coefficient Variation on Rotor Blade.

54
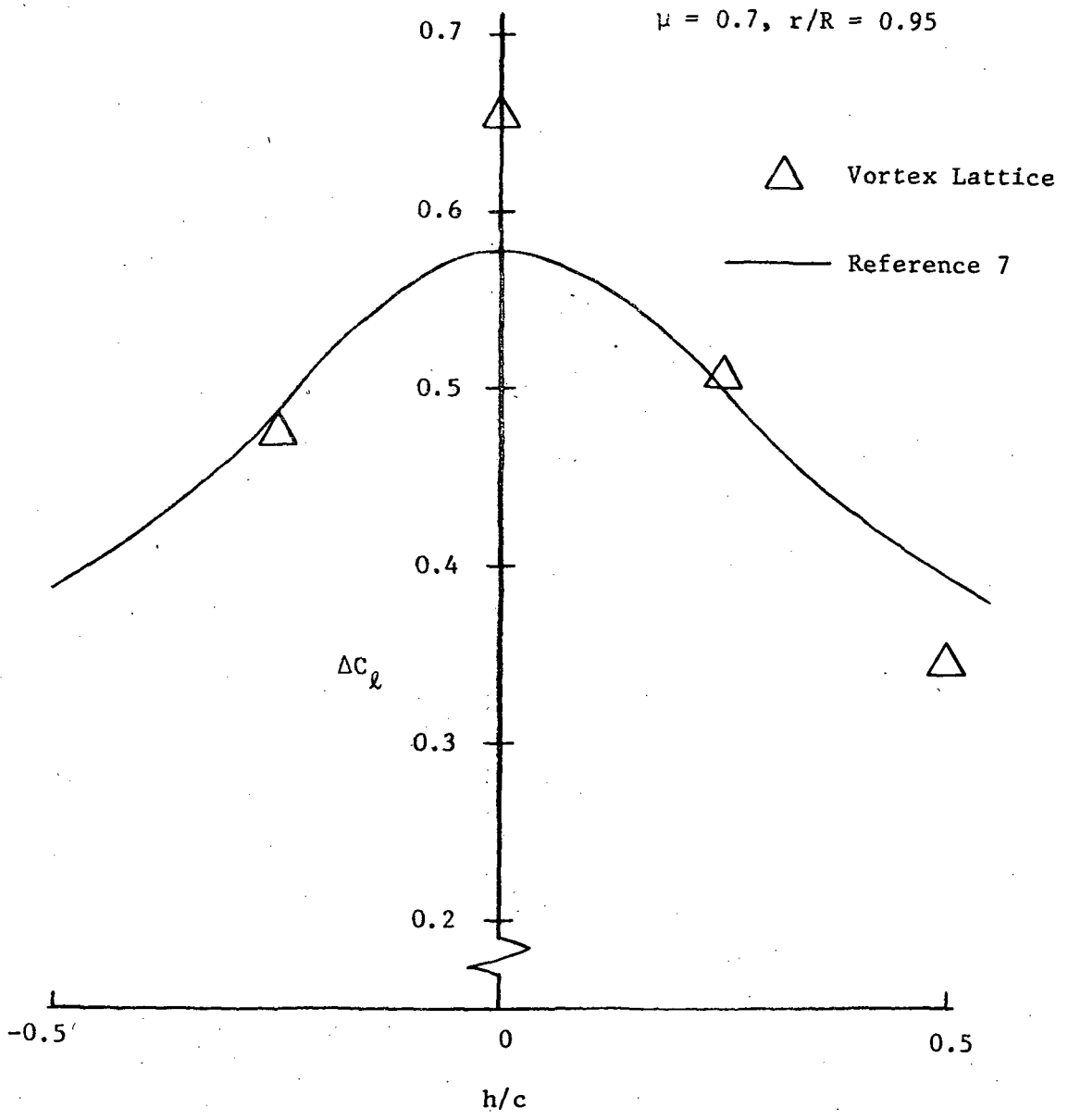
Figure 24a. Variation of Maximum Section Lift Coefficient Difference (ΔC_ℓ) with Rotor Plane Position (h/c); Model Rotor, Z/R = 0.5.
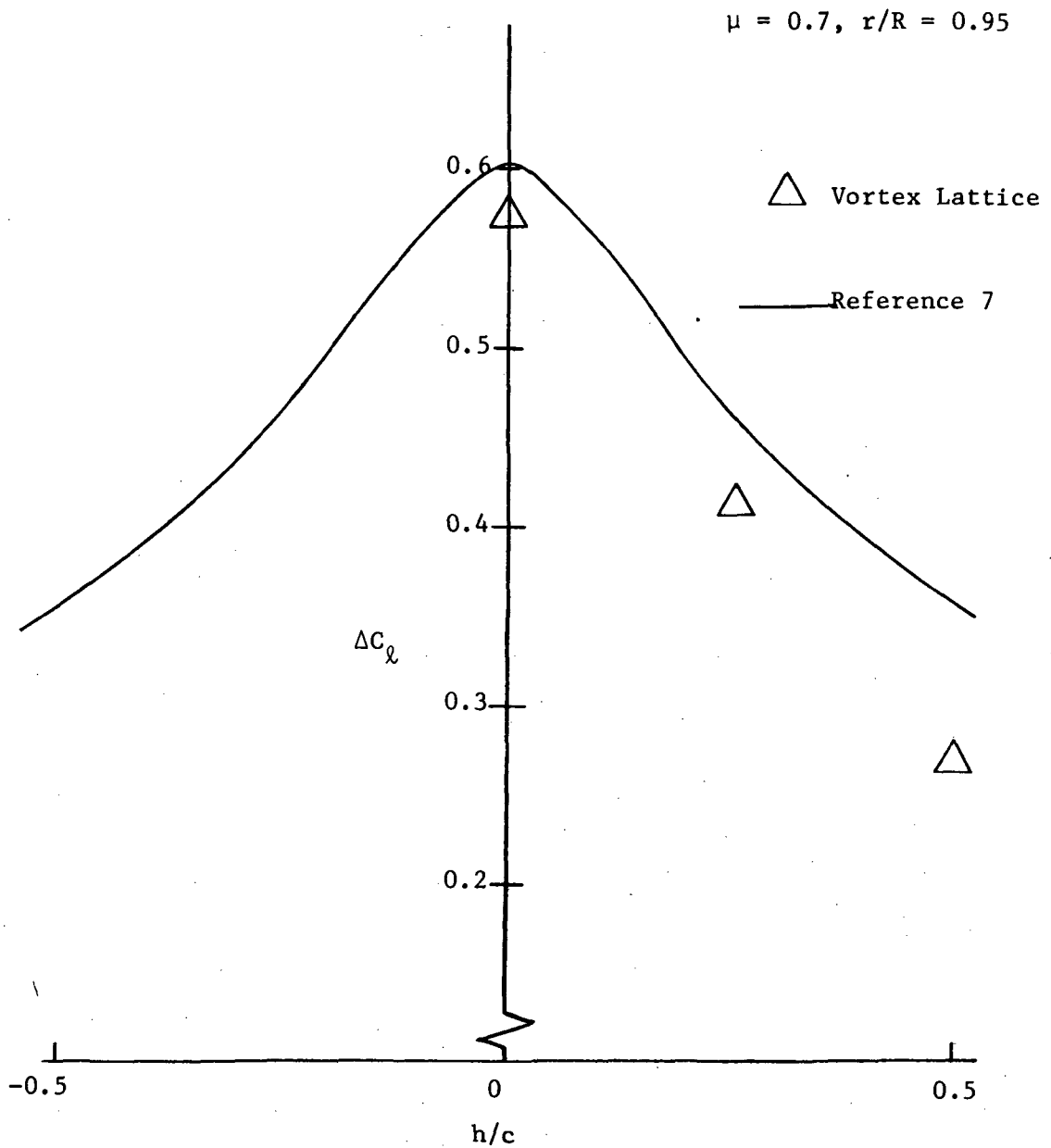
Figure 24b. Variation of Maximum Section Lift Coefficient Difference (ΔC_ℓ) with Rotor Plane Position (h/c); Model Rotor, Z/R = 0.75.
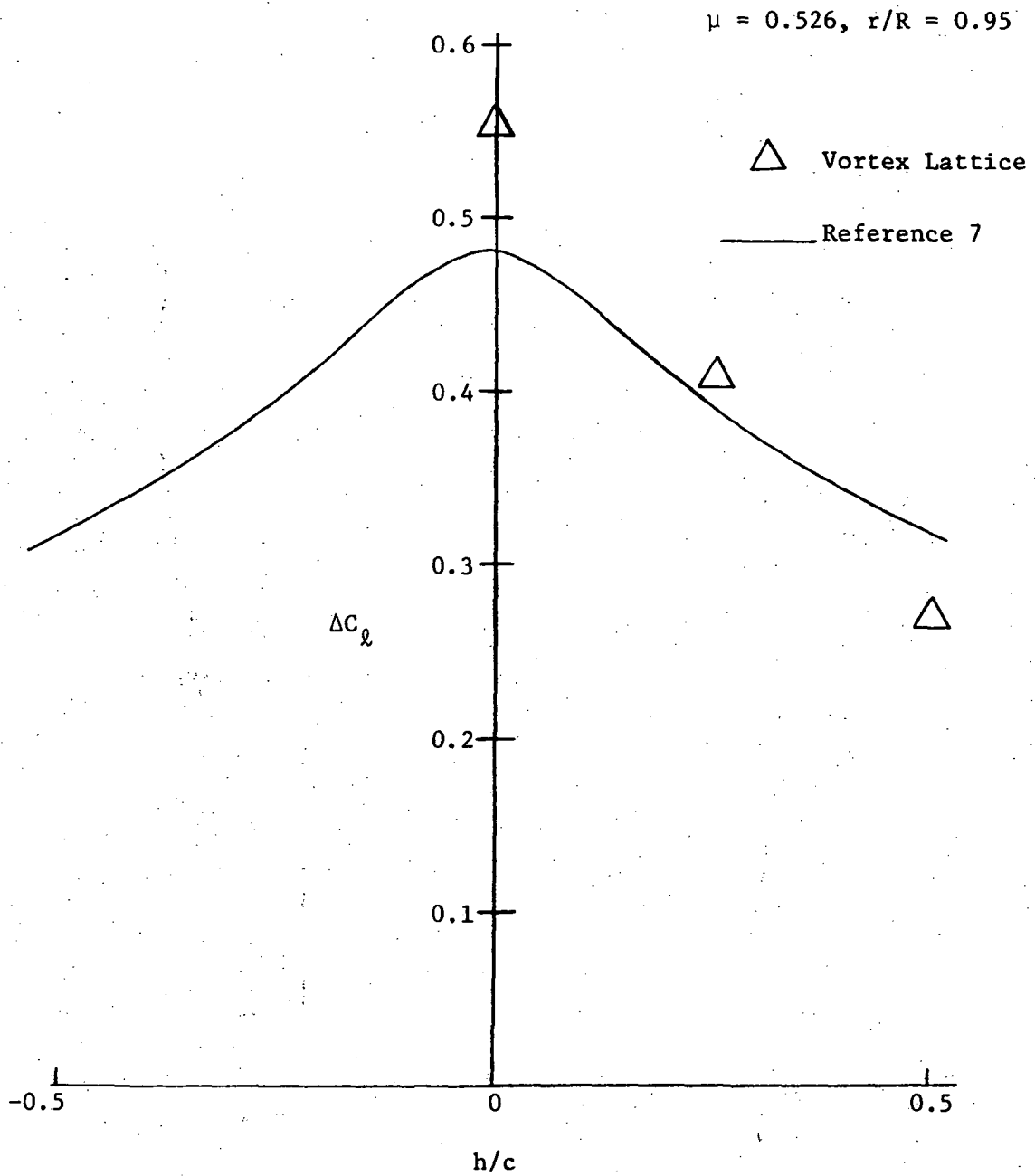
Figure 25. Variation of Maximum Section Lift Coefficient
Difference (ΔC_ℓ) with Rotor Plane Position (h/c);
Model Rotor, Z/R = 0.5.

$\mu = 0.7, \ Z/R = 0.5$

———— Vortex Lattice

△ Experiment
(References 9 and 10)

Figure 26a. Spanwise Variation of Maximum Lift Difference (ΔL) Due to Vortex Interaction;
Model Rotor, h/c = 0.5.

58

Figure 26b. Spanwise Variation of Maximum Lift Difference (ΔL) Due to Vortex Interaction; Model Rotor, h/c = 0.25.
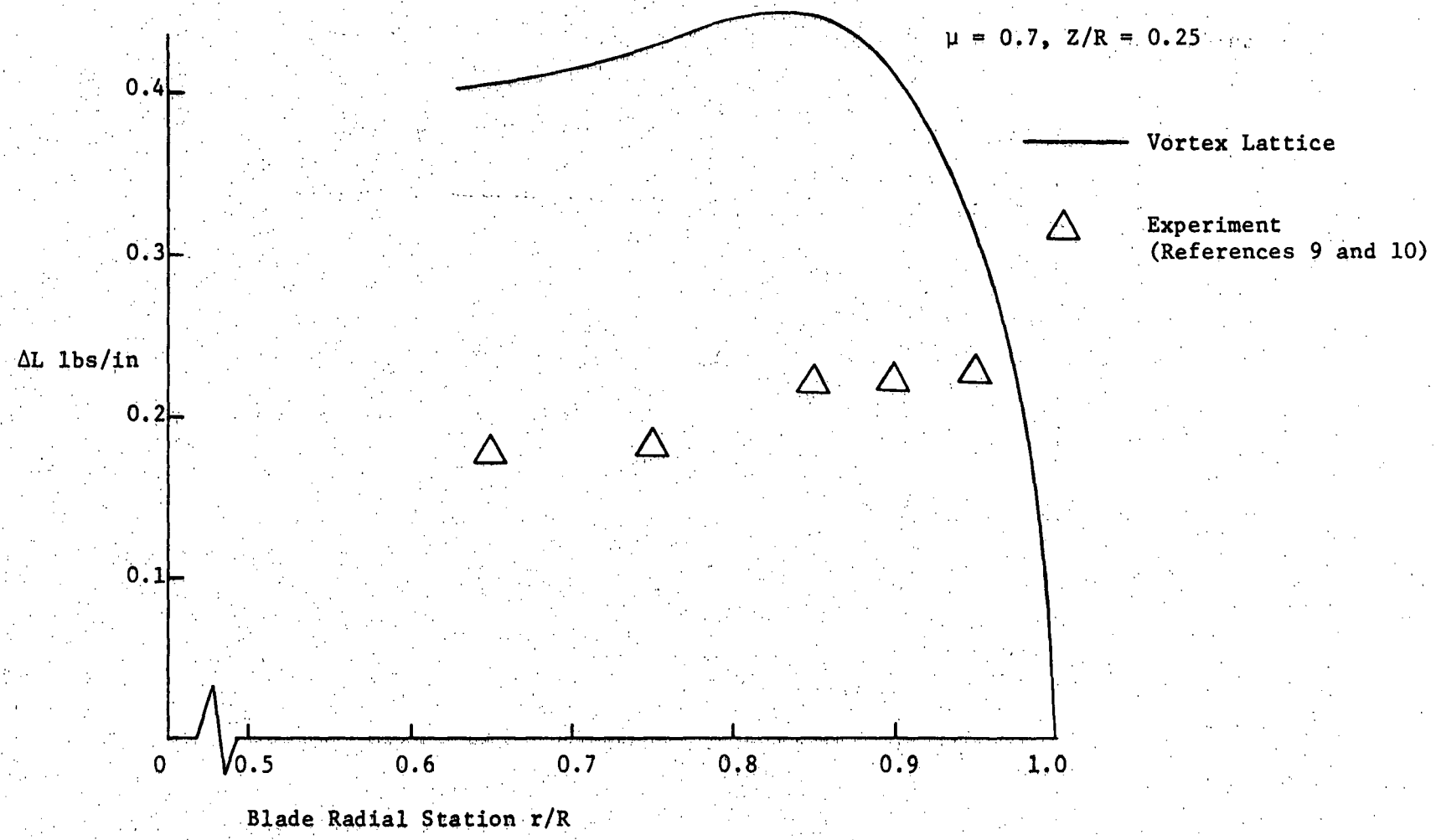
Figure 27. Spanwise Variation of Maximum Lift Difference (ΔL) Due to Vortex Interaction; Model Rotor, h/c = 0.25.

$\mu = 0.526$, $Z/R = 0.5$

——— Vortex Lattice

△ Experiment
(References 9 and 10)

ΔL lbs/in

0.3

0.2

0.1

0

0   0.5   0.6   0.7   0.8   0.9   1.0

Blade Radial Station r/R

61
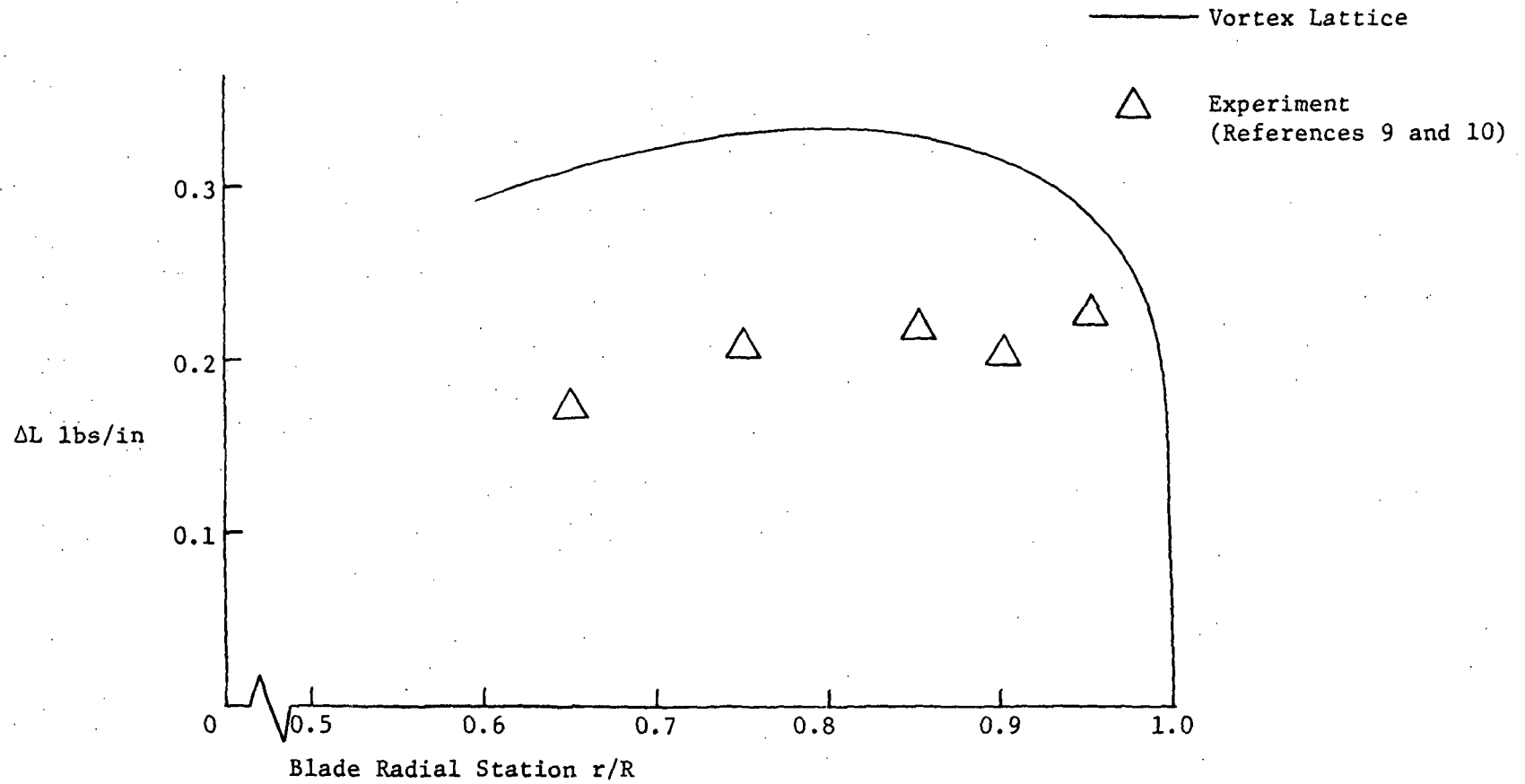
Figure 28.   Spanwise Variation of Maximum Lift Difference (ΔL) Due to Vortex Interaction;
Model Rotor, h/c = 0.5.
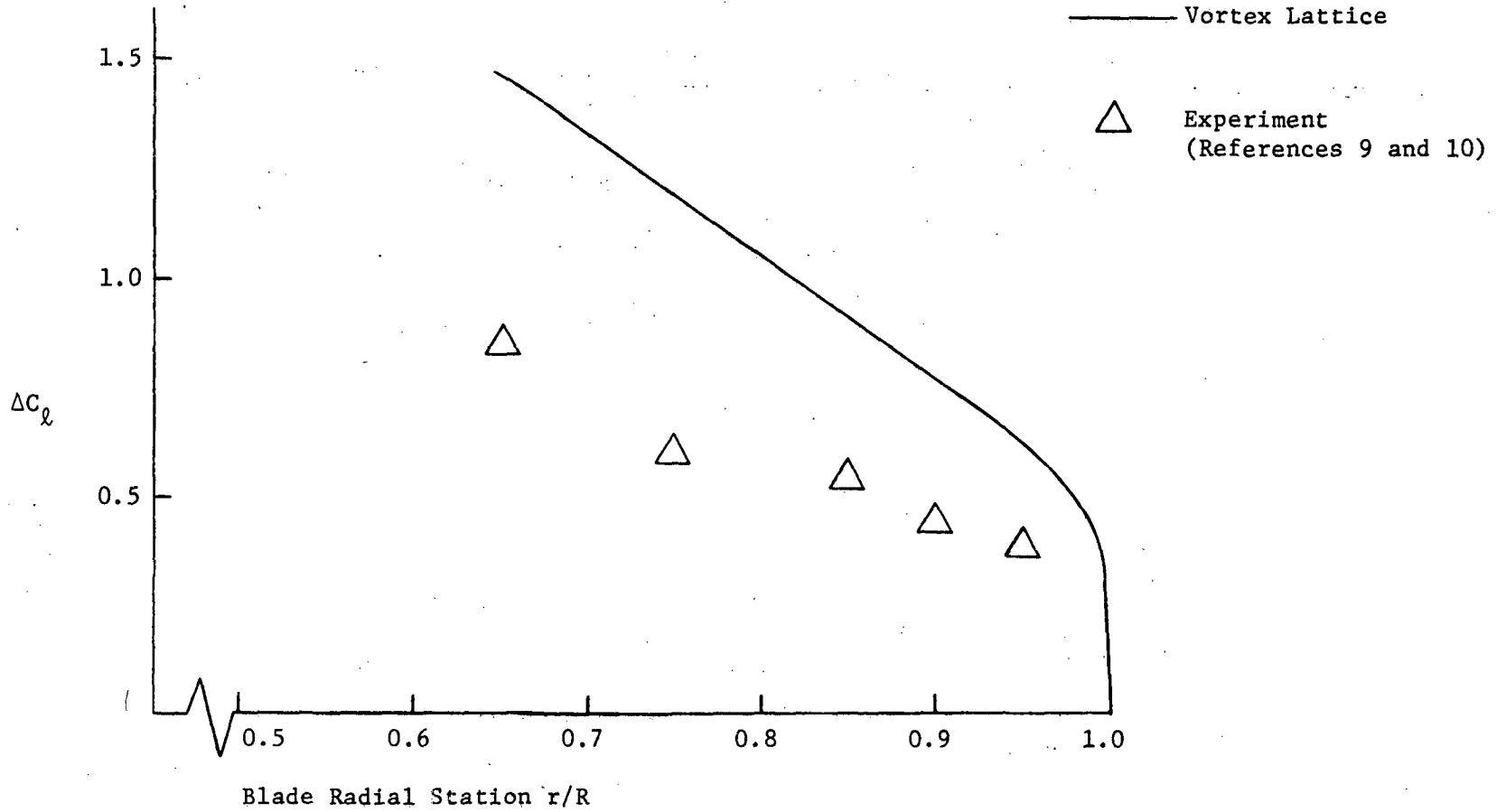
Figure 29a. Spanwise Variation of Maximum Lift Coefficient Difference (ΔC_ℓ) Due to Vortex
Interaction; Model Rotor, h/c = 0.5.

μ = 0.7, Z/R = 0.5

——————— Vortex Lattice

△   Experiment
      (References 9 and 10)
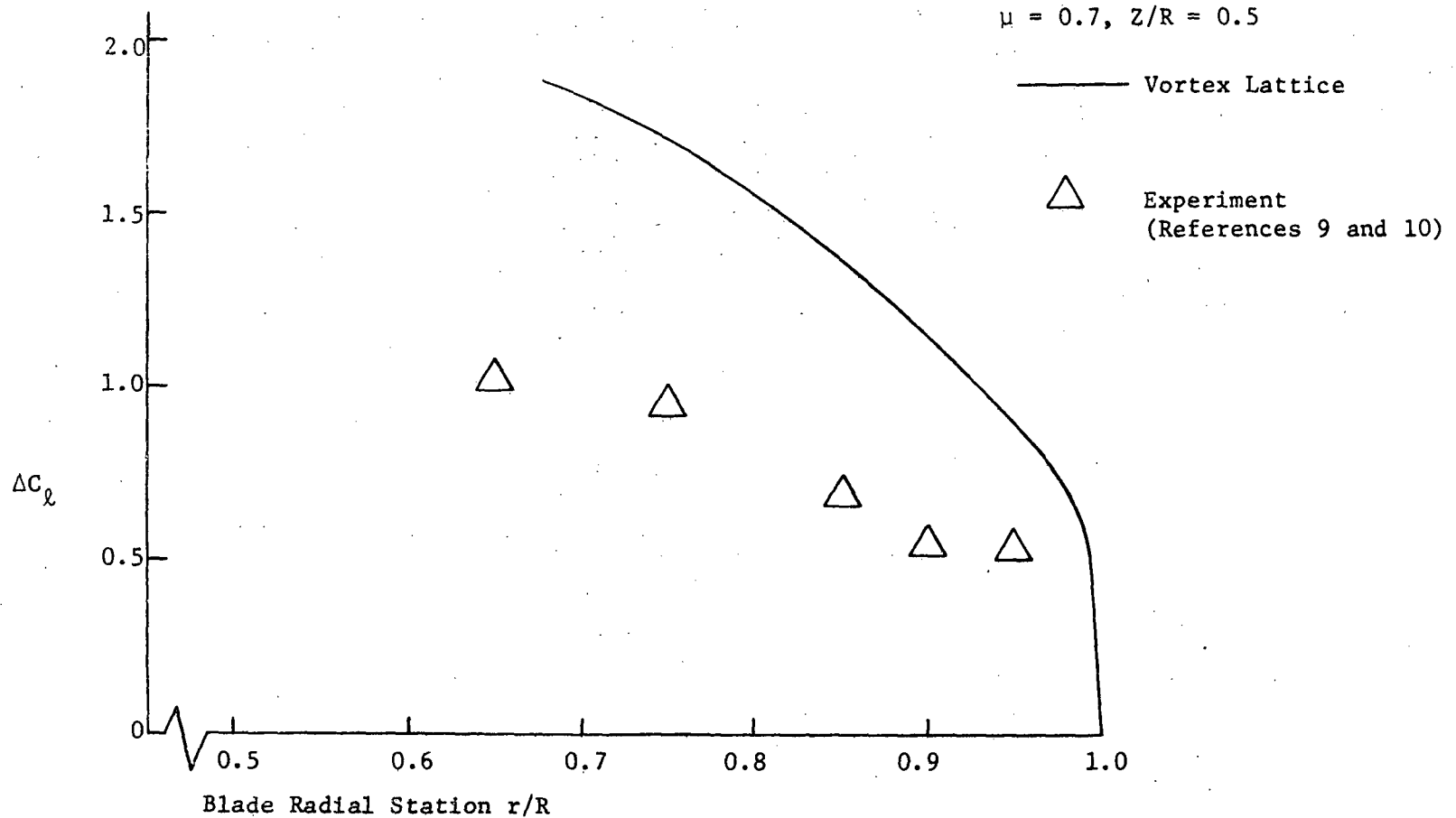
Figure 29b.   Spanwise Variation of Maximum Lift Coefficient Difference (ΔC_ℓ) Due to Vortex
Interaction; Model Rotor, h/c = 0.25.
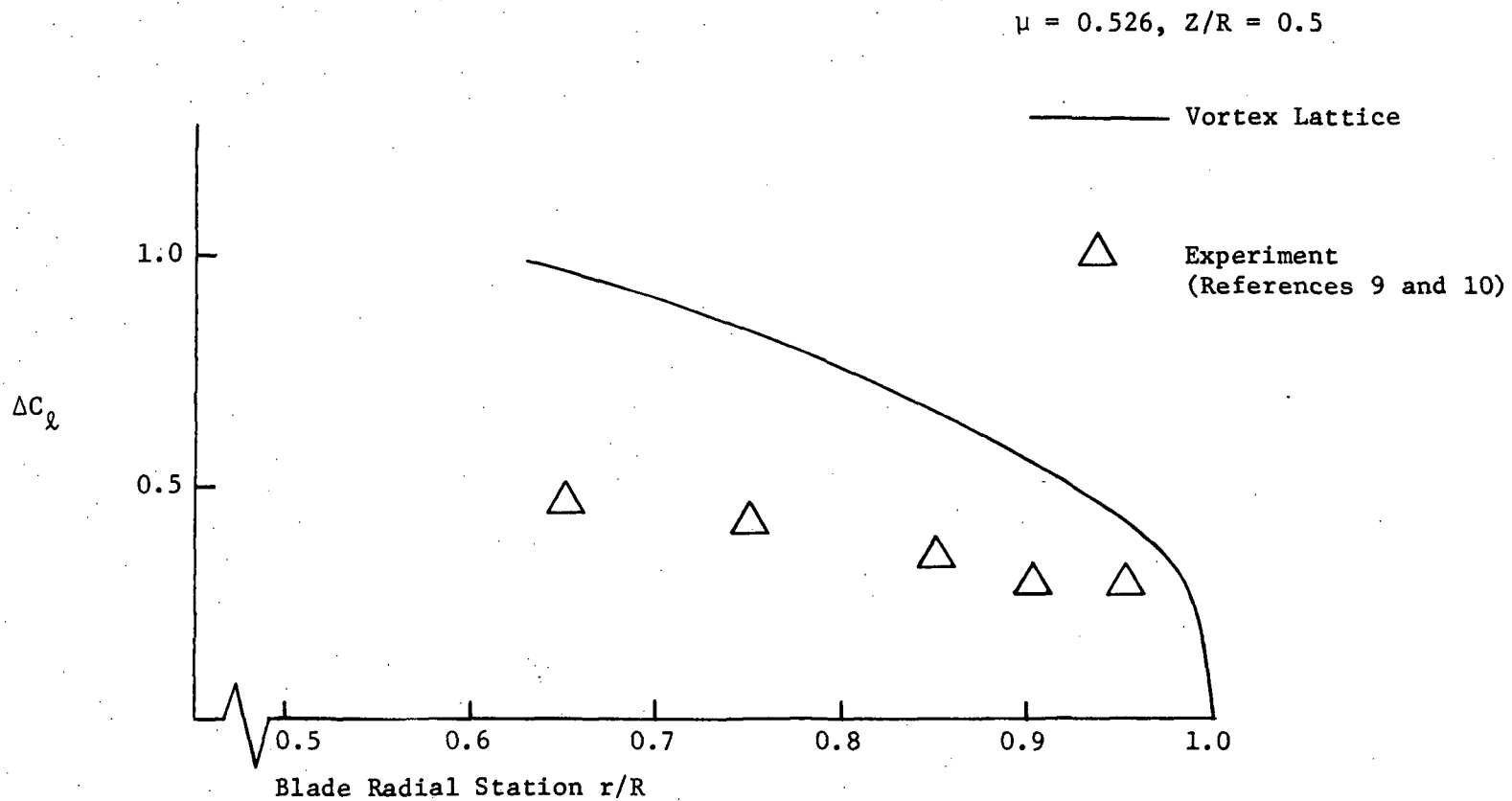
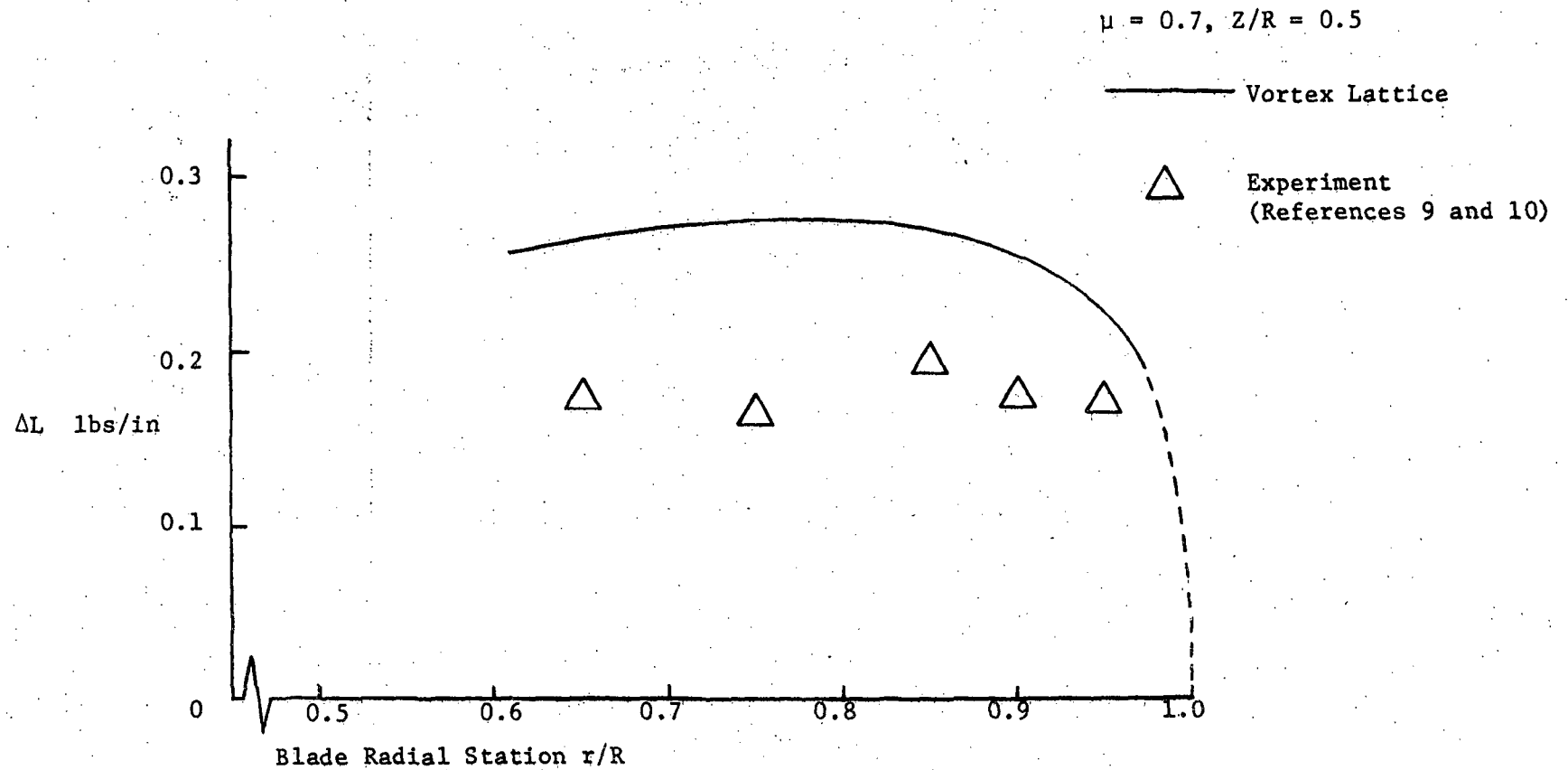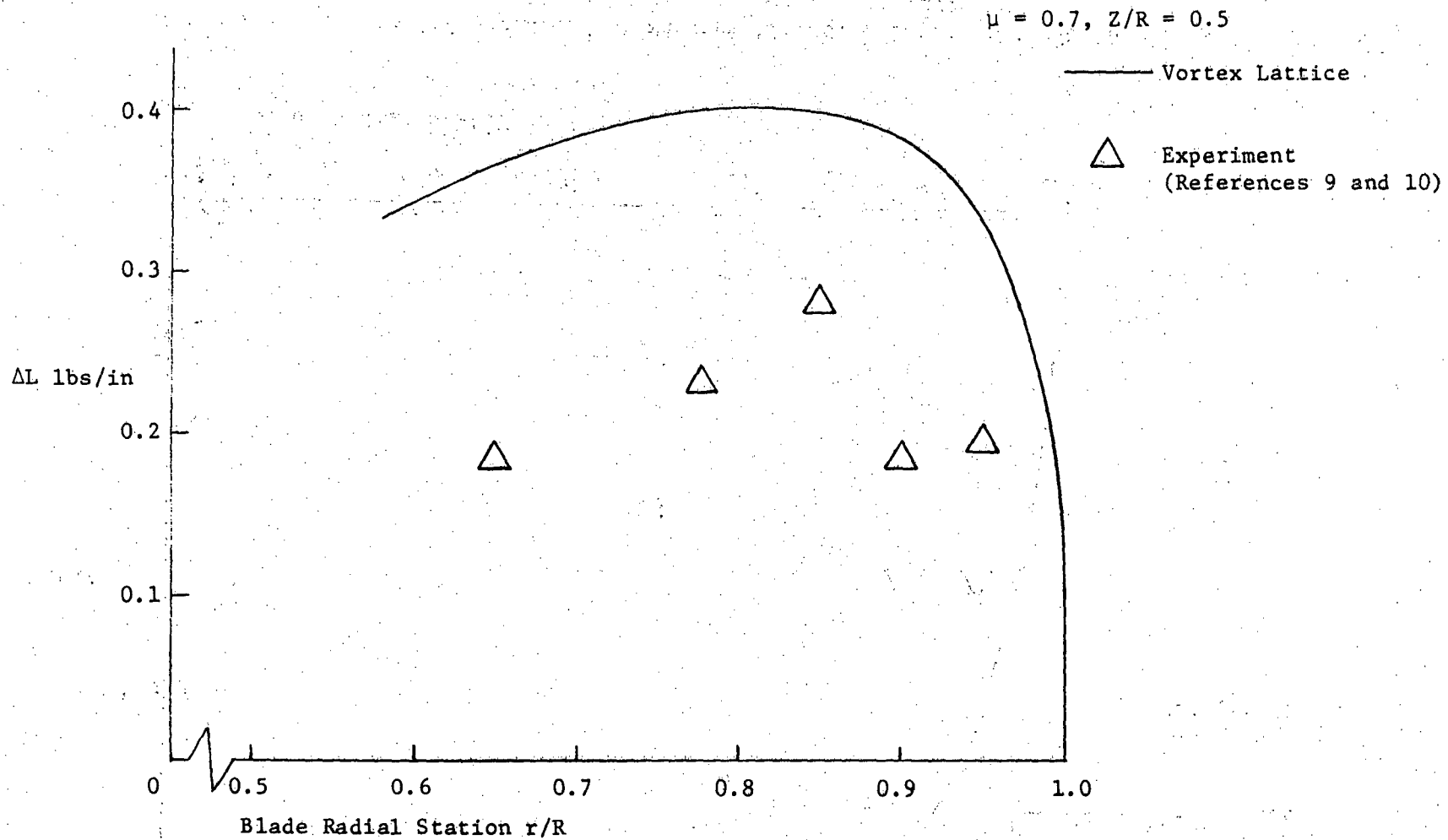Figure 30. Spanwise Variation of Maximum Lift Coefficient Difference (ΔC_ℓ) Due to Vortex Interaction; Model Rotor, $h/c = 0.5$.

in the case of maximum lift difference the predicted and the measured results differ considerably at the inboard radial positions. A typical comparison of the experimental and the predicted lift variation with time is presented in Figure 31. The general shape of the variation of lift is similar but the computations predict a higher negative peak than shown by the experimental results.

In the numerical method the effect of viscosity has been neglected and also the free vortex which is interacting with the rotor blade has been considered as a rigid, infinitely long finite core vortex. The higher predicted value of the load distribution may be due to these assumptions. Measurements of the pressure distribution on a single bladed rotor interacting with a trailing vortex from an upstream wing were also made by Baczek (27). This investigation indicated that the vortex was pushed out of the rotor plane either above or below it, resulting in lower pressure gradients than anticipated. Also Ham (28) has indicated that after a vortex intersects a blade, its strength is weakened, possibly due to counter vortices generated as a result of the loading induced by the vortex on the blade.

4.2 The Calculation of Helicopter Rotor Airloads

4.2.1 Calculation Procedure

Scheiman (12) and Scheiman and Ludi (13) have tabulated experimental data from flight tests of a four bladed H-34 helicopter. The vortex lattice method developed for the model rotor-vortex interaction problem has been extended to the full scale H-34 helicopter rotor. From the experimental data typical flight cases in which vortex induced loads near the tip of the rotor blade are indicated, are chosen for study.

65

$\mu = 0.7$, $Z/R = 0.95$, $h/c = 0.25$, $r/R = 0.95$

△ Vortex Lattice

○ Experiment (Reference 9)

L lbs/in

Time mSecs
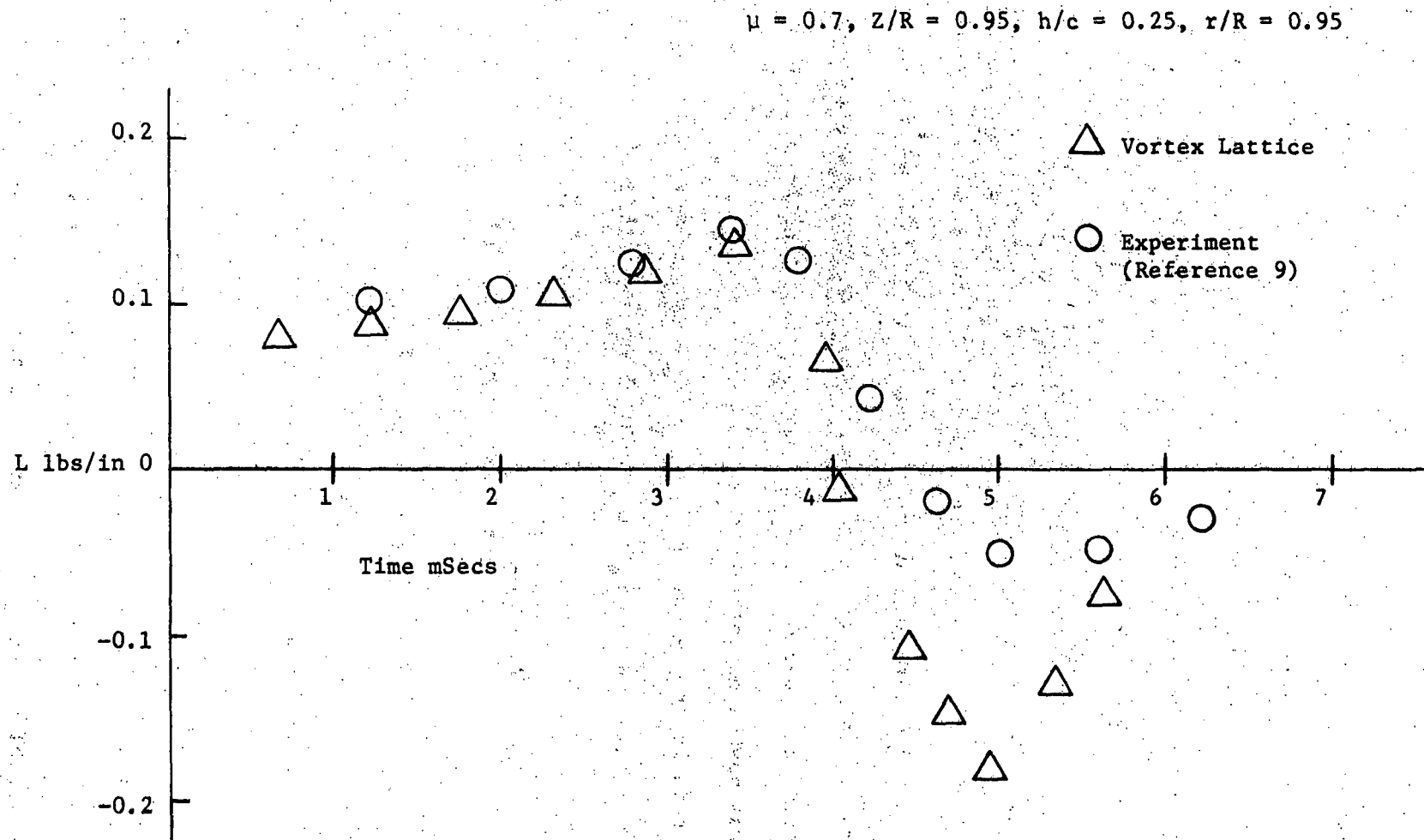
Figure 31. Typical Variation of Section Lift on the Model Rotor Blade with Time (Azimuth).

As in the model rotor configuration the wake behind the rotor blade is represented by a net of finite strength, finite length, straight line trailing and shed vortex elements. The blade coordinates used in the calculation of blade airloads are shown in Figure 21. The wake geometry is calculated starting the rotor from rest in a free stream. The reference blade on which the load distribution is calculated is located initially at a specified azimuthal ($\psi = 0^o$) and flapping and pitching position without any wake vortices. The blades are then rotated through an azimuth increment, $\Delta\psi$, and shed and trailing filaments of unknown strength, but with known positions are deposited in the wake of the reference blade. The blade is replaced by a lattice of vortices of unknown strength. The rolled up tip vortex from the preceding blade is considered to determine the effect of vortex interaction on the load distribution on the following (reference) blade. The strength of the rolled up tip vortex is made equal to the maximum value of the measured radial distribution of the bound vorticity on the blade in the azimuth position from which the element is shed. A finite core tip vortex is considered in order to avoid unrealistically high induced velocities when the vortex is near the plane of the rotor. The core size of the vortex is assumed to be one per cent of the rotor radius which is the value commonly used in the literature. The strength of this concentrated tip vortex varies azimuthally as the maximum value of the radial distribution of the blade loading varies with the azimuth. The tip vortex from the preceding blade can be placed at different heights below the disk plane. The approximate location of the tip vortex below the disk plane can be determined from the rotor advance ratio, μ, rotor thrust coefficient, C_T, and the angle of attack

67

relative to the tip path plane assuming an undistorted wake. Landgrebe and Bellinger (14) have found that the distortion of the wake increases with the decrease in advance ratio. It has also been observed that at very low advance ratios the tip vortex from the preceding blade can lie above the tip path plane over a range of azimuth angles on the advancing side of the disk. Radial contraction of the wake boundaries have been observed in experiments with the contraction of the wake increasing with decreasing advance ratios. Hence the rolled up tip vortex of the preceding can be placed radially at different locations in the wake to account for the contraction of the wake boundary. The radial contraction is zero when the tip vortex is placed at a radial location of $r/R = 1.0$. Relative orientation of the reference blade and tip vortex from the preceding blade on the advancing side of the disk is shown in Figure 32. The root vortex of the preceding blade which is in a sense opposite to that of the tip vortex is usually very weak and hence has been neglected. Piziali (22) has found that adding a concentrated root vortex has a relatively small effect on the rotor blade loading. This rather crude approximation for the tip vortex is hoped to be reasonably good for the areas in which it has a large effect on the induced velocity in the plane of the rotor.

The boundary condition to be satisfied at the control points on the reference blade requires that the sum of the velocities normal to the chord be zero. The total vertical downward velocity, U_p, relative to the blade section is

$$U_p = V \cos \alpha_1 \cos \psi \sin \beta + w + r d\beta/dt - V \sin \alpha_1 \cos \beta$$
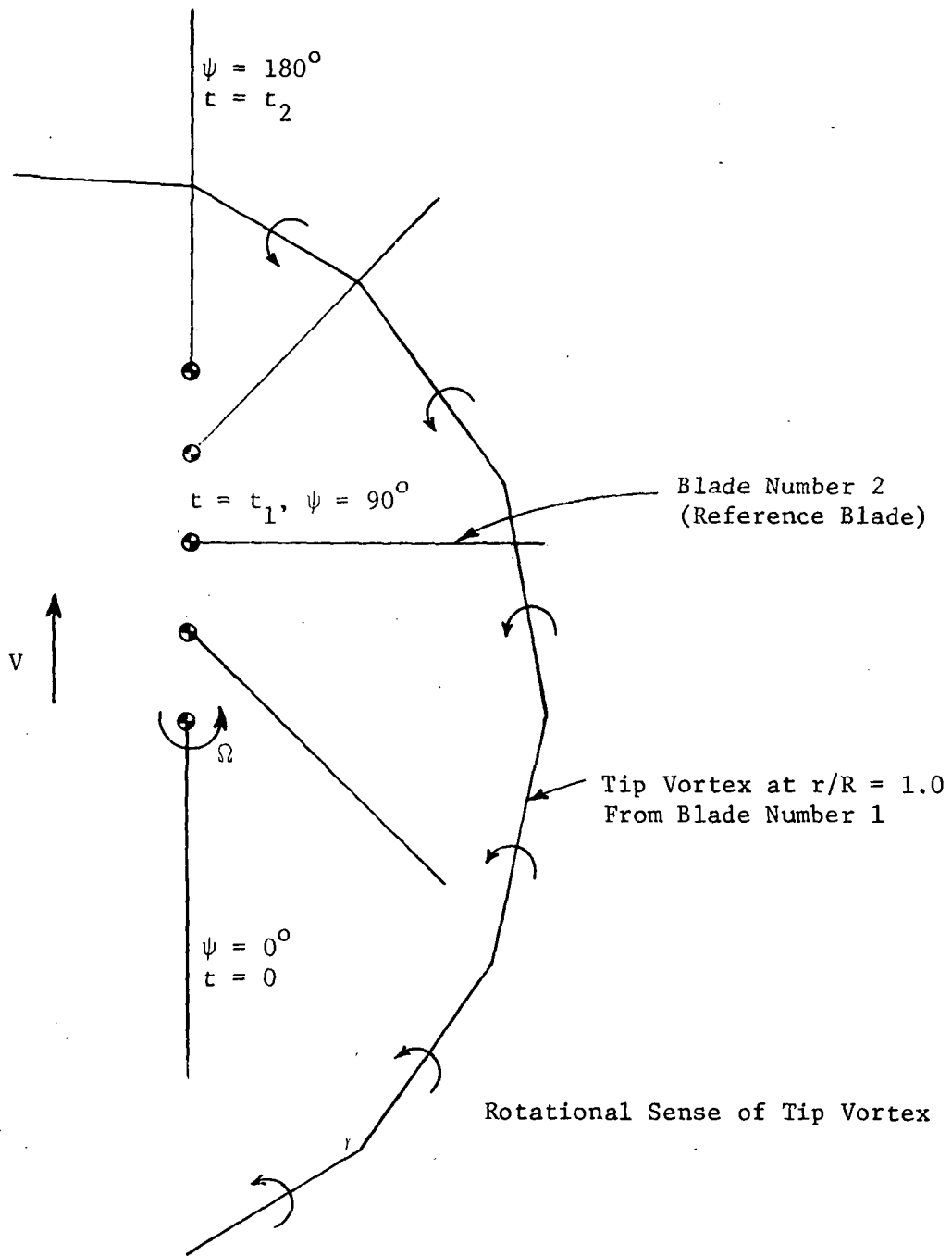
Figure 32. Relative Orientation of Reference Blade and Tip
Vortex on the Advancing Side of Disk.

and the component, U_T, in the disk plane normal to the blade radius is

$$U_T = \Omega r + V \cos \alpha_1 \sin \psi$$

where

α_1 = rotor angle of attack

β = flapping angle

V = free stream velocity

ψ = azimuth angle

w = downwash velocity

r = radial coordinate

Ω = rotational velocity of the blade

Using small angle approximations, the expressions for the velocities can be written as

$$U_p = V\beta \cos \psi + w + r d\beta/dt - V\alpha_1$$

$$U_T = \Omega r + V \sin \psi$$

If θ is the pitch angle relative to the disk plane, the angle of attack of the section from Figure 33 is,

$$\alpha(r,\psi) = \theta - \frac{V \beta \cos \psi + w + r d\beta/dt - V\alpha_1}{\Omega r + V \sin \psi}$$

The wake induced velocity, w, is made up of velocities due to known circulations in the wake and due to the tip vortex of the preceding blade.

dL

ϕ

θ

Disk Plane

$V\beta\cos\psi + w$

$+r\dot{\beta} - V\alpha_1$

ϕ

$\Omega r + V \sin \psi$

$$\alpha(r,\psi) = \theta - \phi$$

θ = Pitch Angle Relative to the Disk Plane.
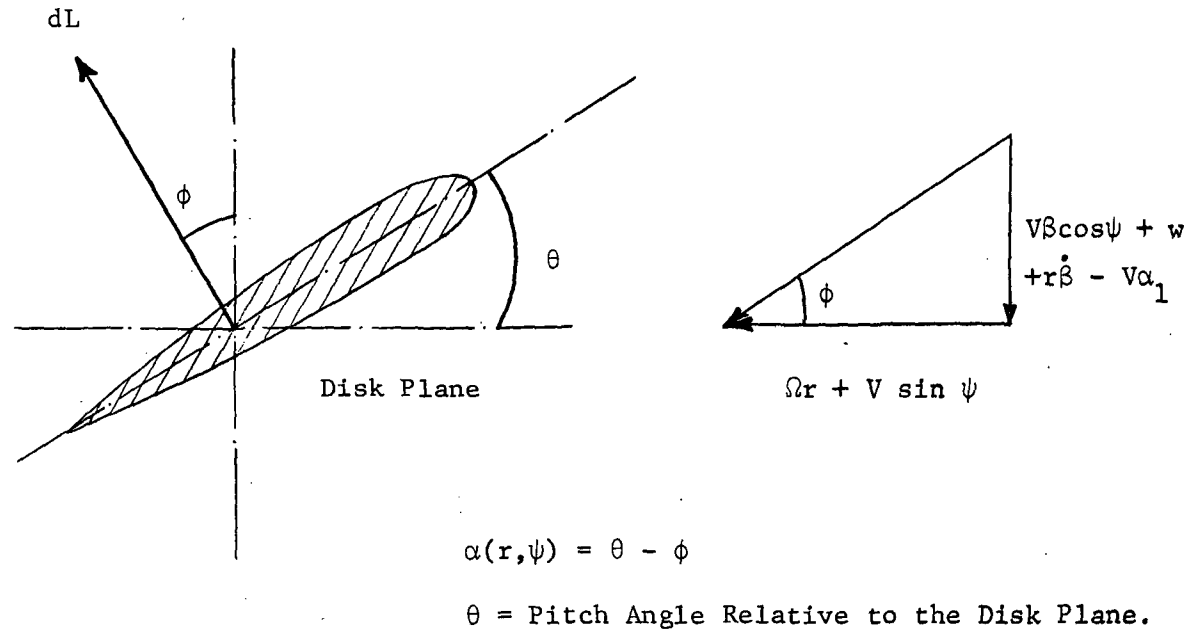
Figure 33.   Velocity Components on a Blade in Forward Flight.

The blade pitch angle for a linearly twisted blade is taken as

$$\theta = \theta_0 + \theta_T x + \theta_1 \cos \psi + \theta_2 \sin \psi$$

where

θ_0 = collective pitch

θ_T = total twist

θ_1 = lateral cyclic

θ_2 = longitudinal cyclic

$x = r/R$ = radial coordinate

Only first harmonic flapping is considered.

$$\beta = \beta_0 + \beta_1 \cos \psi + \beta_2 \sin \psi$$

where β_0 = coning angle

β_1 = longitudinal flapping

β_2 = lateral flapping

The radial component of the velocity is neglected as it does not significantly effect the lift. The blade is assumed infinitely rigid in all directions, i.e. the effects of torsional deflection and blade-bending deflections on the velocity and the angle of attack distributions are neglected.

Satisfaction of the boundary condition at all the control points results in a set of simultaneous equations for the unknown vortex strengths on the blade. Solving these equations gives the strengths of the vortices that are shed immediately behind the blade. The reference blade is then advanced through an azimuth increment, $\Delta\psi$, and each vortex end point which is not attached to the blade is allowed

72

to translate with the velocity $(V \sin \psi + \Omega r)$, i.e. a flat, rigid wake is assumed. The entire computational process for the new position of the reference blade is then repeated. In this manner arrays of discrete shed and trailing vortices are generated immediately behind the reference blade with strengths corresponding to the blade loads.

Considerable computational simplifications are achieved through the assumption of a flat rigid wake. At low rotor thrusts or high forward velocities, the downwash becomes small in comparison to the free stream velocity and hence this assumption is a good approximation at large advance ratios. In a recent paper, Ormiston (29) has presented rotor wake induced velocities of helicopter rotors in forward flight assuming a flat planar wake. The results indicated that a simple, flat planar wake is a valid configuration for the wake vorticity down to advance ratios of around 0.15 for nominal thrust coefficients.

Once the circulations at each section of the blade are known from the solution of the simultaneous equations, the section lift can be determined from

$$\ell_j(y,t) = \rho U \underset{i}{\Sigma} \Gamma_{ij}(x,y,t) + \rho \int_0^c [\frac{\partial}{\partial t} \int_0^x \Gamma_{ij}(\xi,y,t) \, d\xi] \, dx$$

where $U = V \sin \psi + \Omega r_j$

Compressibility effects are included in the calculations through the use of the Prandtl-Glauret correction factor based on the local Mach number of the flow normal to the span of the blade.

$$\therefore \ell_{comp} = \frac{1}{\sqrt{1 - M^2}} \ell_{incomp}$$

where M = Mach number

ℓ = lift at any section of the blade

All of the input information for the computations, such as the flapping angle, the blade pitch angle, the shaft tilt angle and blade twist are taken from the report by Scheiman (12). The strength of the tip vortex of the preceding blade was calculated from the tabulated measured load distributions. The time interval Δt is chosen to correspond to the finite change $\Delta\psi$ in the azimuth position of the blades.

$$\Delta t = \Delta\psi/\Omega$$

where Ω is the rotor angular speed.

The accuracy of the predicted load distribution depends on the number of vortices and the azimuth increment. An azimuth increment of about 15 degrees was found to be sufficiently small for the prediction of vortex induced velocities. Ten spanwise and three chordwise vortices were considered on the blade.

For the computations of load distribution, both the IBM 360/67 and the IBM 370/165 computers of the Pennsylvania State University were used. The present calculations required about 200 secs on the IBM 360/67 computer for an azimuth travel of 180 degrees with an azimuth increment of 15 degrees. The same calculations required only 50 secs on the IBM 370/165 computer.

4.2.2 Results and Discussion

This section presents and discusses the results of the computations and compares predicted blade loads with the measured values. The rotor blade dimensions and operating conditions are given in Table 2. The azimuth increment ($\Delta\psi$) in the calculations was 15 degrees. Ten spanwise and three chordwise vortices were considered on the rotor blade.

74

Table 2

Rotor Dimensions and Operating Conditions

Number of blades	4
Rotor blade radius	28 ft
All metal, constant chord rotor blade	
Twist	-8 deg
Airfoil section	Modified NACA 0012
Blade chord	1.367 ft.
Rotor solidity	0.0622
Normal rotor tip speed	623 fps
Normal rotor angular velocity	22.2 rad/sec
Test disk loading	4.79 lbs/ft^2
Forward rotor shaft tilt	3.0 deg

Calculations were done both with equally spaced and unequally spaced spanwise vortices. The number of vortices on the blade and the azimuth increment in the calculations were chosen taking into account computing economy.

Comparisons of the results of the vortex lattice method and the experimental data, for radial stations r/R = 0.95, 0.85, 0.55 and 0.25 are presented in Figures 34 through 37 for an advance ratio of 0.2. Scheiman (12) and Scheiman and Ludi (13) have tabulated flight test data of a H-34 helicopter. These flight test values are the experimental data used for the comparisons. In-flight measured flapping angles were used in the calculation of airloads. Blade pitch angles and the height of the preceding blade tip vortex below the reference blade were adjusted to give agreement of the loads at the r/R = 0.95 station. For the advance ratio of 0.2 the tip vortex was placed at a height of three-quarter's of a chord below the plane of the rotor. This is approximately the undistorted wake location near the azimuth location (ψ) of 90 degrees where the vortex interaction effect is large. Landgrebe and Bellinger (14) have indicated that the experimental axial wake position and undistorted wake position do not differ much on the advancing side of a rotor at an advance ratio of 0.2.

As can be seen in these figures the large fluctuations in the measured airloads near the tip of the rotor blade on the advancing side are predicted closely by the present lifting surface method. For the advance ratio of 0.2 calculations were repeated for two different radial locations (r/R = 1.0 and r/R = 0.90) of the tip vortex to determine the effect of radial contraction of the tip vortex (observed experimentally) on the airloads. The results of the computations with

76

Figure 34. Comparison of Computed and Measured Section Lift; H-34 Helicopter Rotor, $\mu = 0.2$, $r/R = 0.95$.

Figure 35. Comparison of Computed and Measured Section Lift; H-34 Helicopter Rotor, $\mu = 0.2$, $r/R = 0.85$.
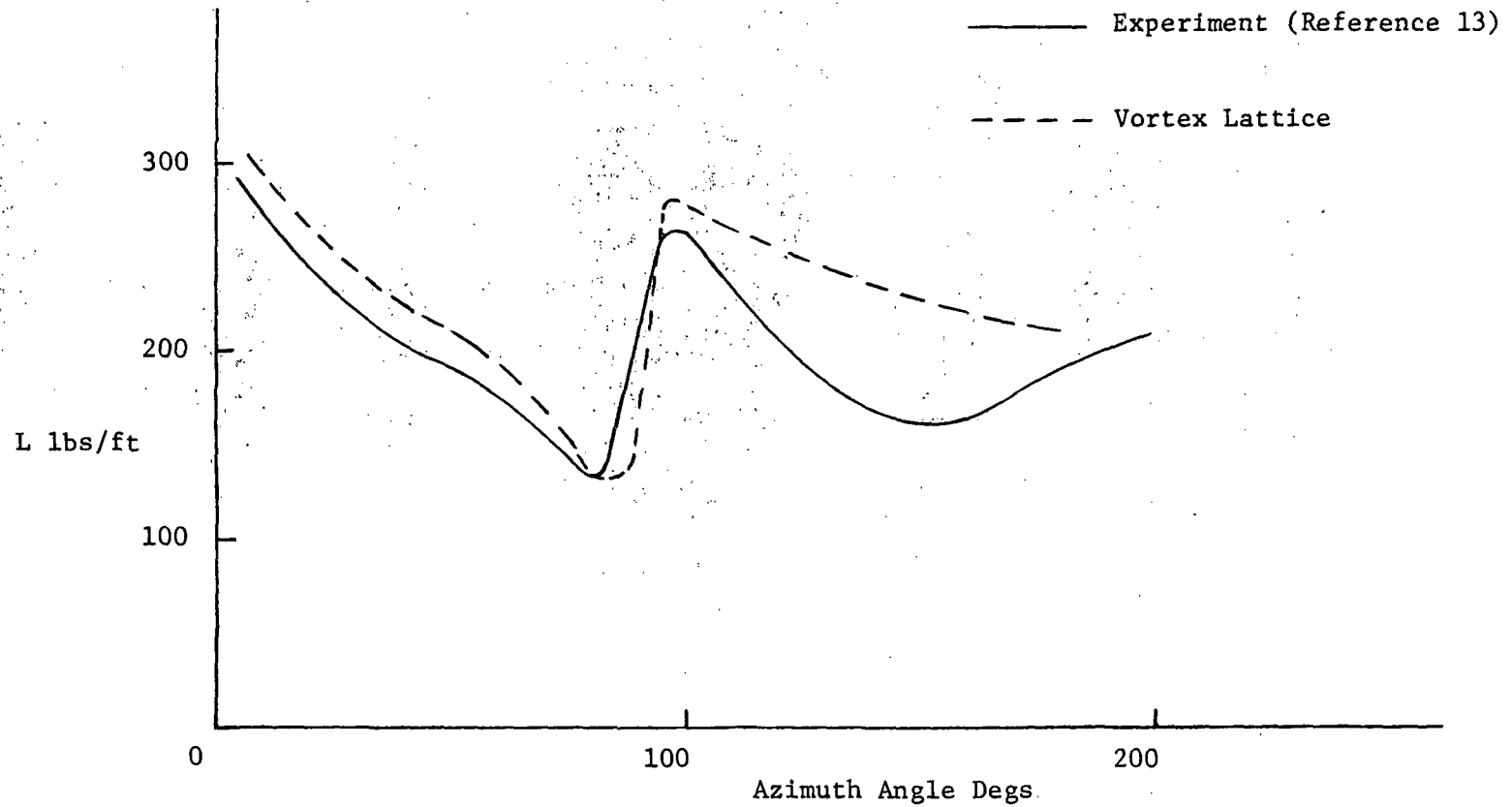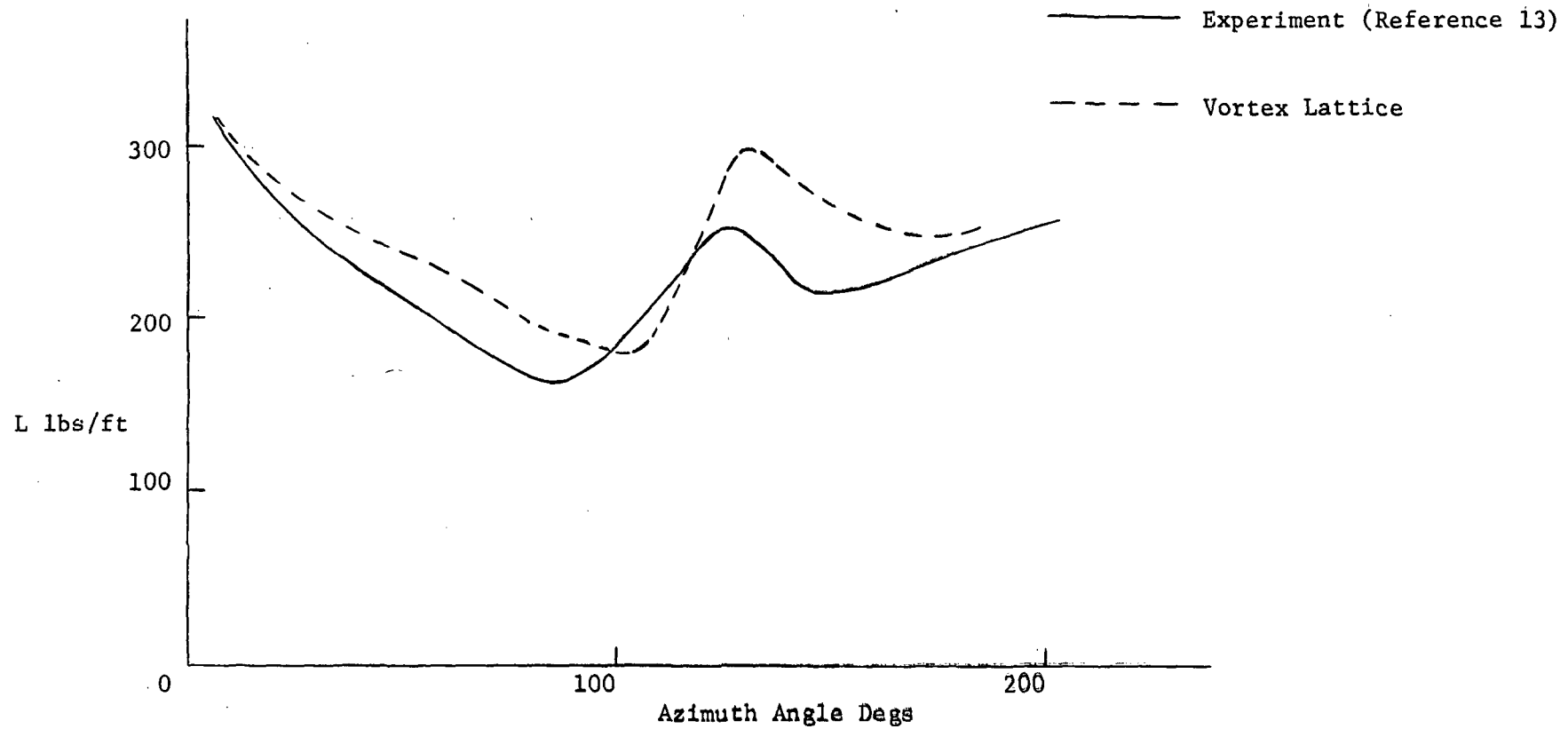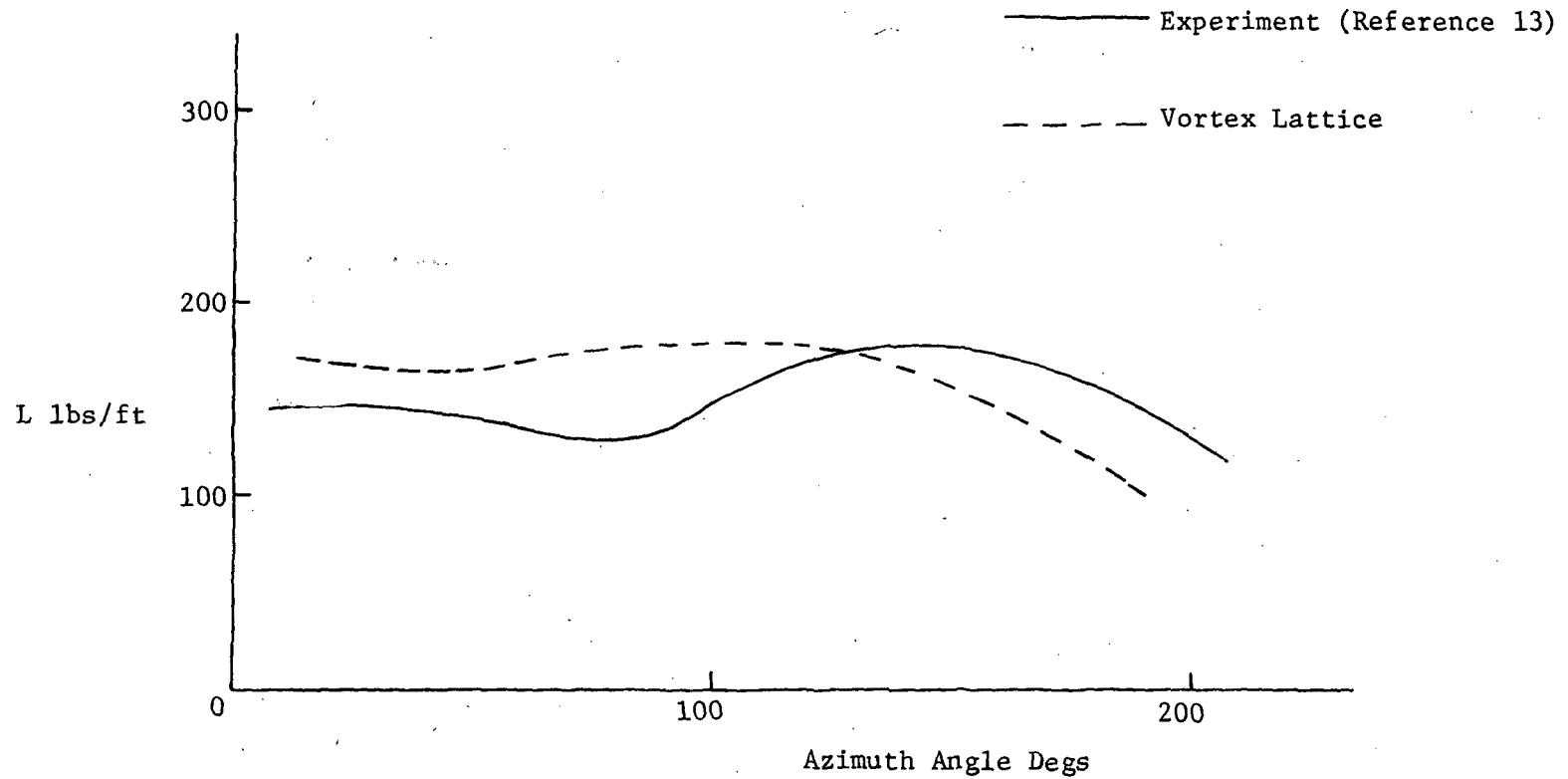
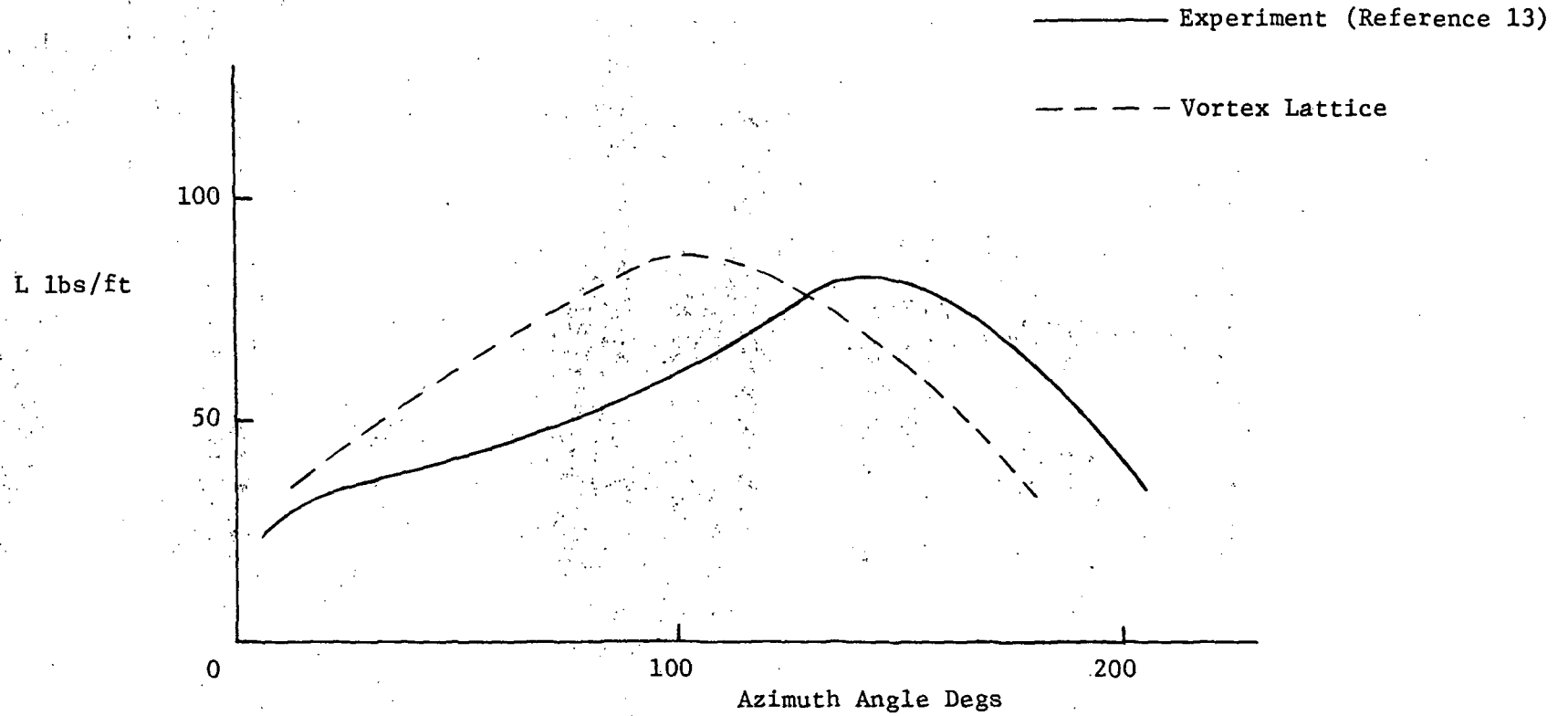Figure 36. Comparison of Computed and Measured Section Lift; H-34 Helicopter Rotor, $\mu = 0.2$, $r/R = 0.55$.

Figure 37. Comparison of Computed and Measured Section Lift; H-34 Helicopter Rotor, μ = 0.2, r/R = 0.25.

different radial locations of the tip vortex are presented in Figures 38
and 39 for radial stations r/R = 0.95 and r/R = 0.85 respectively. As
can be seen in these figures there is a noticeable difference in the
airloading due to the change in the orientation of blade passage over
the two radial locations of the tip vortex. Hence radial contraction of
the tip vortex is a significant parameter in the prediction of vortex
induced airloads especially at low advance ratios since the vortex
remains closer to the rotor. The effect of the vertical location of
the tip vortex on the blade loads is shown in Figure 40. As expected
the vortex induced load increases as the vortex gets closer to the blade
since the induced velocity on the blade increases with the decrease in
distance between the blade and the vortex. The radial variation of load
distribution on a rotor blade at an azimuth location (ψ) of 90 degrees
for unequal and equal spacing of spanwise vortices in the vortex lattice
method is shown in Figure 41. As expected the radial load distribution
is not very sensitive to the spacing of vortices except near the tip of
the blade where the vortex induced load is predominant.

A comparison of the calculated and the experimental section lift
with azimuth for an advance ratio of 0.1 is presented in Figures 42
through 45 for radial stations of r/R = 0.95, 0.85, 0.55 and 0.25.
The experimental data is from Scheiman's (12) report. In the
calculations the tip vortex was placed radially at r/R = 1.0 and
vertically 0.6 chord below the plane of the rotor. The vortex
interaction effect has been predicted reasonably well. From the wake
pattern studies in a water tunnel Landgrebe and Bellinger (14) have
indicated that large axial and radial distortions of the wake occur at
low advance ratio of approximately 0.1. As the local blade loading is
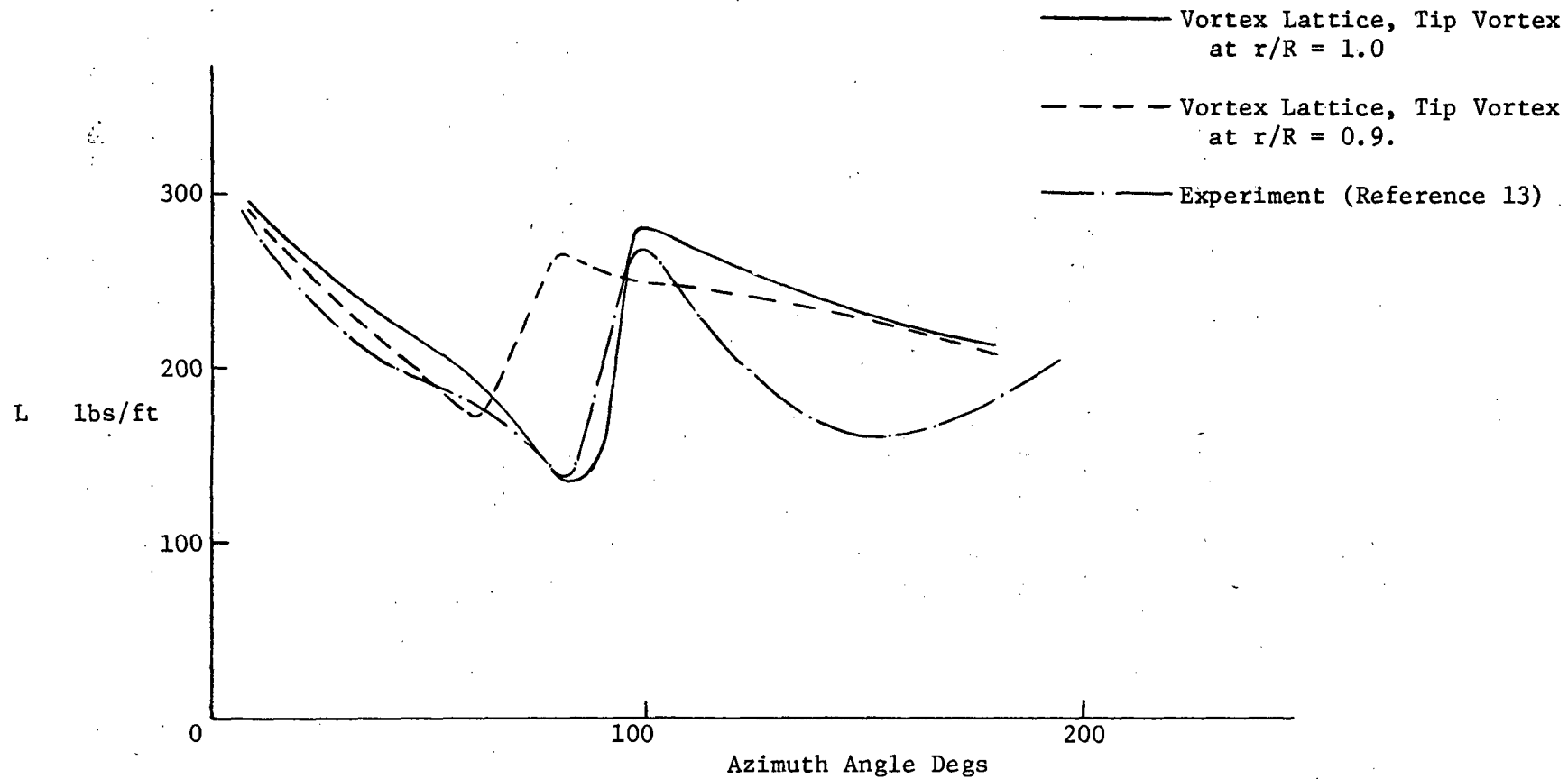
Figure 38. Comparison of Section Lift for Two Positions of Tip Vortex in the Wake; H-34 Helicopter Rotor, $\mu = 0.2$, $r/R = 0.95$.
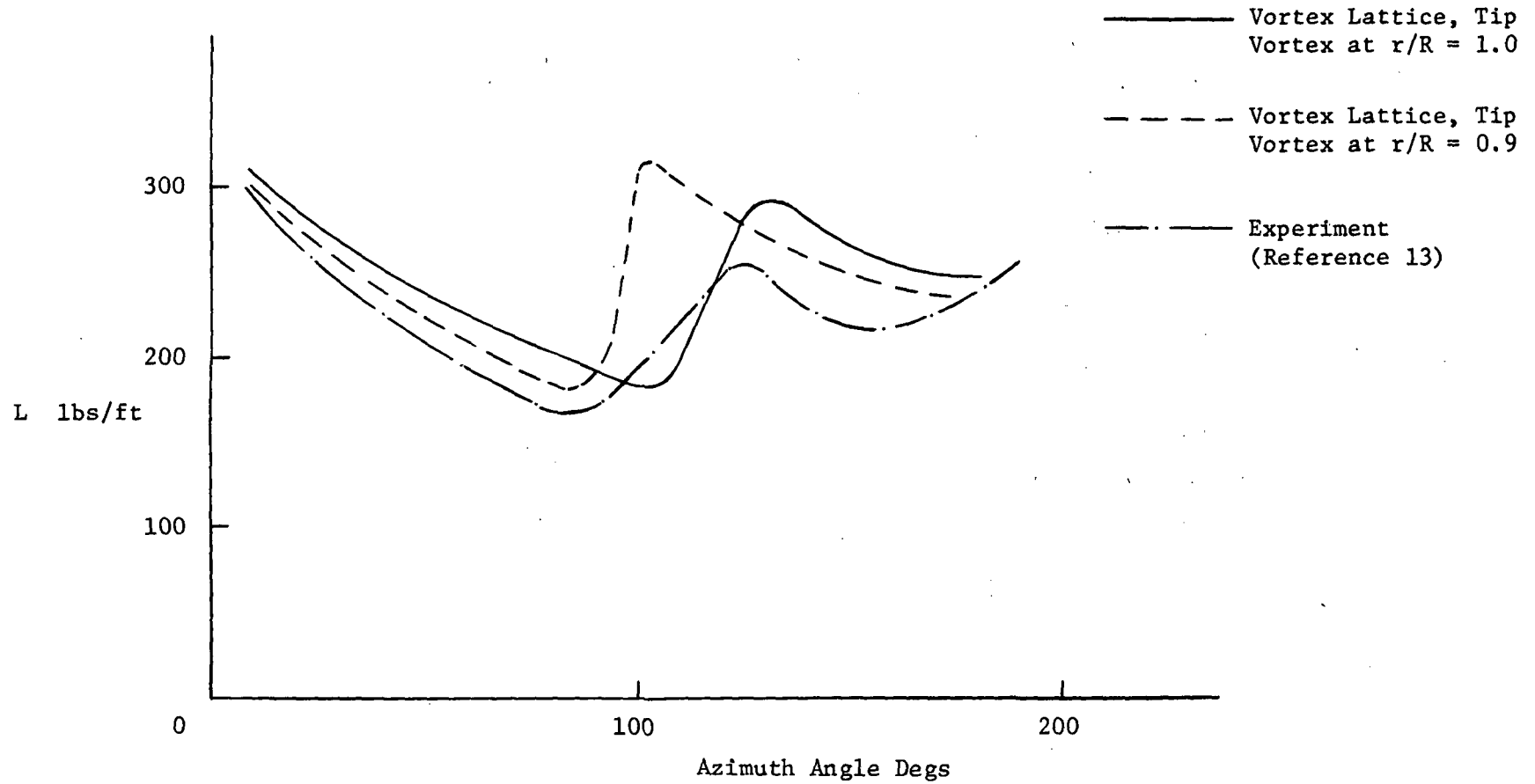
Figure 39. Comparison of Section Lift for Two Positions of Tip Vortex in the Wake; H-34 Helicopter Rotor, $\mu = 0.2$, $r/R = 0.85$.

$\mu = 0.2, \; r/R = 0.95$

——————— Z = 0.75C

———·——— Z = 0.50C

————— Z = 0.25C

L lbs/ft

300

200

100

0   100   200

Azimuth Angle Degs
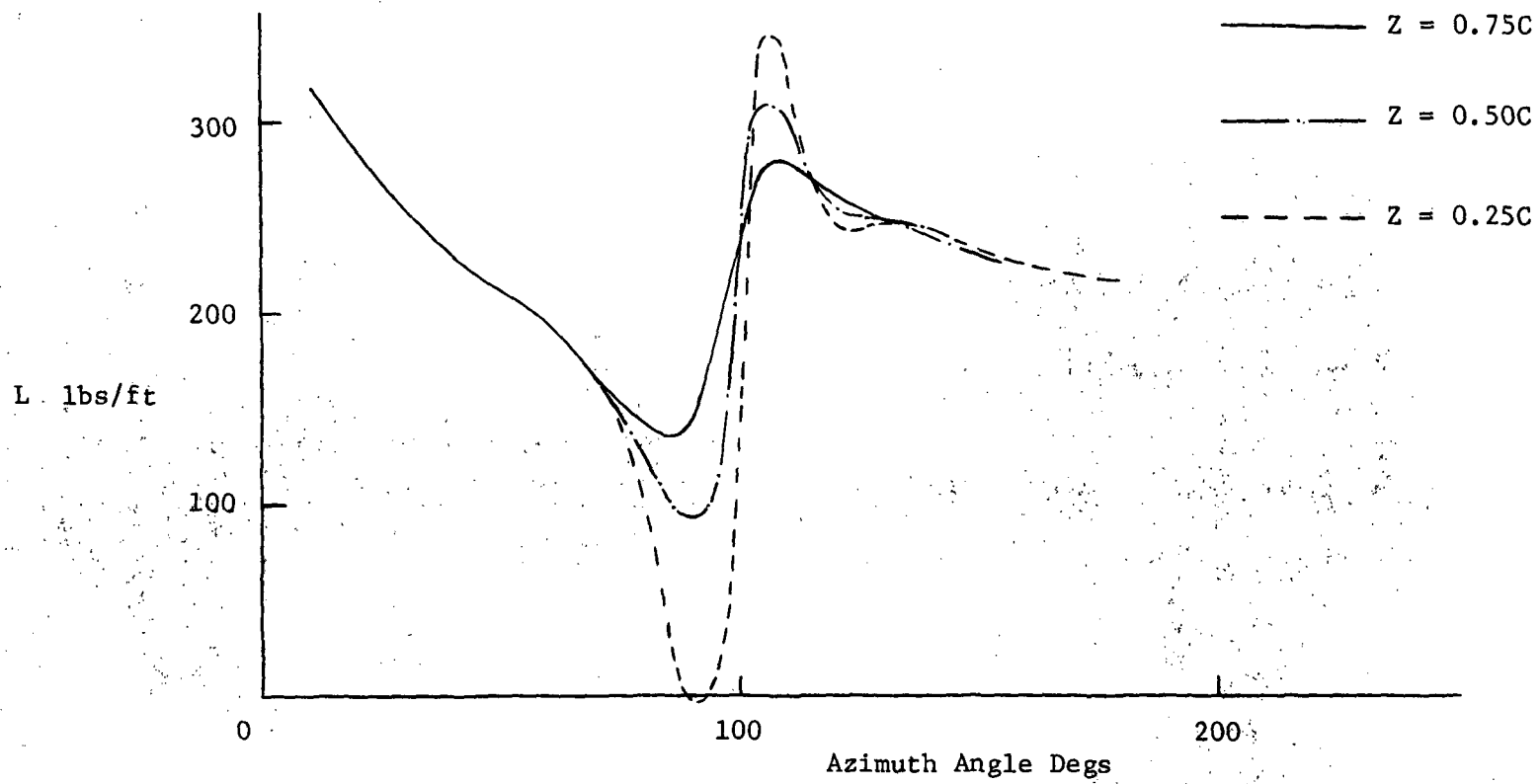
Figure 40. Effect of Vertical Location (Z) of Tip Vortex on the Computed Section Lift;
H-34 Helicopter Rotor.
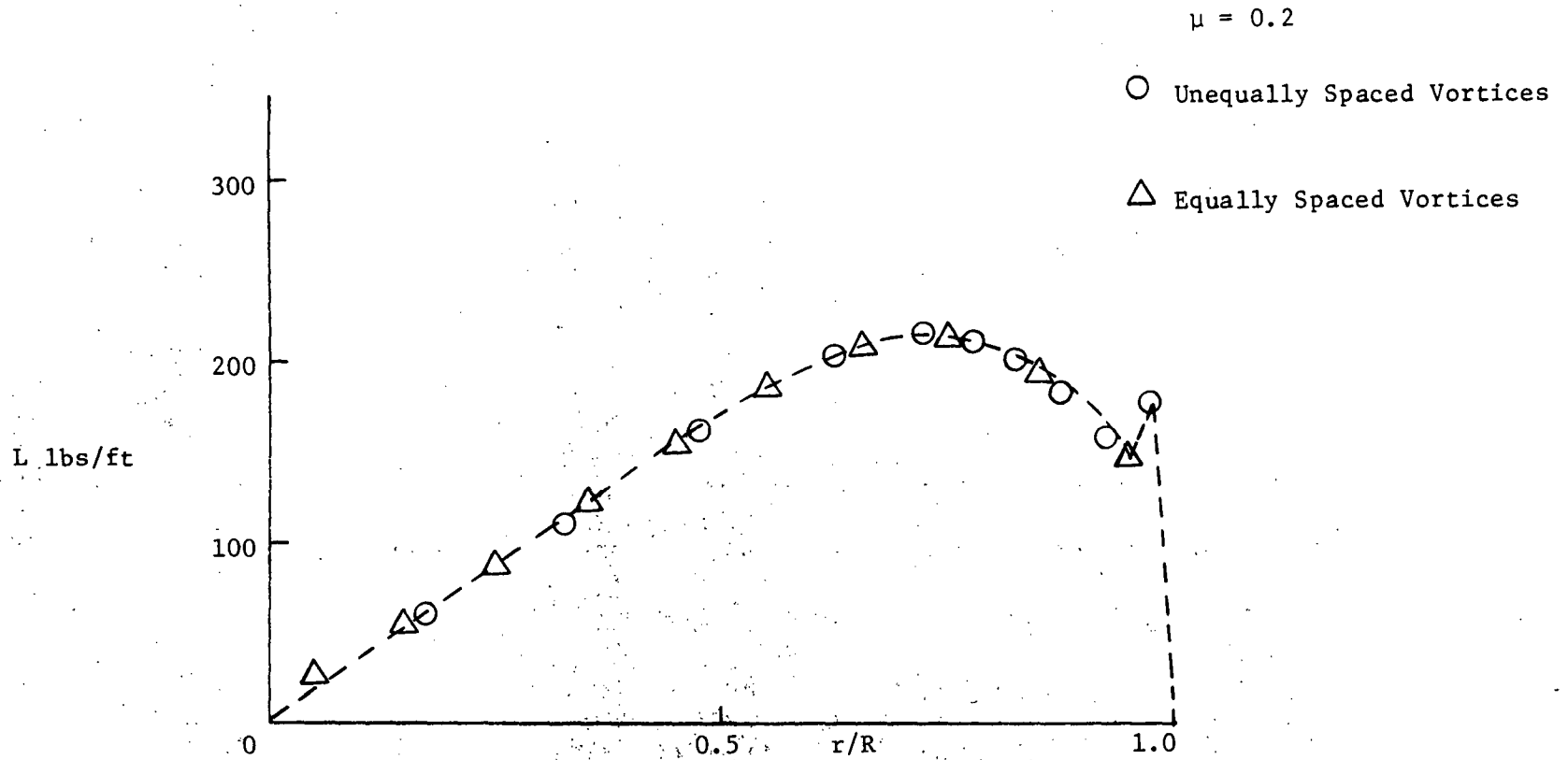
Figure 41. Computed Radial Lift Distribution at the 90 Degrees Azimuth Position; H-34 Helicopter Rotor.
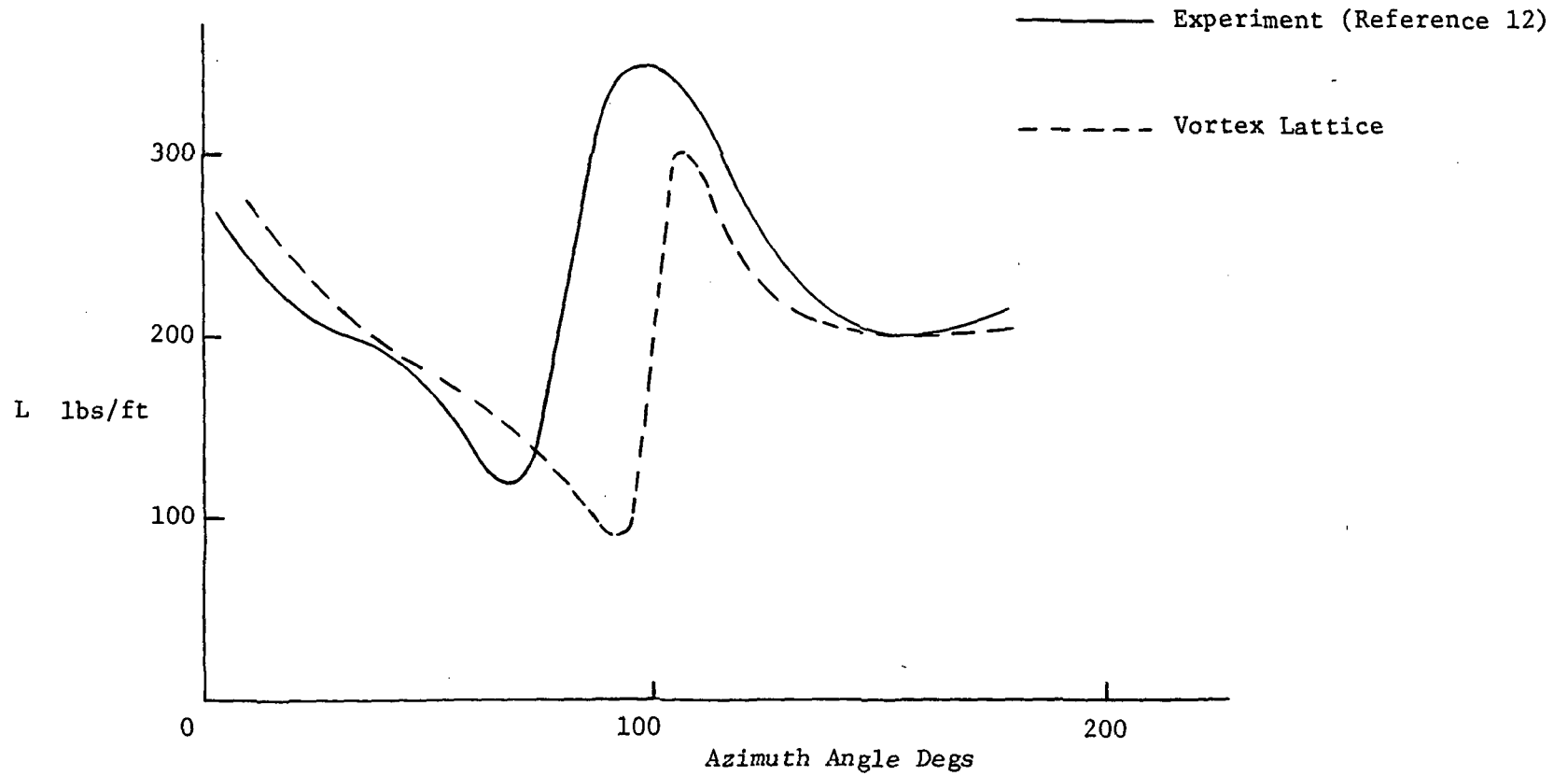
Figure 42. Comparison of Computed and Measured Section Lift; H-34 Helicopter Rotor, $\mu = 0.13$, $r/R = 0.95$.
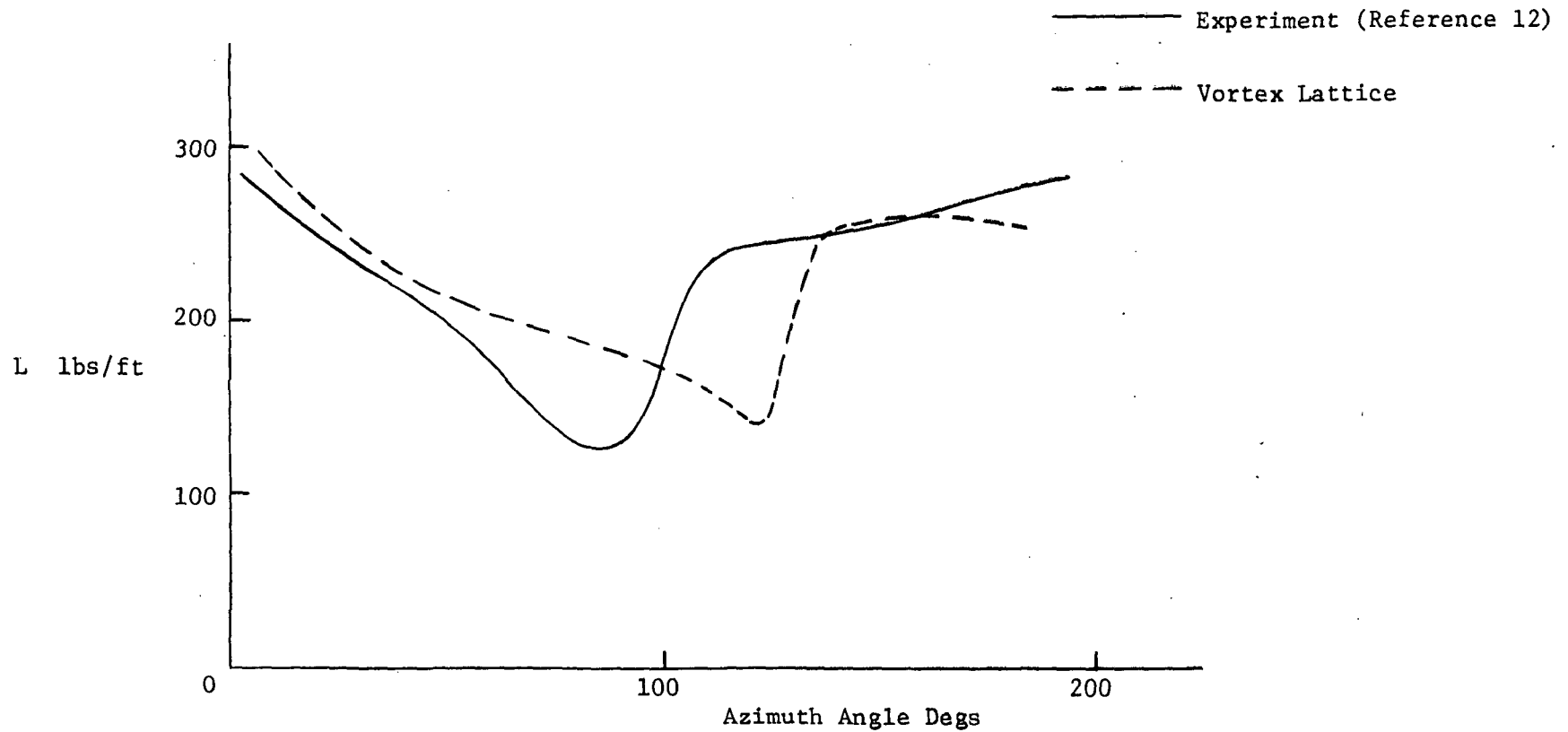
Figure 43. Comparison of Computed and Measured Section Lift; H-34 Helicopter Rotor, μ = 0.13, r/R = 0.85.
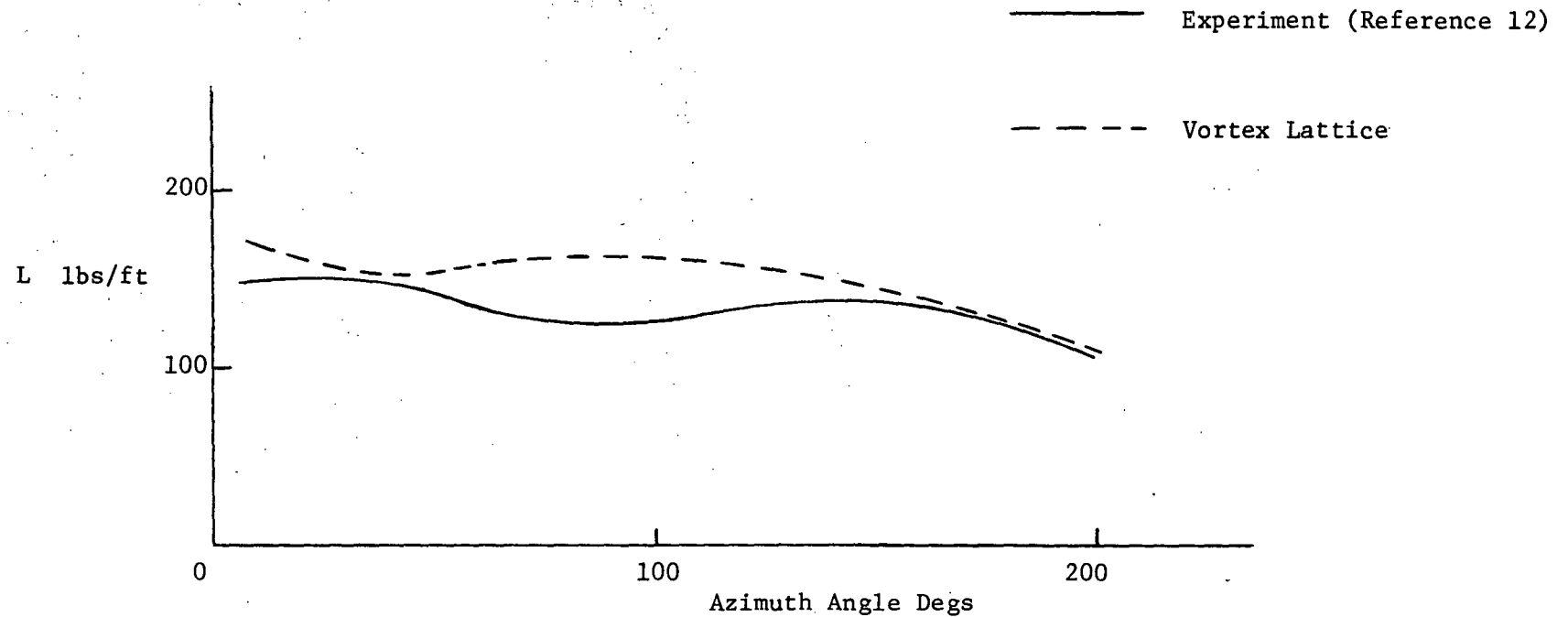
Figure 44. Comparison of Computed and Measured Section Lift; H-34 Helicopter Rotor, $\mu = 0.13$, $r/R = 0.55$.
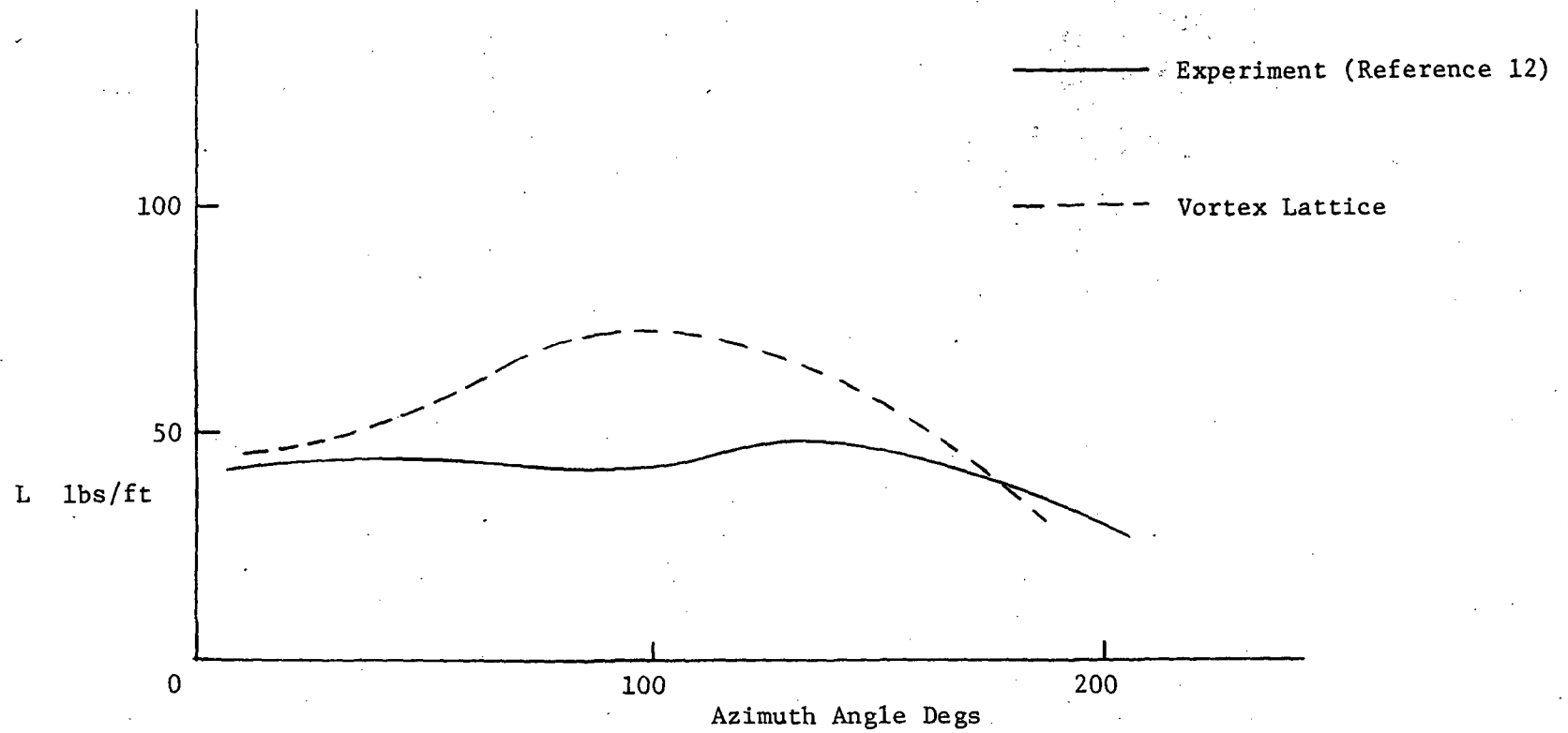
Figure 45. Comparison of Computed and Measured Section Lift; H-34 Helicopter Rotor, $\mu = 0.13$, $r/R = 0.25$.

very sensitive to wake distortions, wake distortion effects should be included in the calculations for a better correlation of the calculated and experimental section lifts at this low advance ratio.

The section lift variation with azimuth angle at radial stations r/R = 0.95, 0.85, and 0.75 is shown in Figure 46. The results are from the flight test data of a H-34 helicopter operating at an advance ratio of 0.11. This figure indicates the decrease in effectiveness of the tip vortex for inducing loads at the inboard sections. This feature has been found in all cases of the present study, cases which were chosen because they show large vortex-induced loads near the tip of the blade. Figure 47 shows the variation of section lift with azimuth angle at the radial station r/R = 0.95 for advance ratios of approximately 0.1, 0.2, and 0.3. The results are from the flight test data of a H-34 helicopter. As can be seen in this figure the effect of tip vortex on the blade loading reduces as the advance ratio increases. At low advance ratios the extent to which the wake is transported away is limited and results in blade-vortex intersections close to the rotor.

The wake behind a helicopter rotor remains in close proximity to the rotor for a long time because of the rotation of the rotor whereas a wing moves continually away from its wake. Hence, it might be expected that wake distortions which could be neglected for a fixed wing would be more important in the case of a rotor. Although lifting surface theories allow accurate calculation of airloads on a rotor blade, its use requires an accurate knowledge of the relative position of the vortex and the blade. Hence a very high degree of accuracy is required to correctly predict the close passages of the tip vortex and the blade, as the downwash is very sensitive to the tip vortex location. Johnson
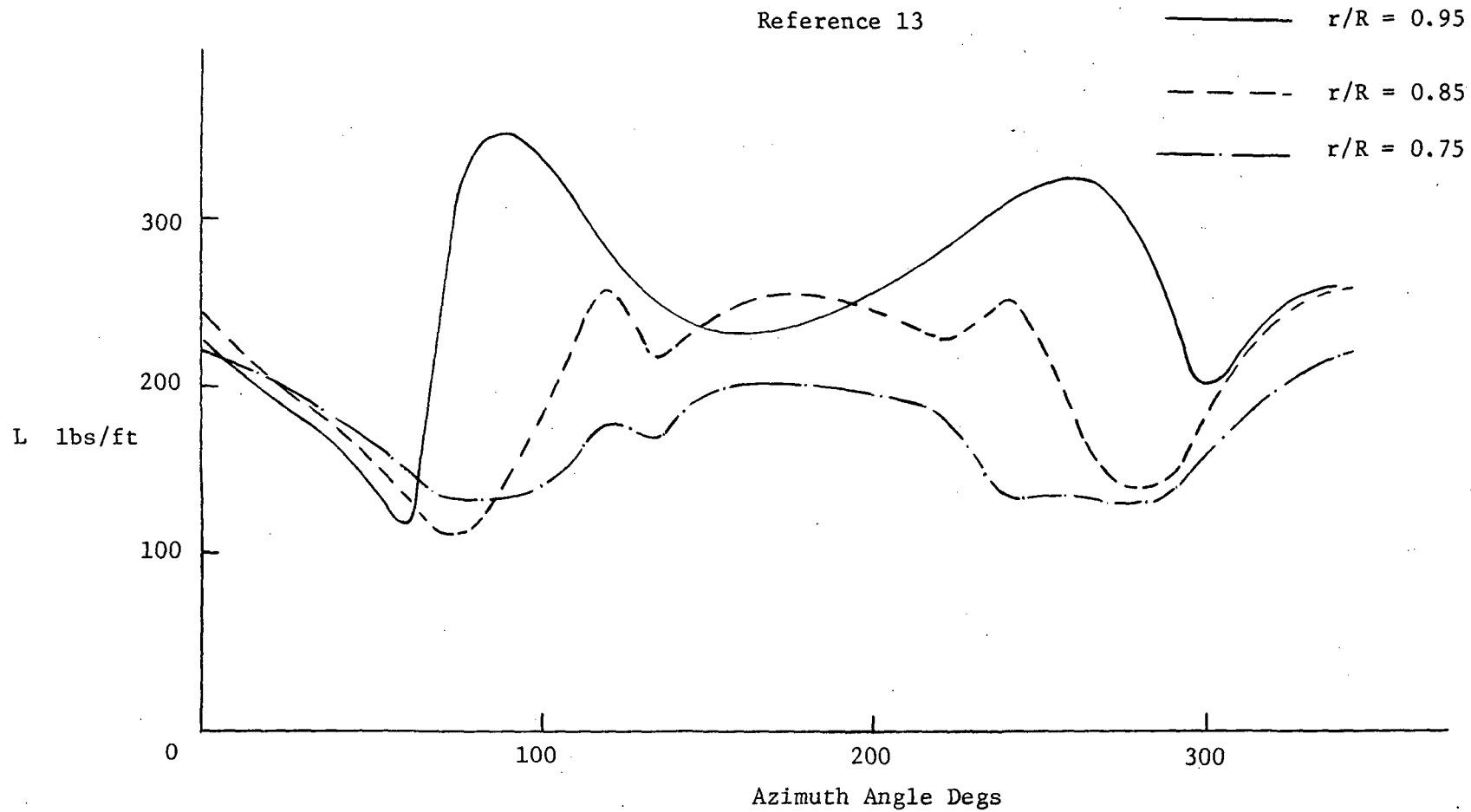
Figure 46. Experimental Section Lift Variation with Azimuth Angle; H-34 Helicopter Rotor, $\mu = 0.11$.
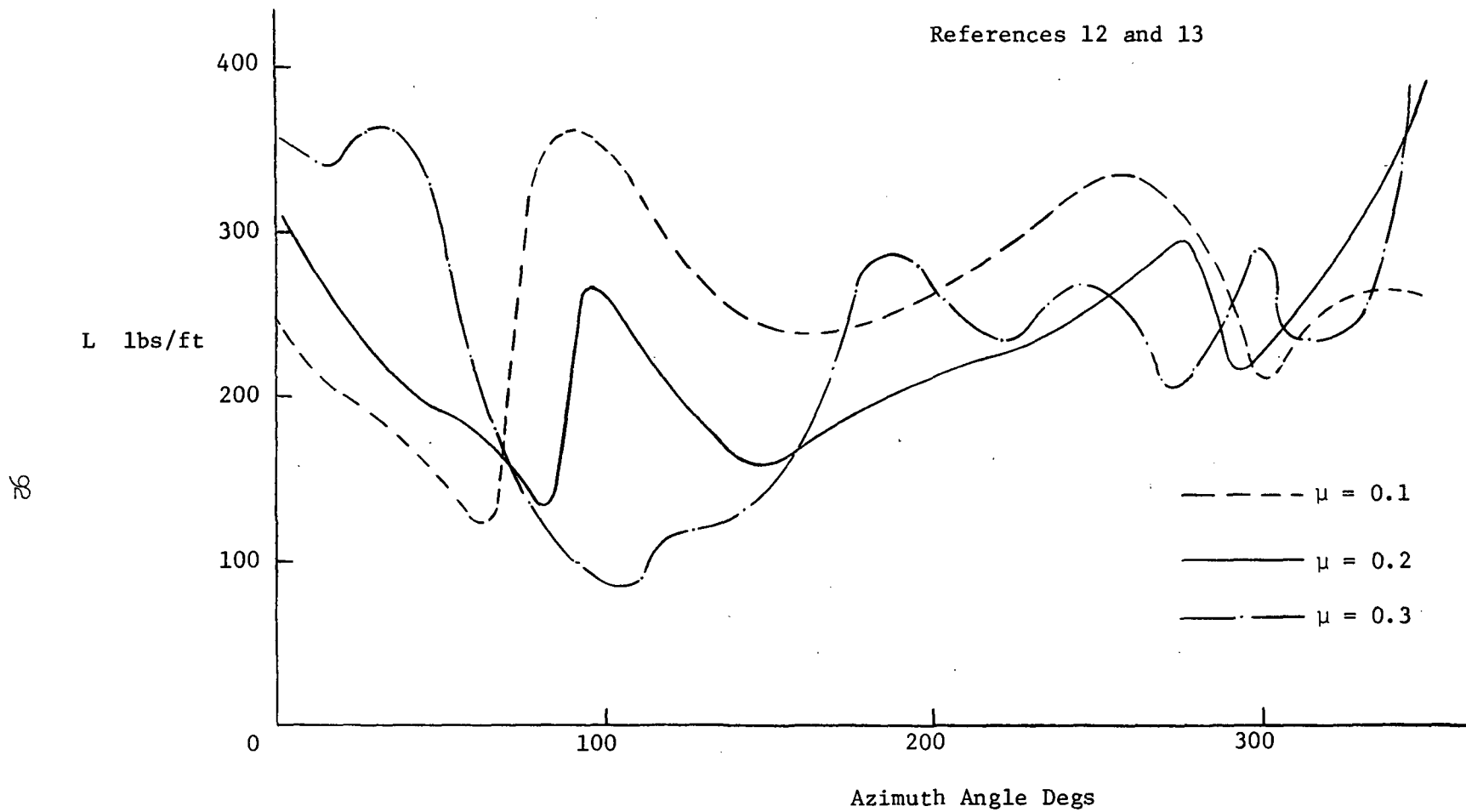
Figure 47. Experimental Section Lift Variation with Azimuth Angle; H-34 Helicopter Rotor, r/R = 0.95.

and Scully (30) have indicated that the combination of lifting surface and distorted wake geometry does not necessarily result in accurate airloads as shown in Figure 48. Calculations using distorted wake geometry predicted higher loads and hence the distorted wake should be closer to the tip path plane. It has been suggested by these authors that real fluid interaction of the blade and vortex (such as local vortex-induced flow separation) or local changes of the nature of the tip vortex viscous core due to the blade-vortex interaction (such as interaction induced bursting) may be important to be included in the airload calculations for a better correlation of experimental and predicted results.

Rotor blades have large aspect ratios and hence their structural stiffness is much smaller than that of a fixed wing designed to carry the same lift. Sadler (31) considered the effects of flexible blade motion on wake geometry and thereby on the wake's contribution to blade loads. The elevation at which the trailing vortices were deposited corresponded to the flapping positions of the flexible blade. As can be seen in this Figure 49, the general trends are very similar, but there are small differences in the airloads over the aft half of the rotor disk due to the effect of flexible blade on the wake geometry.

In a review paper, Johnson and Scully (30) have indicated that, for current wake geometry models (theoretical and experimental), on the advancing side of the rotor disk the tip vortex remains very close to the plane of the rotor and is pushed downward after the passage of the following blade. Hence on the advancing side a finite core vortex should be considered in the airloads calculations to avoid unrealistically high vortex-induced velocities. Most existing analyses currently assume

Figure 48.   Comparison of Experimental and Lifting Surface Theory Section Lift;
H-34 Helicopter Rotor, a = 0.005R.

——————— Without Blade Motion
Effects

— — — — With Blade Motion
Effects
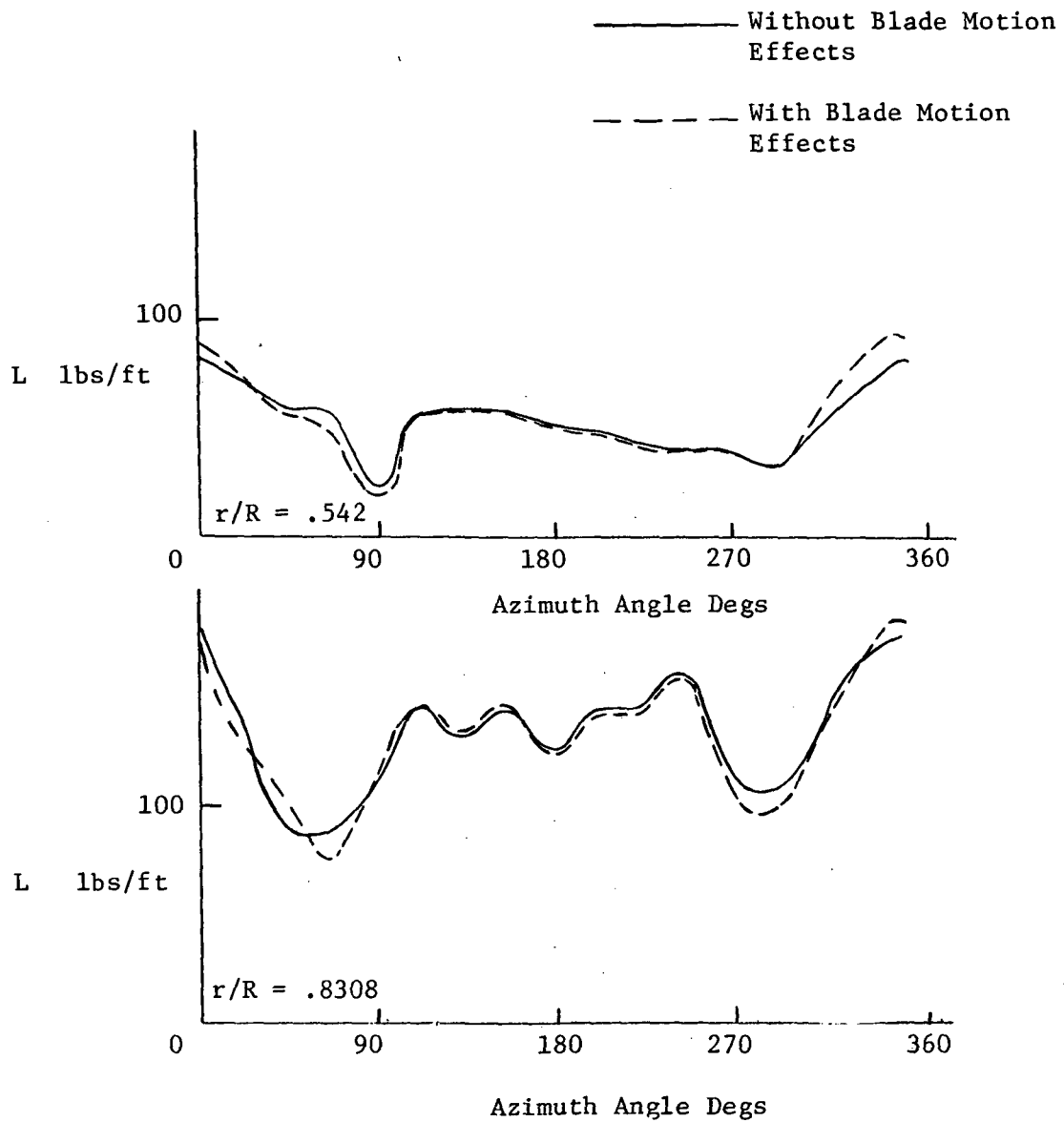
Figure 49. Airloads Without and With Blade Motion Effects in Wake-Induced
Velocity Calculations; H-34 Helicopter Rotor, μ = 0.2.

a core diameter of approximately ten percent of the blade chord or one percent of the rotor radius. A comparison of the results from the paper by Johnson and Scully (30) presented in Figures 48 and 50 for vortex core radii of 0.005R and .02R respectively, indicates that assuming a large core radius eliminates the difference between the rigid and distorted tip vortex geometries. Rorke and Moffitt (32) have recently measured the flow field in the core of the vortex behind a rectangular wing model which is a segment of a CH-53A helicopter rotor blade section with a revolved airfoil tip cap. The measurements were made at Mach numbers from 0.2 to 0.6 and Reynolds numbers ranging from 4.4×10^5 to 7.0×10^6 which are comparable to those at the tip of a full scale helicopter main rotor blade. As shown in Figures 51 and 52 for rectangular wings, the measured vortex core diameter to chord ratios and the peak tangential velocity ratios are functions only of wing lift coefficient and elapsed time from vortex formation, and appear to be independent of both Mach number and Reynolds number. In these figures, the vortex age (t) is the time required for an air particle to travel at the free stream velocity from the wing quarter-chord to the downstream location at which the vortex was surveyed. The trends of vortex core diameters and peak tangential velocities presented in these figures could be used to get a good approximation for the core diameter of the tip vortex of a rotor blade.

Cook (33) has very recently presented the measured velocity distribution through the tip vortex of a single bladed full scale rotor operating on a whirl tower at a representative tip speed of 600 ft/sec. The measurements were made using a hot wire anemometer. The rotor was 28 ft. radius, with a blade chord of 1.367 ft., 8° overall washout and
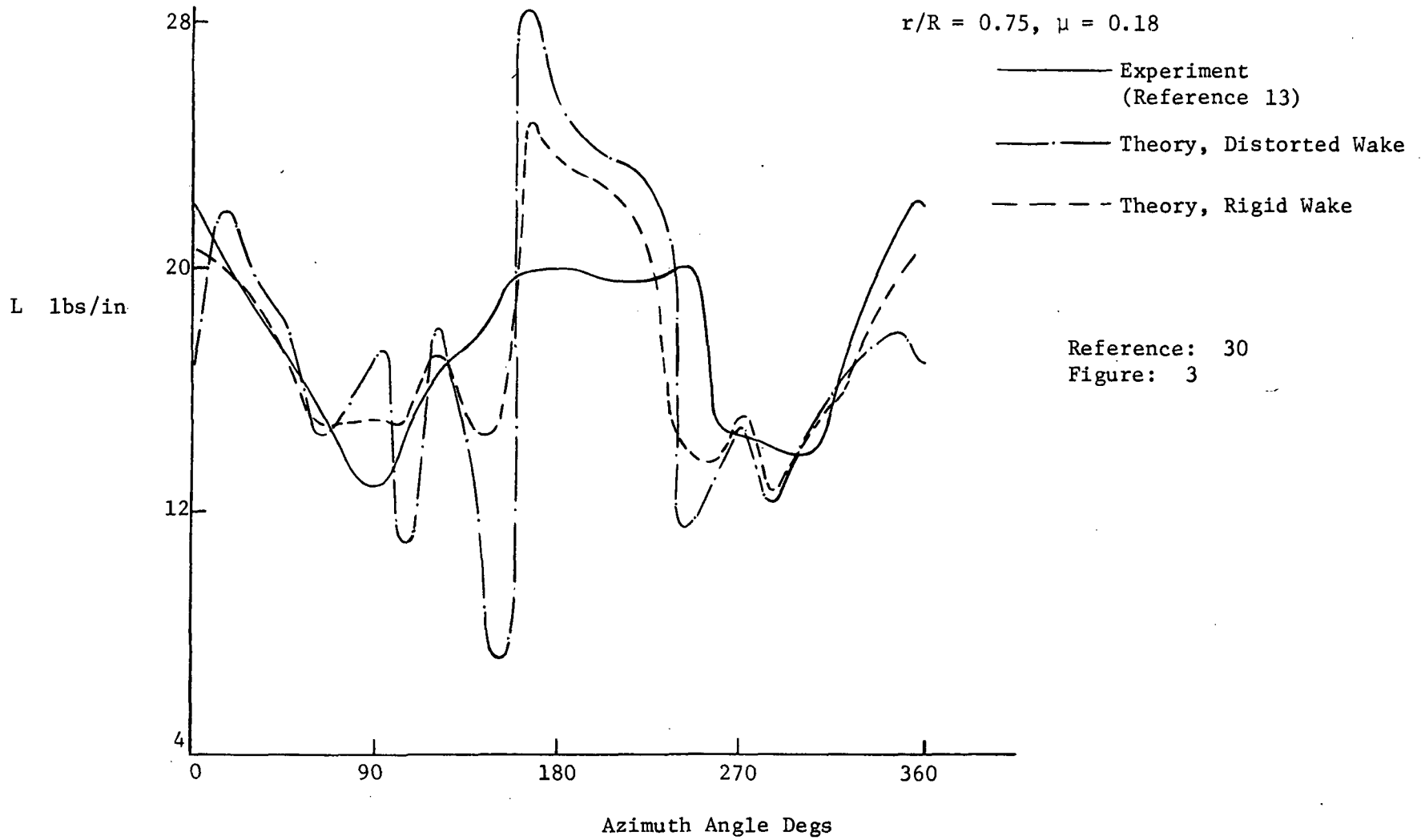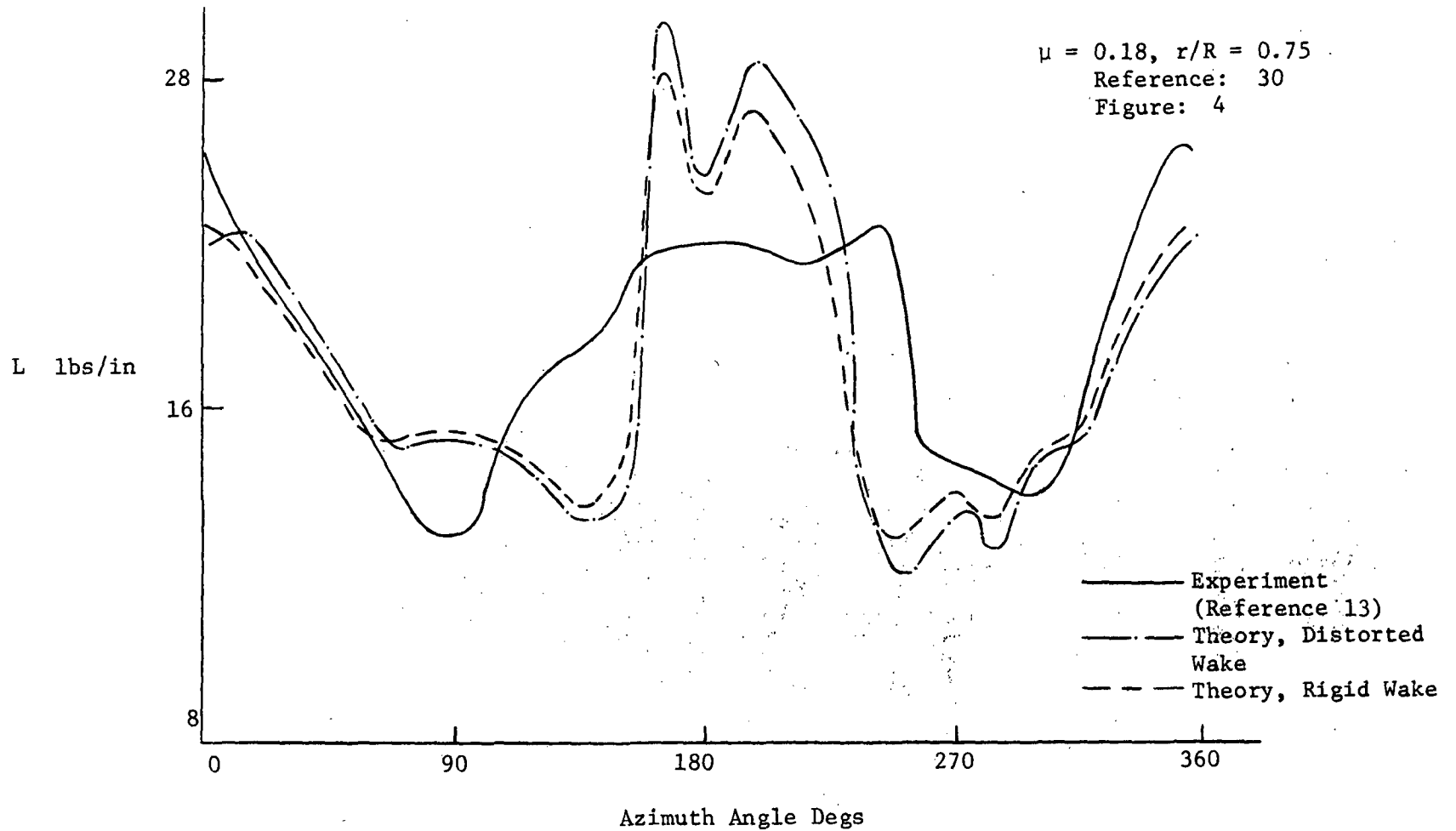
Figure 50. Comparison of Experimental and Lifting Surface Theory Section Lift; H-34 Helicopter Rotor, a = 0.02R.
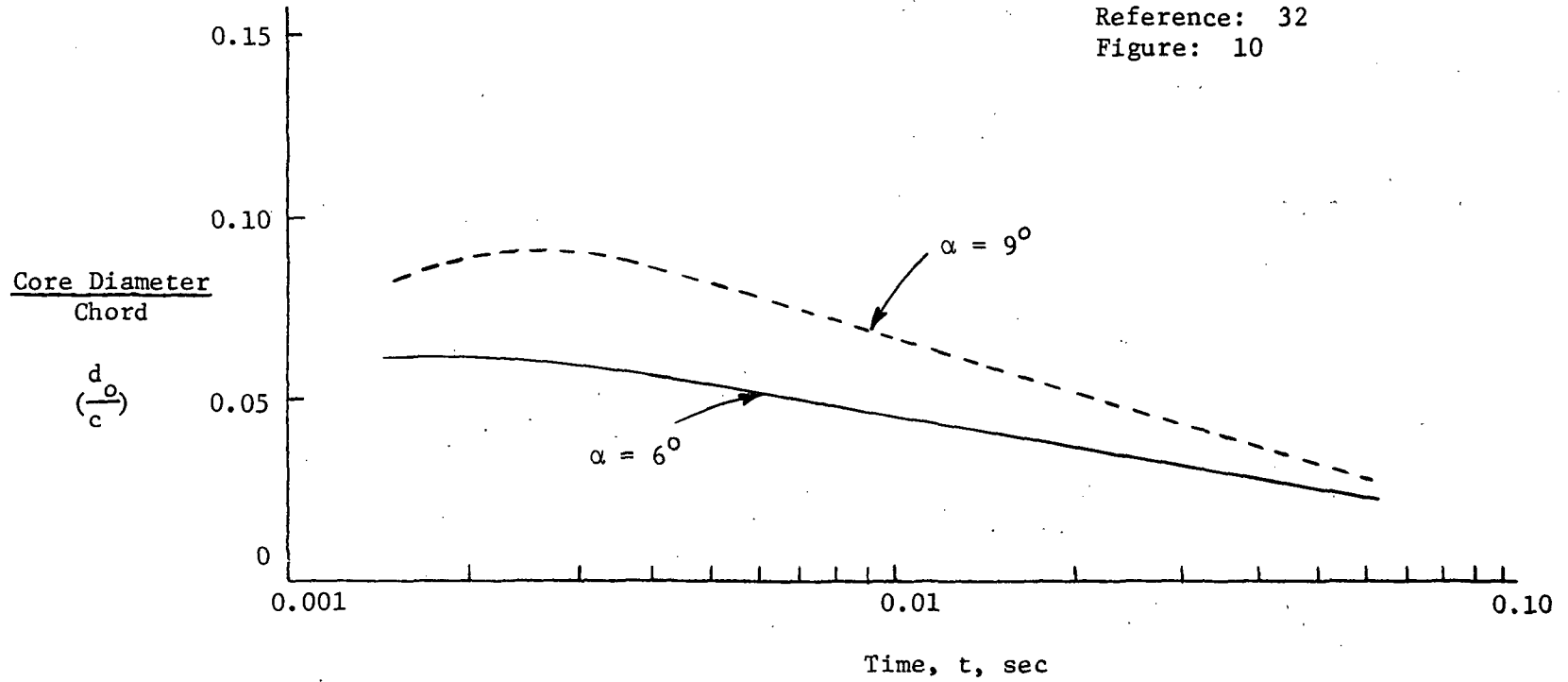
Figure 51. Vortex Core Diameter as a Function of Vortex Age.
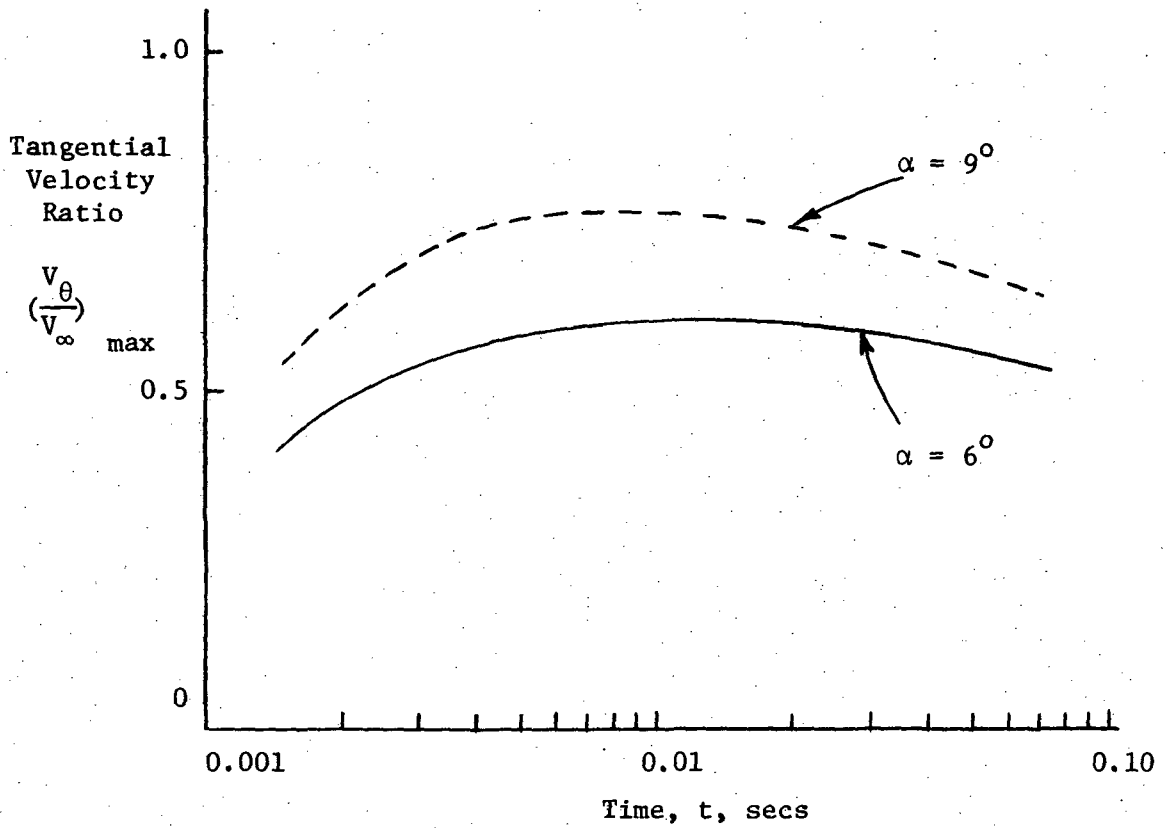
Figure 52. Maximum Tangential Velocity as a Function of Vortex Age.

99

NACA 0012 section. As shown in Figure 53, the viscous core diameter, defined as the distance between the measured velocity peaks, is very small. For the same total circulation of the vortex, a typical comparison of the measured velocity distribution and two Rankine vortex velocity distributions, one with the same maximum velocity as the measured and the other with half the core size, indicated a significant difference as shown in Figure 54. Since the scatter in the experimental data is very large as shown in a typical Figure 55, more measurements will have to be made before any data can be used in the analytical investigations with confidence. In reference 33, a point was noted on the measured vortex velocity profile outboard of which the curve obeyed the (1/r) law. This point has been designated by that reference as the core diameter indicated in Figure 55.

Reference: 33
Figure: 11

Thrust = 4400 lbs.

1.2

Viscous Core Diameter ins.

0.8

Thrust Conditions
2300 - 3750 lbs.

0.4

0   100   200   300   400   500

Vortex Age ψ degs
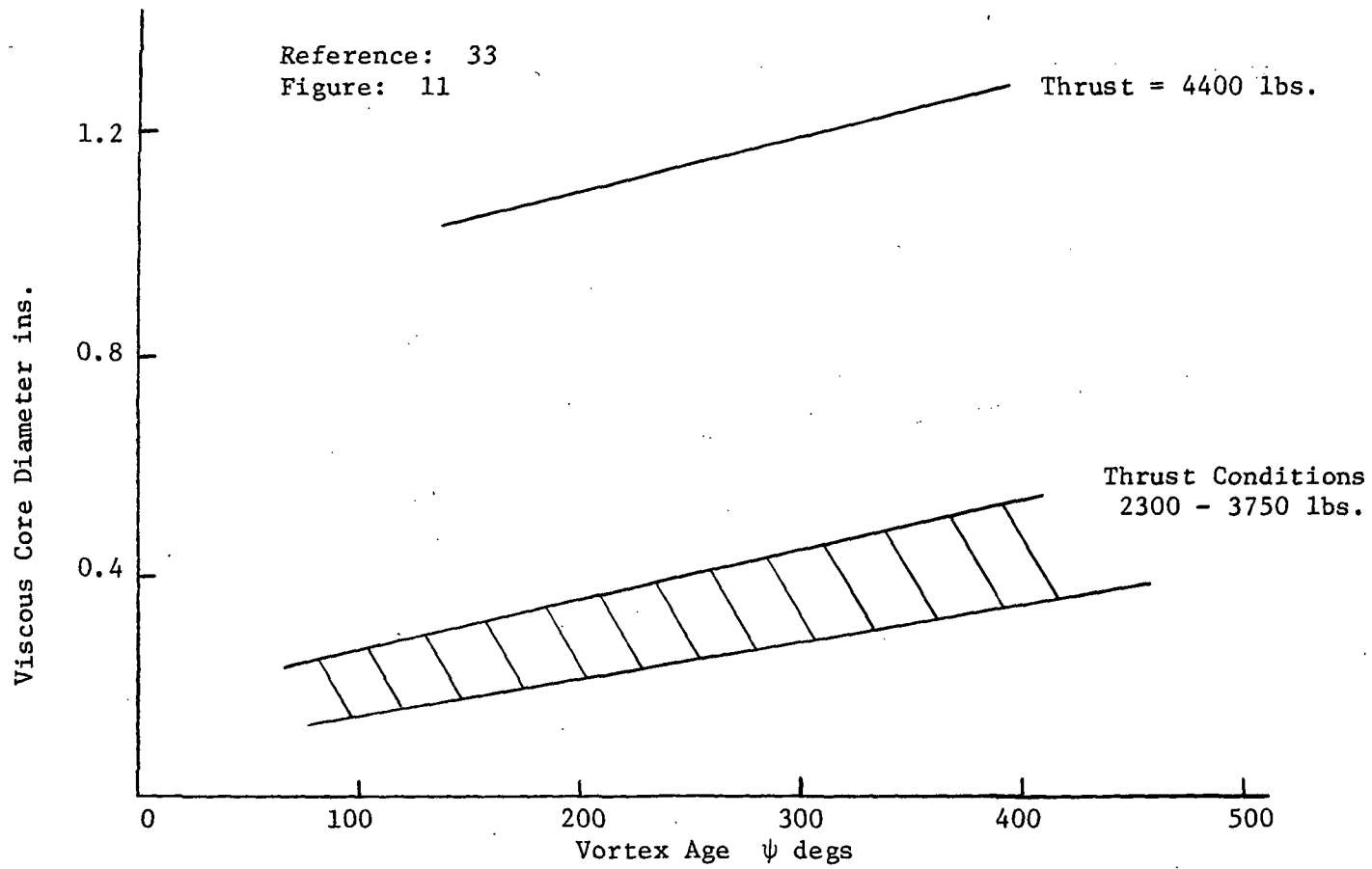
Figure 53.   Variation of Viscous Core Diameter with Vortex Age.
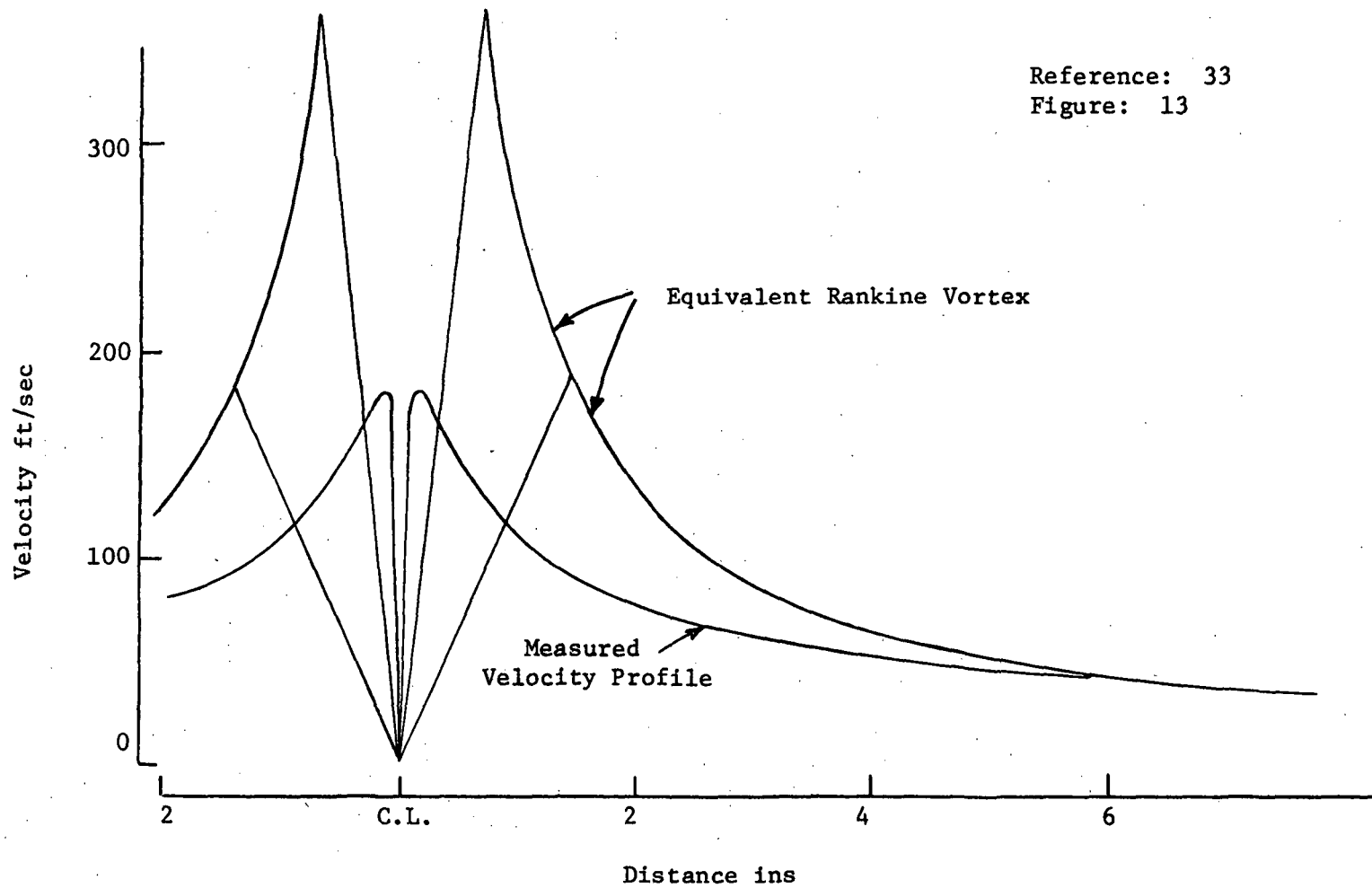
Figure 54. A Comparison of Rankine and Measured Vortex Velocities (with the Same Total Circulation).
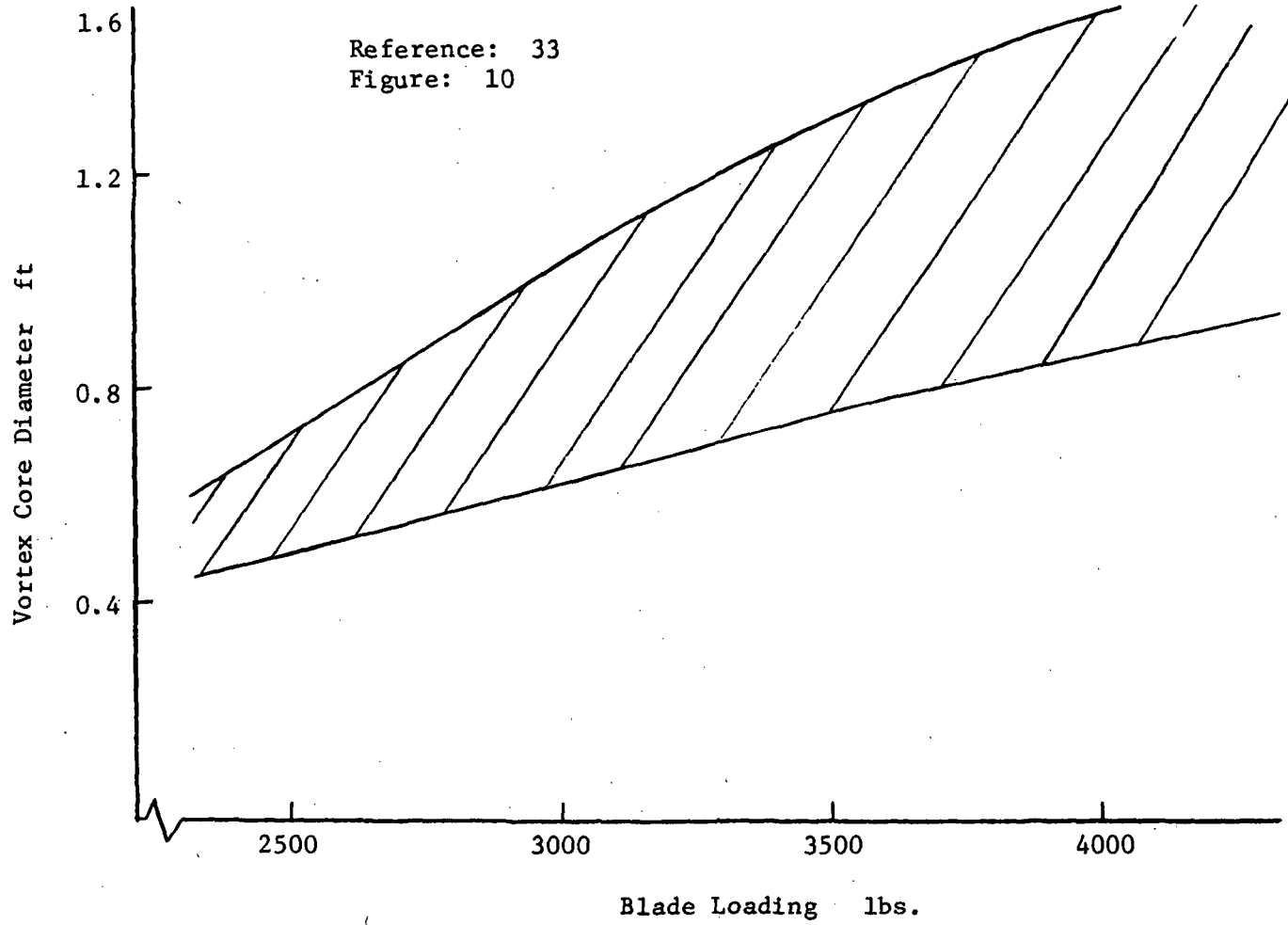
Figure 55. Variation of Vortex Size with Blade Loading.

CHAPTER V

CONCLUSIONS AND RECOMMENDATIONS

The foregoing analysis has developed a numerical lifting surface method to predict unsteady aerodynamic forces induced on a finite aspect ratio rectangular wing by a straight, free vortex placed at an arbitrary angle in a subsonic, incompressible free stream. This vortex lattice method has been applied to a single bladed rotor operating at high advance ratios and encountering a free vortex from a fixed upstream wing. The method has also been extended to full scale rotor flight cases in which vortex induced loads near the tip of a rotor blade were indicated. The calculated results were compared with planar lifting surface theory results and also with available experimental results. The following conclusions can be drawn from this investigation.

1. This investigation establishes the feasibility of a simple vortex lattice method to predict the unsteady forces due to complex vortex interactions. This method uses discrete vortices to represent the lifting surface and the wake.

2. In wing-vortex interaction problems, comparison of the vortex lattice method with linear lifting surface theory shows good agreement.

3. In the numerical calculations of lift due to a lifting surface-vortex interaction the interval between successive time steps and also the number of vortices on the lifting surface has considerable influence on the peak lift coefficients. The time step size and the number of vortices on the lifting surface must be chosen as a compromise between the accuracy and computer time and storage requirements.

4. Steady state or quasi-steady assumptions are inadequate to predict the unsteady nature of the lift fluctuation due to a lifting surface-vortex interaction.

5. Good agreement is shown between the vortex lattice method results and the planar lifting surface theory results in the case of a model rotor intersecting a free vortex.

6. The vortex induced loads on the model rotor blade are generally overestimated by the numerical lifting surface method when compared to experimental results. The computed time interval between peak values is in good agreement with experimental measurements.

7. The numerical lifting surface method predicts closely the large fluctuations in the measured airloads near the tip of a rotor blade on the advancing side of the disk.

8. Accurate information concerning the vertical location and the radial location of the tip vortex are required for an accurate prediction of vortex induced airloads. For close blade-vortex interactions, tip vortex core size is an important parameter in the prediction of vortex induced loads.

9. Rotor blade loads are very sensitive to the azimuthal variation of flapping and pitching angles.

10. The flat planar wake configuration is satisfactory for most of the advance ratios considered in the present investigation as at large advance ratios the downwash becomes small in comparison to the free stream velocity.

Since an accurate knowledge of the wake geometry is required to obtain accurate vortex-induced loads it is recommended that the present numerical lifting surface method be used with a deformed wake model,

105

especially at small advance ratios ($\mu \leq 0.15$). However, Moore (34) has shown by examination of the rolling up of a vortex sheet of an elliptically loaded wing that the approximation of replacing a finite vortex sheet by an array of line vortices can be unreliable regardless of the number of vortices used. It was suggested by the author that the strong coupling between line vortices causes chaotic motion of the tip vortices which affects inboard vortices. Hence caution must be exercised in using the deformed wake configuration.

One can attempt to calculate the unsteady airloads for close blade-vortex spacing. However blade loads are very sensitive to vortex locations and the sensitivity increasing with decreasing distance from the blade and hence such a calculation is questionable. It will be preferred to use measured blade-vortex spacing as high degree of accuracy is required of the location of the vortex. Since it determines the maximum tangential velocity near the vortex, the viscous core radius of the tip vortex is a very important parameter for the calculation of induced velocity. Hence for close blade-vortex interactions a more realistic value of the core radius from a very recent paper by Cook (33) could be used instead of the usually assumed value of 10 percent of the chord or one percent of the blade radius. Also for close blade-vortex interactions real fluid effects such as local separation on the blade due to large induced velocity gradients and local changes in the nature of the tip vortex viscous core due to blade-vortex interaction could be very important factors. The present investigation has neglected the effects of viscosity.

Finally, it is recommended that accurate azimuthal variation of flapping and pitching angles of the blade should be used in the present

analysis as the blade loads are sensitive to these. Accurate azimuthal variations of flapping and pitching angles of the blade could be obtained from an iterative calculation of blade motion and blade airloads.

BIBLIOGRAPHY

References Cited

1. Lehman, A. F., "Model Studies of Helicopter Rotor Flow Patterns in a Water Tunnel," American Helicopter Society, 24th Annual National Forum, May 1968.

2. Jenney, D. S., Olson, J. R., and Landgrebe, A. J., "A Reassessment of Rotor Hovering Performance Prediction Methods," American Helicopter Society, 23rd Annual National Forum, May 1967.

3. Simons, I. A., "Some Aspects of Blade-Vortex Interaction on Helicopters in Forward Flight," Journal of Sound and Vibration, Vol. 4, No. 3, November 1966, pp. 268-281.

4. Kfoury, D. J., "A Routine Method for the Calculation of Aerodynamic Loads on a Wing in the Vicinity of Infinite Vortices," ASRL TR 133-2, M.I.T. Aeroelastic and Structures Research Lab., May 1966.

5. Jones, W. P., and Rao, B. M., "Wing-Vortex Interaction," Texas Engineering Experiment Station, Texas A and M University, January 1970.

6. Johnson, W., "A Lifting Surface Solution for Vortex Induced Airloads and Its Application to Rotary Wing Airloads Calculations," ASRL TR 153-2, M.I.T. Aeroelastic and Structures Research Lab., April 1970.

7. Johnson, W., "A Comparison Between Experimental Data and a Lifting Surface Theory Calculation of Vortex Induced Loads," ASRL TR 153-3, M.I.T. Aeroelastic and Structures Research Lab., August 1970.

8. Johnson, W., "A Comparison Between Experimental Data and Helicopter Airloads Calculated Using a Lifting Surface Theory," ASRL TR 157-1, M.I.T. Aeroelastic and Structures Research Lab., July 1970.

9. Surendraiah, M., "An Experimental Study of Rotor Blade-Vortex Interaction," NASA CR-1573, May 1970.

10. Padakannaya, R., "Experimental Study of Rotor Unsteady Airloads Due to Blade-Vortex Interaction," NASA CR-1909, November 1971.

11. Pruyn, R. R., and Alexander, W. T., "USAAVLABS Tandem Rotor Airloads Measurement Program," Journal of Aircraft, Vol. 4, No. 3, May-June 1967, pp. 255-260.

12. Scheiman, J., "A Tabulation of Helicopter Rotor Blade Differential Pressures, and Motions as Measured in Flight," NASA TM X-952, March 1964.

13. Scheiman, J., and Ludi, L. H., "Qualitative Evaluation of Effect of Helicopter Rotor Blade Tip Vortex on Blade Airloads," NASA TND-1637, May 1963.

14. Landgrebe, A. J., and Bellinger, E. D., "An Investigation of the Quantitative Applicability of Model Helicopter Rotor Wake Patterns Obtained from a Water Tunnel," USAAMDRL Technical Report 71-69, December 1971.

15. Kantha, H. L., Lewellan, W. S., and Durgin, F. H., "Qualitative Responses of a Vortex Core to Tip Blowing and Intersecting Airfoils," ASRL TR 153-4, M.I.T. Aeroelastic and Structures Research Lab., August 1971.

16. Scully, M. P., and Sullivan, J. P., "Helicopter Rotor Wake Geometry and Airloads and Development of Laser Doppler Velocimeter for Use in Helicopter Rotor Wakes," M.I.T. Aerophysics Laboratory TR 179, August 1972.

17. Albano, E., and Rodden, W. P., "A Doublet-Lattice Method for Calculating Lift Distributions on Oscillating Surfaces in Subsonic Flows," AIAA Journal, Vol. 7, No. 2, February 1969, pp. 279-285.

18. James, R. M., "On the Remarkable Accuracy of the Vortex Lattice Discretization in Thin Wing Theory," Douglas Aircraft Company Report No. DAC 67211, February 1969.

19. De Young, J., "Convergence – Proof of Discrete Panel Wing Loading Theories," Journal of Aircraft, Vol. 8, No. 10, October 1971, pp. 837-839.

20. Djojodihardjo, R. H., and Widnall, S. E., "A Numerical Method for the Calculation of Nonlinear, Unsteady Lifting Potential Flow Problems," AIAA Journal, Vol. 7, No. 10, October 1969, pp. 2001-2009.

21. Giesing, J. P., "Nonlinear Two-Dimensional Unsteady Potential Flow with Lift," Journal of Aircraft, Vol. 5, No. 2, March-April, 1968, pp. 135-143.

22. Piziali, R. A., "Method for the Solution of the Aeroelastic Response Problem for Rotating Wings," Journal of Sound and Vibration, Vol. 4, No. 3, November 1966, pp. 445-486.

23. Bisplinghoff, R. L., Ashley, H., and Halfman, R. L., "Aeroelasticity," Addison-Wesley, Reading, Massachusetts, 1955.

24. Jones, W. P., "Aerodynamic Forces in Nonuniform Motion," ARC, R and M, No. 2117 (1945).

25. Rudhman, W. E., "A Numerical Solution of the Unsteady Airfoil with Application to the Vortex Interaction Problem," M.S. Thesis, December 1970, Dept. of Aerospace Engineering, The Pennsylvania State University.

26. McCormick, B. W., Tangler, J. M., and Sherrieb, H. E., "Structure of Trailing Vortices," Journal of Aircraft, Vol. 5, No. 3, May-June 1968, pp. 260-267.

27. Baczek, L. J., "An Experimental Investigation Concerning Trailing Vortex and Helicopter Rotor Blade Interaction," M.S. Thesis, Dept. of Aeronautics and Astronautics, M.I.T., February 1970.

28. Ham, N. D., "Discussion of Papers on Aerodynamics of Rotary Wings," AGARD-CP-111, September 1972.

29. Ormiston, R. A., "An Actuator Disc Theory for Rotor Wake Induced Velocities," AGARD-CP-111, September 1972.

30. Johnson, W., and Scully, M. P., "Aerodynamic Problems in the Calculation of Helicopter Airloads," Paper presented at the Symposium on Status of Testing and Model Techniques for V/STOL Aircraft, American Helicopter Society, October 1972.

31. Sadler, G. S., "Development and Application of a Method for Predicting Rotor Free Wake Positions and Resulting Rotor Blade Airloads, Vol. I - Model and Results," NASA CR-1911, December 1971.

32. Rorke, J. B., and Moffitt, R. C., "Wind Tunnel Simulation of Full Scale Vortices," NASA CR-2180, March 1973.

33. Cook, C. V., "The Structure of the Rotor Blade Tip Vortex," AGARD-CP-111, September 1972.

34. Moore, D. W., "The Discrete Vortex Approximation of a Finite Vortex Sheet," AFOSR-TR-72-0034, October 1971.

35. Durand, W. F., "Aerodynamic Theory, A General Review of Progress," Vol. II, Dover Publications, Inc., New York, 1963.

General References

Abbott, I. H., and Von Doenhoff, A. E., "Theory of Wing Sections," Dover Publications, Inc., New York.

Arcidiacono, P. J., and Carlson, R. G., "Helicopter Rotor Loads Prediction," Paper presented at the AGARD Specialists meeting on Prediction and Verification of Loads on Helicopters, Italy, April 1973.

Bellinger, E. D., "Analytical Investigation of Effects of Blade Flexibility, Unsteady Aerodynamics, and Variable Inflow on Helicopter Rotor Stall Characteristics," Journal of the American Helicopter Society, Vol. 17, No. 3, July 1972, pp. 35-44.

Belotserkovskii, S. M., "The Theory of Thin Wings in Subsonic Flow," Plenum Press, New York, 1967.

Beno, E. A., "Analysis of Helicopter Maneuver-Loads and Rotor-Loads Flight-Test Data," NASA CR-2225, March 1973.

Crimi, P., "Theoretical Prediction of the Flow in the Wake of a Helicopter Rotor, Part 1," Cornell Aero Lab. Report BB-1994-S-1, September 1965.

Daughaday, H., and Piziali, R. A., "An Improved Computational Model for Predicting the Unsteady Aerodynamic Loads of Rotor Blades," Journal of the American Helicopter Society, Vol. 11, No. 4, October 1966, pp. 3-10.

Davenport, F. J., "A Method for Computation of the Induced Velocity Field of a Rotor in Forward Flight, Suitable for Application to Tandem Rotor Configurations," Journal of the American Helicopter Society, Vol. 9, No. 3, July 1964, pp. 26-33.

Falabella, G., and Meyer, J. R., "Determination of Inflow Distributions from Experimental Aerodynamic Loading and Blade Motion on a Model Helicopter Rotor in Hovering and Forward Flight," NASA TN-3492, November 1955.

Falkner, V. M., "The Calculations of Aerodynamic Loading on Surfaces of Any Shape," ARC, R and M No. 1910 (1941).

Fung, Y. C., "An Introduction to the Theory of Aeroelasticity," Dover Publications, Inc., New York.

Gessow, A., and Meyers, G. C., Jr., "Aerodynamics of the Helicopter," Frederick Ungar Publishing Co., New York, Third Printing, 1967.

Gray, R. B., and Brown, G. W., "A Vortex-Wake Analysis of a Single Bladed Hovering Rotor and a Comparison with Experimental Data," AGARD-CP-111, September 1972.

Halfman, R. L., Johnson, H. C., and Haley, S. M., "Evaluation of High-Angle-of-Attack Aerodynamic Derivative Data and Stall-Flutter Prediction Techniques," NACA TN 2533 (1951).

Ham, N. D., "An Experimental Investigation of the Effect of a Non-Rigid Wake on Rotor Blade Airloads in Transition Flight," Proceedings CAL/TRECOM Symposium on Dynamic Load Problems Associated with Helicopters and V/STOL Aircraft, Vol. 1, June 1963.

Hedman, S. G., "Vortex Lattice Method for the Calculation of Quasi-Steady State Loadings on Thin Elastic Wings," Aeronautical Research Institute of Sweden Report 105, October 1965.

Hough, G. R., "Remarks on Vortex Lattice Methods," Journal of Aircraft, Vol. 10, No. 5, May 1973, pp. 314-316.

Ichikawa, T., "Linear Aerodynamic Theory of Rotor Blades," Journal of Aircraft, Vol. 4, No. 3, May-June 1967, pp. 210-218.

Johnson, W., "The Effect of Dynamic Stall on the Response and Airloading of Helicopter Rotor Blades," Journal of the American Helicopter Society, Vol. 14, No. 2, April 1969, pp. 68-79.

Jones, J. P., "An Extended Lifting Line Theory for the Loads on a Rotor Blade in the Vicinity of a Vortex," ASRL TR 123-3, M.I.T. Aeroelastic and Structures Research Lab., December 1965.

Jones, W. P., "Vortex-Elliptic Wing Interaction," AIAA Journal, Vol. 10, No. 2, February 1972, pp. 225-227.

Jones, W. P., and Rao, B. M., "Tip Vortex Effects on Oscillating Rotor Blades in Hovering Flight," AIAA Journal, Vol. 9, No. 1, January 1971, pp. 106-113.

Kalman, T. P., Giesing, J. P., and Rodden, W. P., "Spanwise Distribution of Induced Drag in Subsonic Flow by the Vortex Lattice Method," Journal of Aircraft, Vol. 7, No. 6, Nov.-Dec. 1970, pp. 574-576.

Kalman, T. P., Rodden, W. P., and Giesing, J. P., "Application of the Doublet-Lattice Method to Nonplanar Configurations in Subsonic Flows," Journal of Aircraft, Vol. 8, No. 6, June 1971, pp. 406-413.

Landahl, M. T., and Stark, V. J. E., "Numerical Lifting Surface Theory - Problems and Progress," AIAA Journal, Vol. 6, No. 11, November 1968, pp. 2049-2060.

Landgrebe, A. J., "An Analytical Method for Predicting Rotor Wake Geometry," AIAA Paper No. 69-196, February 1969.

Landgrebe, A. J., and Cheney, M. C., Jr., "Rotor Wakes - Key to Performance Prediction," Paper presented at the Symposium on Status of Testing and Modeling Techniques for V/STOL Aircraft, American Helicopter Society, October 1972.

Lehrian, E. D., "A Calculation of the Complete Downwash in Three Dimensions Due to a Rectangular Vortex," ARC, R and M No. 2771 (1949).

Leverton, J. W., "Helicopter Noise-Blade Slap" Part 1; Review and Theoretical Study, NASA CR-1221, October 1968.

Leverton, J. W., "Helicopter Noise-Blade Slap" Part 2; Experimental Results, NASA CR-1983, March 1972.

Loewy, R. G., "A Two Dimensional Approach to the Unsteady Aerodynamics of Rotary Wings," Journal of Aerospace Sciences, Vol. 24, No. 3, March 1957, pp. 82-98.

McCormick, B. W., Jr., "Aerodynamics of V/STOL Flight," Academic Press, New York, 1967.

Miller, R. H., "Rotor Blade Harmonic Airloading," AIAA Journal, Vol. 2, No. 7, July 1964, pp. 1254-1269.

Miller, R. H., "A Discussion of Rotor Blade Harmonic Airloading," Proceedings CAL/TRECOM Symposium on Dynamic Load Problems Associated with Helicopters and V/STOL Aircraft, Vol. 1, June 1963.

Piziali, R. A., and DuWaldt, F. A., "Computation of Rotary Wing Harmonic Airloads and Comparison with Experimental Results," American Helicopter Society, 19th Annual National Forum, May 1962.

Rabbott, J. P., Jr., and Paglino, V. M., "Aerodynamic Loading of High Speed Rotors," CAL/USAAVLABS Symposium Proceedings, Vol. 1, June 1966.

Rodden, W. P., Giesing, J. P., and Kalman, T. P., "New Developments and Application of the Subsonic Doublet-Lattice Method for Nonplanar Configurations," AGARD Symposium, Unsteady Aerodynamics of Aeroelastic Analyses of Interfering Surfaces, AGARD Paper No. 4, Tansberg Oslofjorden, Norway, November 1970.

Rubbert, P. E., "Theoretical Characteristics of Arbitrary Wings by a Nonplanar Vortex Lattice Method," The Boeing Company, Seattle, Washington, Report D6-9244, 1964.

Runyan, H. L., and Woolston, D. S., "Method for Calculating the Aerodynamic Loading on an Oscillating Finite Wing in Subsonic and Sonic Flow," NACA TR 1322 (1957).

Sadler, G. S., "Main Rotor Free Wake Geometry Effects on Blade Airloads and Response for Helicopters in Steady Maneuvers, Vol. I – Theoretical Formulation and Analysis of Results," NASA CR-2110, September 1972.

Scully, M. P., "A Method of Computing Helicopter Vortex Distortion," ASRL TR 138-1, M.I.T., Aeroelastic and Structures Research Lab., June 1967.

Segel, L., "A Method for Predicting Nonperiodic Airloads on a Rotary Wing," Journal of Aircraft, Vol. 3, No. 6, Nov.-Dec. 1966, pp. 541-548.

Silver, L. W., "An Investigation of the Interaction of a Trailing Vortex with a Lifting Surface," M.I.T., S.M. Thesis, June 1967.

Simons, I. A., Pacifico, R., and Jones, J. P., "The Movement, Structure and Breakdown of Trailing Vortices from a Rotor Blade," CAL/USAAVLABS Symposium Proceedings, Vol. 1, June 1966.

Spencer, R. H., Sternfeld, H., and McCormick, B. W., "Tip Vortex Core Thickening for Application to Helicopter Rotor Noise Reduction," USAAVLABS Technical Report 66-1, September 1966.

Tangler, J. L., Wohlfeld, R. M., and Miley, S. J., "An Experimental Investigation of Vortex Stability, Tip Shapes, Compressibility, and Noise for Hovering Model Rotors," Bell Report No. 299-099-641.

Tangler, J. L., "Investigation of the Stability of the Tip Vortex Generated by Hovering Propellers and Rotors," Paper presented at the AIAA Second Atmospheric Flight Mechanics Conference, September 1972.

Von Karman, Th., and Sears, W. R., "Airfoil Theory for Non-uniform Motion," Journal of the Aeronautical Sciences, Vol. 5, No. 10, August 1938, pp. 379-390.

Walsh, G. R., "Leading-edge Pressure Measurements of Airfoil Vortex Interaction," ASRL TR 153-1, M.I.T. Aeroelastic and Structures Research Lab., January 1970.

Ward, J. F., "Helicopter Rotor Periodic Differential Pressures and Structural Response Measured in Transient and Steady-State Maneuvers," American Helicopter Society, 26th Annual National Forum, June 1970.

Ward, J. F., and Young, W. H., Jr., "A Summary of Current Research in Rotor Unsteady Aerodynamics with Emphasis on Work at Langley Research Center, AGARD-CP-111, September 1972.

White, R. P., "VTOL Periodic Aerodynamic Loadings: The Problems, What is being done and what needs to be done." Journal of Sound and Vibration, Vol. 4, Number 3, November 1966.

Widnall, S., "Helicopter Noise Due to Blade-Vortex Interaction," Journal of Acoustical Society of America, Vol. 50, July 1971, Part 2, pp. 354-365.

Willmer, M. A. P., "The Loading of Helicopter Rotor Blades in Forward Flight," ARC, R and M No. 3318 (1963).

Woodley, J. G., "The Influence of Near Wake Assumptions on the Lifting Characteristics of a Rotor Blade," RAE TR 71046, March 1971.

Young, M. I., "An Engineering Approximation for the Aerodynamic Loading of Helicopter Rotor Blades," Journal of Sound and Vibration, Vol. 4, No. 3, November 1966, pp. 282-304.

EFFECT OF THICKNESS ON THE LIFT DUE TO WING-VORTEX INTERACTION

In the following analysis conformal transformation methods have been used to study the effect of thickness on the lift due to a two-dimensional wing-vortex interaction. A circle can be transformed by the Joukowski transformation into a shape resembling that of a wing section. The flow about a circulat cylinder having a radius slightly larger than a, and so placed that the circumference passes through the point x = a, on the z-plane is transformed to the flow about an airfoil on the ζ-plane using the mapping function

$$\zeta = z + a^2/z$$

If, in addition, the center of the larger cylinder (of radius larger than a) is placed on the x-axis, the transformed curve will be that of a symmetrical wing section (Figure 56). Let the radius of the larger cylinder be a + ε. The complex potential of a circular cylinder with a circulation of strength Γ, placed in a stream of velocity along the x-axis is

$$w_1 = V[(z_1 + \varepsilon) + \frac{(a+\varepsilon)^2}{(z_1+\varepsilon)}] + \frac{i\Gamma}{2\pi} \ln (\frac{z_1+\varepsilon}{a+\varepsilon})$$

Consider a vortex of strength Γ_1 located at z_{01} outside the cylinder of radius (a + ε). If the motion is due solely to the vortex the circle theorem gives the complex potential

$$w_2 = - \frac{i\Gamma_1}{2\pi} \ln [(z_1+\varepsilon) - z_{01}] + \frac{i\Gamma_1}{2\pi} \ln [\frac{(a+\varepsilon)^2}{(z_1+\varepsilon)} - z_{01}]$$
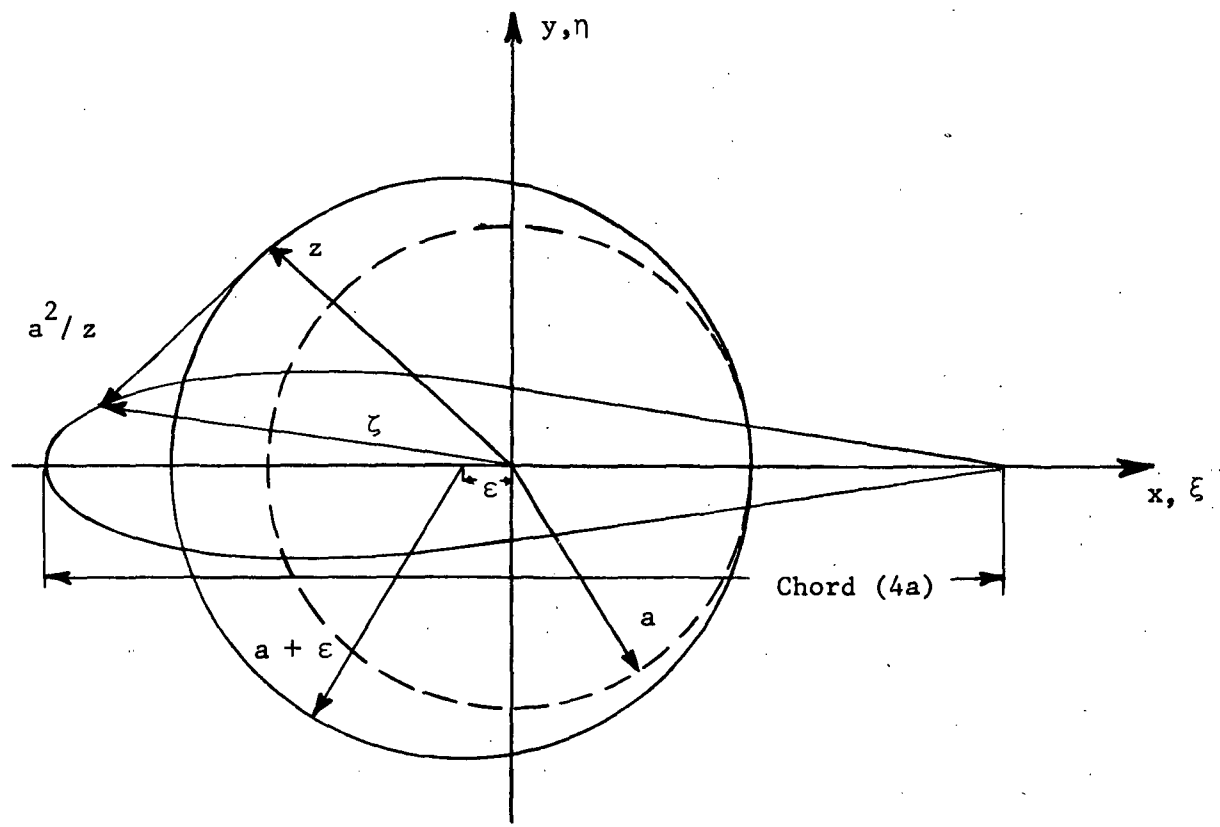
Figure 56.   Conformal Transformation of a Circle into a Symmetrical Wing Section.

The more general expression for the flow about the circular cylinder with flow at infinity inclined at an angle α_0 to the z-axis in the presence of a vortex outside the cylinder can be written by substituting

$$z + \varepsilon = (z_1 + \varepsilon) e^{i\alpha_0}$$

and

$$z_0 = z_{01} e^{i\alpha_0}$$

In the case of α_0 zero, the lift is due only to the interacting vortex. For this case of $\alpha_0 = 0$, $w = w_1 + w_2$ can be written as

$$w = V[(z+\varepsilon) + \frac{(a+\varepsilon)^2}{z+\varepsilon}] + \frac{i\Gamma}{2\pi} \ln (\frac{z+\varepsilon}{a+\varepsilon})$$

$$- \frac{i\Gamma_1}{2\pi} [\ln \{(z+\varepsilon) - z_0\}]$$

$$+ \frac{i\Gamma_1}{2\pi} [\ln \frac{(a+\varepsilon)^2}{z+\varepsilon} - z_0 \}]$$

The velocity $(dw/d\zeta)$ at the point $z = a$ (corresponding to the trailing edge) must satisfy the Kutta condition of smooth flow at the trailing edge which determines the value of circulation Γ around the airfoil.

$$\text{Equating } \frac{dw}{d\zeta} = \frac{dw}{dz} \frac{dz}{d\zeta} \Big|_{z=a} = 0$$

$$\Gamma = 2\Gamma_1 (a+\varepsilon) [\text{Real part } \{\frac{1}{(a+\varepsilon)-z_0}\}]$$

Neglecting powers of ε greater than one the chord of the airfoil is 4a. The lift on the wing section is $\rho V \Gamma$ and the lift coefficient is

$$C_\ell = \frac{\Gamma_1}{V} (1+\varepsilon/a) \left[\frac{a(1+2\varepsilon/a) - x}{\{a(1+2\varepsilon/a)-x\}^2+y^2} \right]$$

Durand (35) has shown that the thickness ratio of the wing section is nearly equal to $3\sqrt{3}/4$ (ε/a)

$$C_\ell = \frac{\Gamma_1}{V} (1 + 0.77 \ t/c) \left[\frac{a(1 + 1.54 \ t/c) - x}{\{a(1 + 1.54 \ t/c) - x\}^2 + y^2} \right]$$

where $a = c/4$

For $t/c = 0$ this expression reduces to

$$C_\ell = \frac{\Gamma_1}{V} \left[\frac{a - x}{(a-x)^2+y^2} \right]$$

For a given value of y

$$C_{\ell_{max}} = \Gamma_1/V \ [1 + 0.77 \ t/c] \ (1/2y)$$

This value of maximum lift coefficient occurs at

$$x = a \ (1 + 1.54 \ t/c) - y$$

For $t/c = 0$ $\qquad C_{\ell_{max}} = \Gamma_1/V \ (1/2y)$

This maximum lift coefficient occurs at

$$x = a - y$$

therefore

$$\frac{C_{\ell_{max}} (t/c)}{C_{\ell_{max}} (t/c=0)} = (1 + 0.77 \, t/c)$$

For a thickness ratio of 12 percent this ratio is 1.0924.

The variations of lift coefficient with (x/c) for a given (y/c) are presented in Figures 57 and 58 for thickness ratios of zero and 12 per cent respectively. As expected the lift coefficient is higher for the thicker wing.
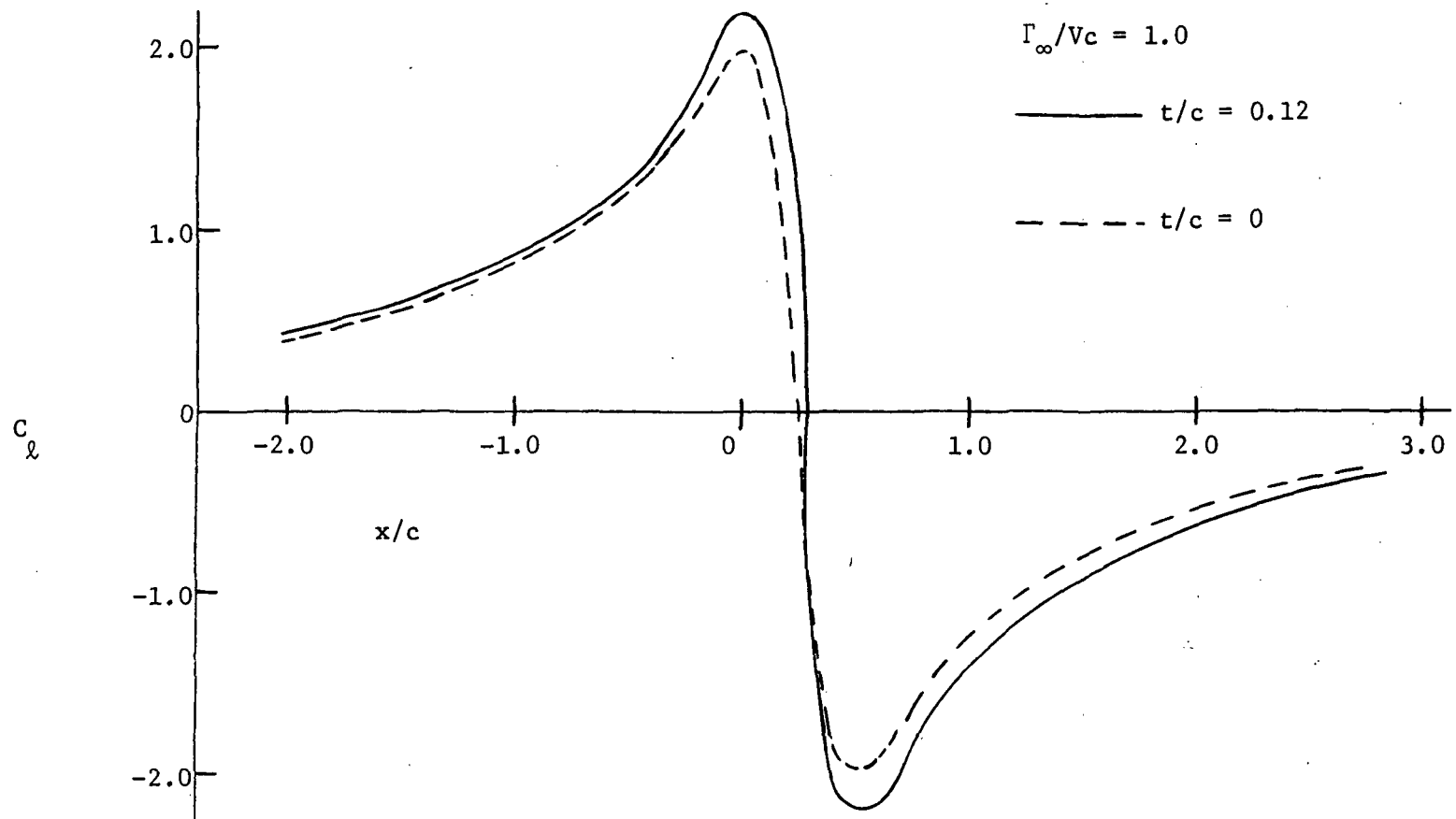
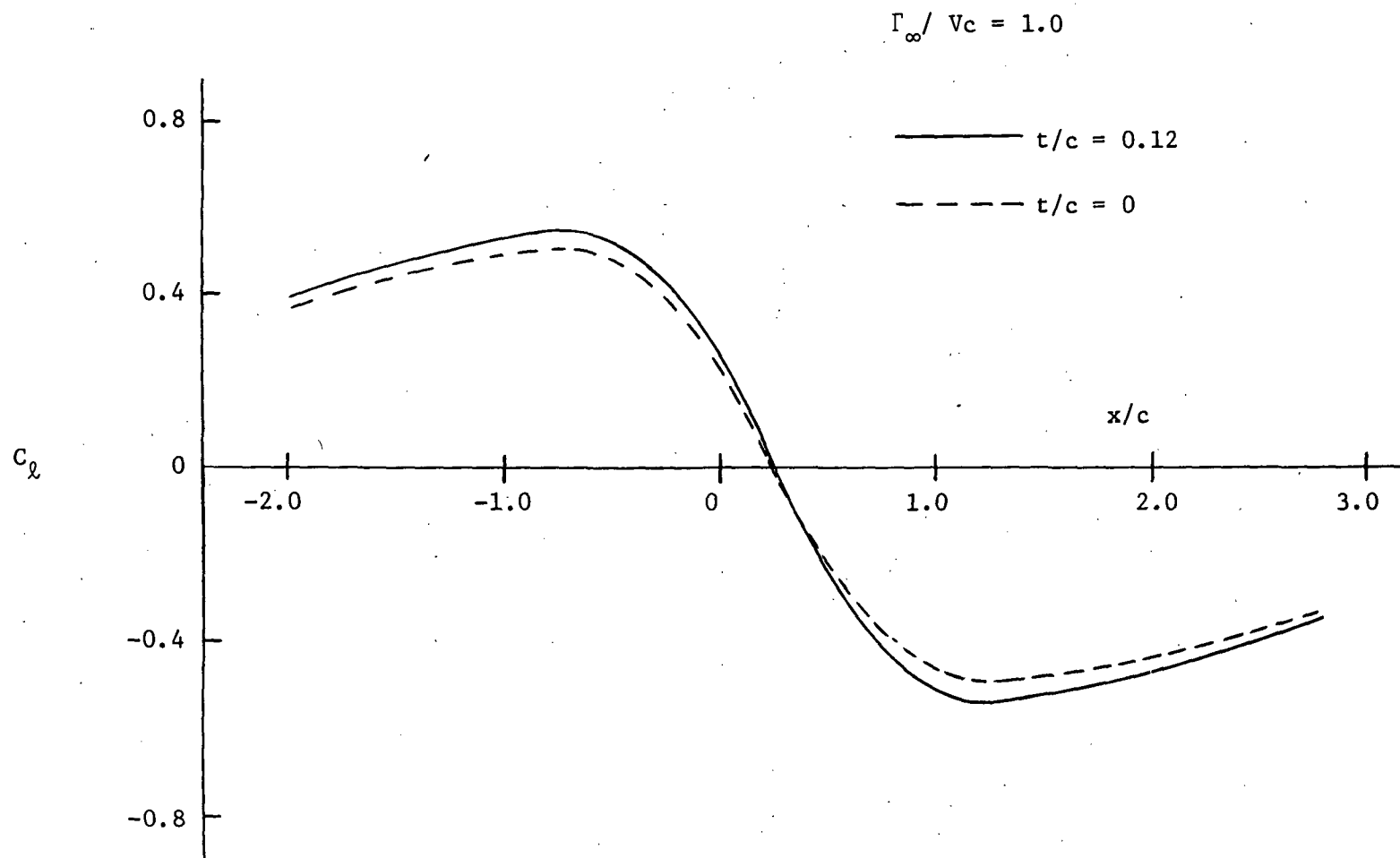Figure 57. Effect of Thickness on the Lift Coefficient Due to Vortex Interaction, y/c = 0.25.

Figure 58. Effect of Thickness on the Lift Coefficient Due to Vortex Interaction; y/c = 1.0.

APPENDIX B

RADIAL LOCATIONS AND ANGLE OF INTERSECTIONS ASSOCIATED
WITH BLADE-VORTEX INTERSECTIONS

In the calculation of airloads on a helicopter rotor blade due to vortex interaction the radial location and the angle of intersection of the tip vortex with the following blade is required. Helicopter rotor wake studies (experimental) have indicated that there are no significant wake distortions in the top view of the wake in the vicinity of the rotor for moderate and high speed conditions. Hence assuming an undistorted top view of the wake the radial locations at which the following blade intersects the tip vortex from the preceding blade at different advance ratios are presented in Figures 59, 60 and 61 for two, three and four bladed rotors respectively. The angles of intersection of the tip vortex with the following blade at different advance ratios are presented in Figures 62, 63, and 64 for two, three and four bladed rotors respectively. These figures show a typical variation of the radial locations and the intersection angles associated with blade-vortex intersections. As can be seen in these figures, for an advance ratio of 0.3, the azimuth region over which intersection occurs increases with increasing number of blades of a rotor. For a given rotor the radial extent over which blade-vortex intersections occur decreases with a decrease in advance ratio. However, the vortex-interaction effect is predominant at the lower advance ratios as the wake remains close to the blades. For some low speed flight conditions tip vortices pass above the blades. As can be seen in these figures, the angles of intersection of the blade and the tip vortex are smaller for lower advance ratios.
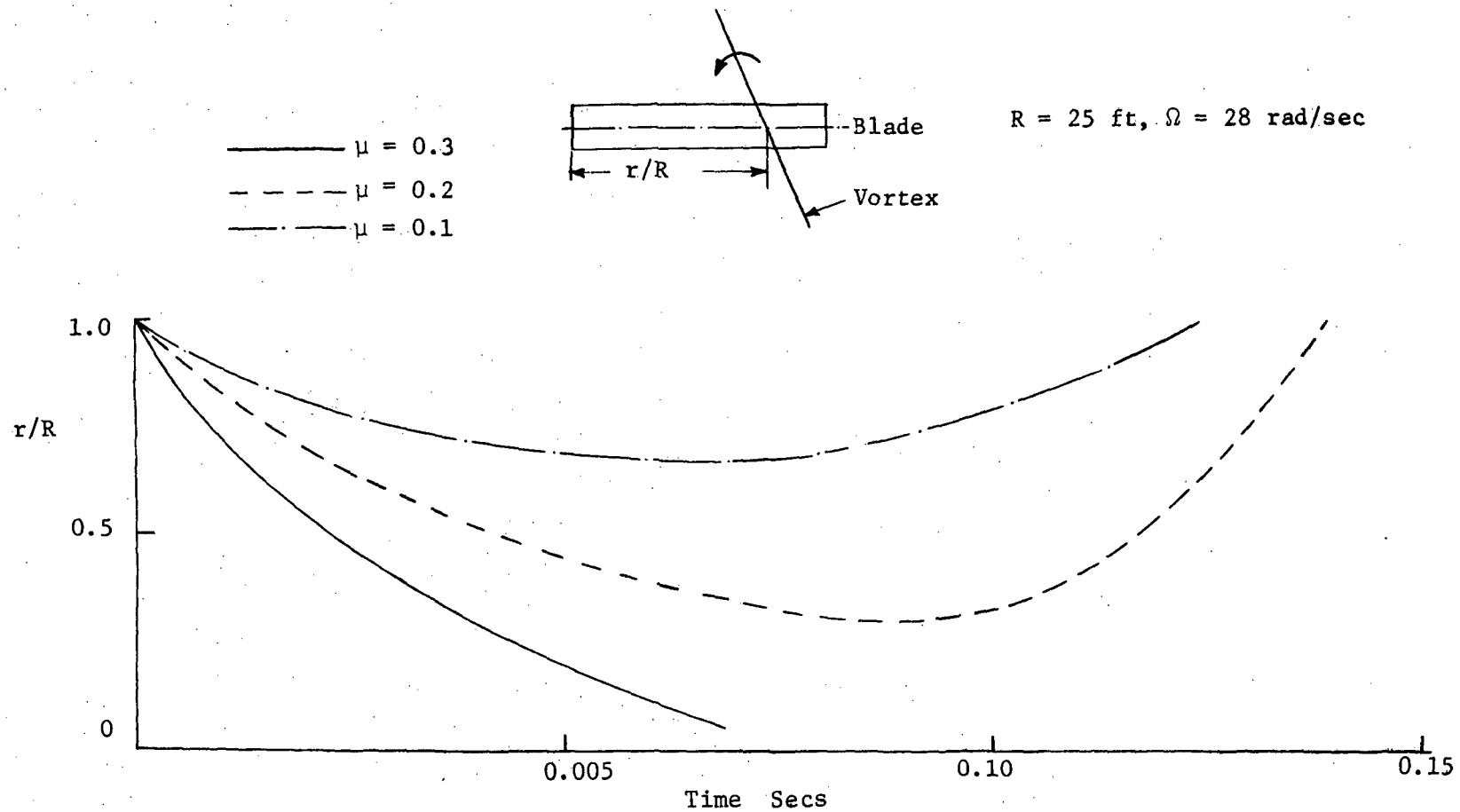
Figure 59. Radial Location of Blade-Vortex Intersection for a Two Bladed Rotor.
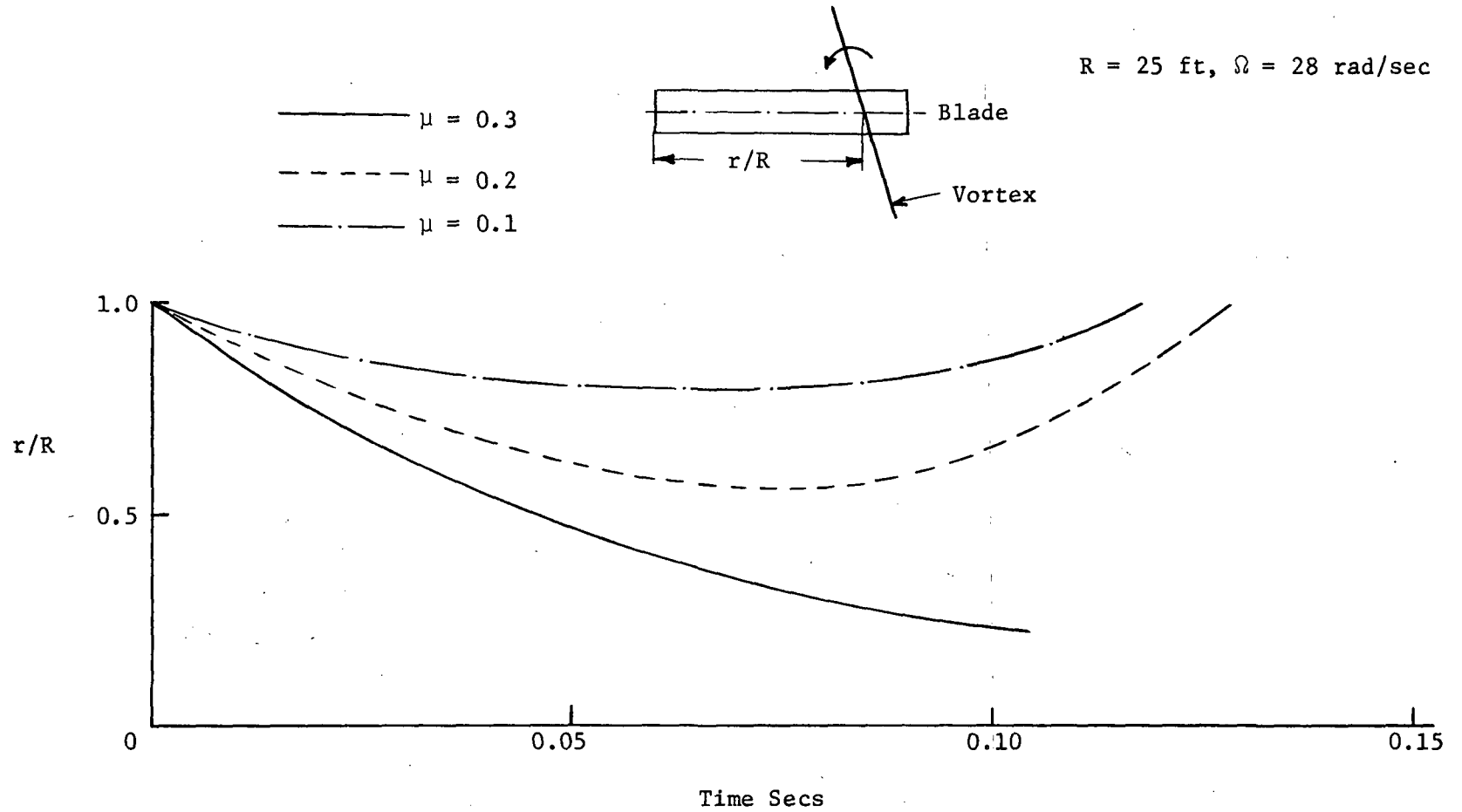
Figure 60.   Radial Location of Blade-Vortex Intersection for a Three Bladed Rotor.
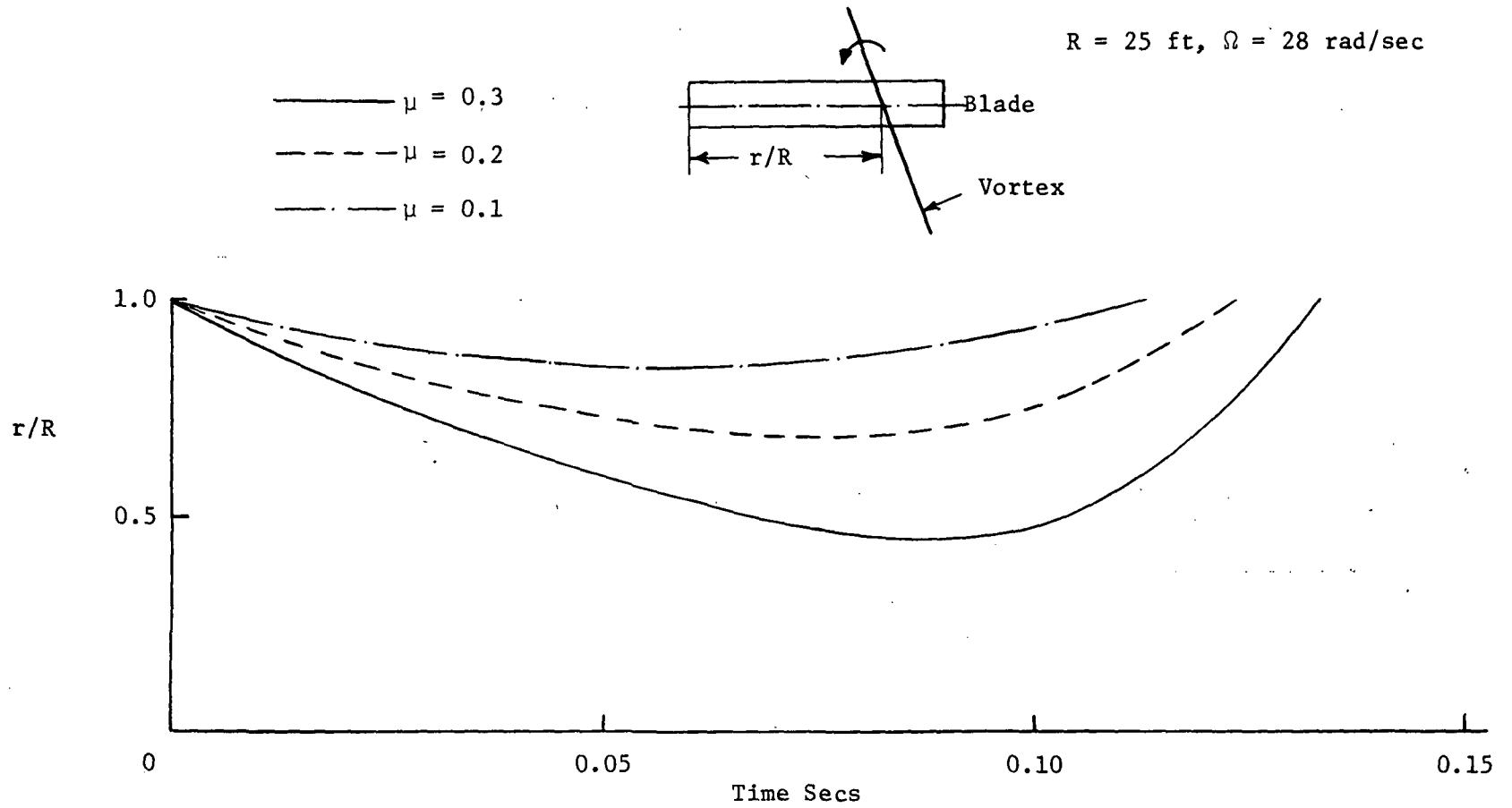
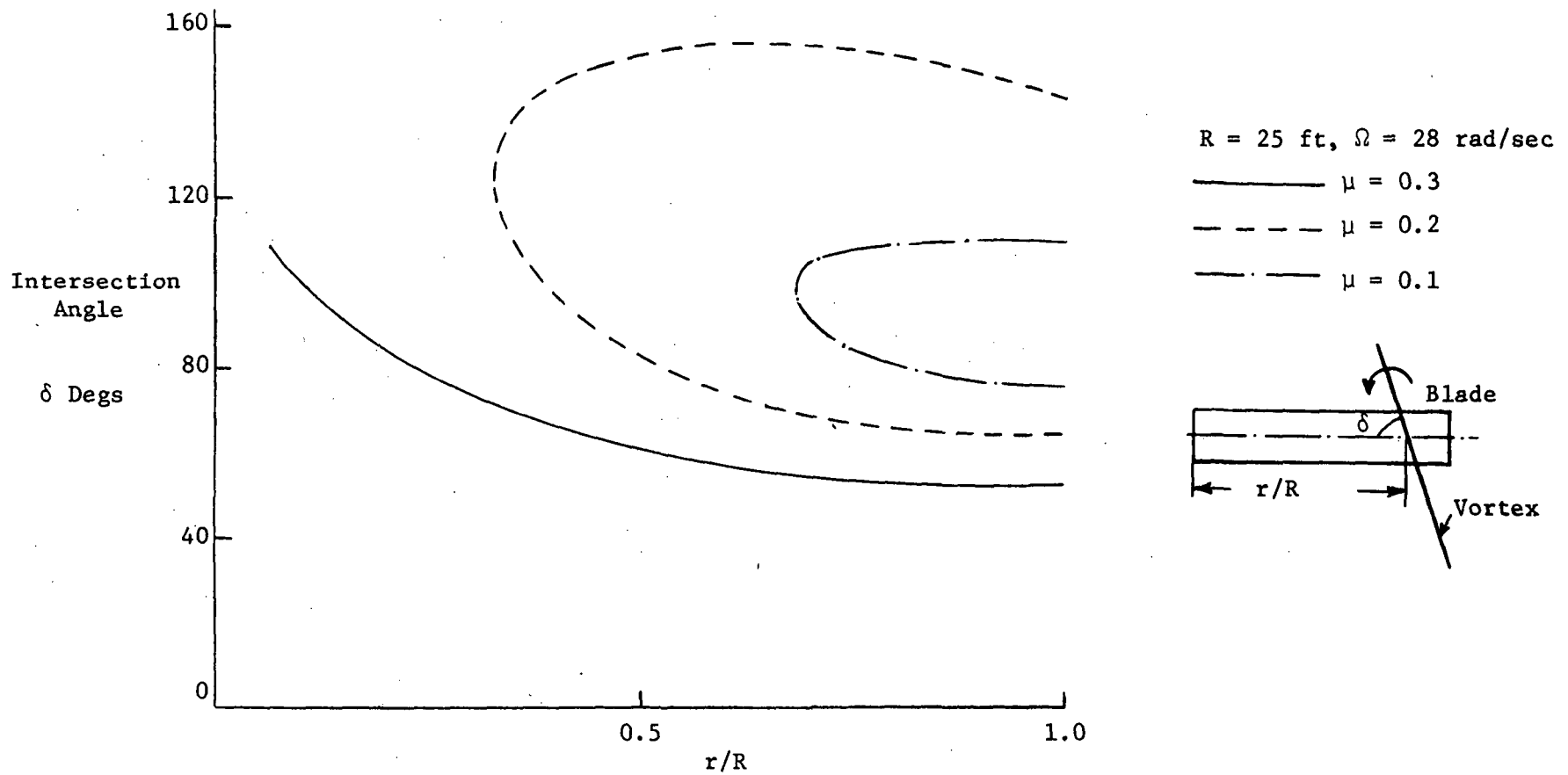Figure 61. Radial Location of Blade-Vortex Intersection for a Four Bladed Rotor.

Figure 62.   Angle of Intersection and Radial Location of Blade-Vortex Intersection
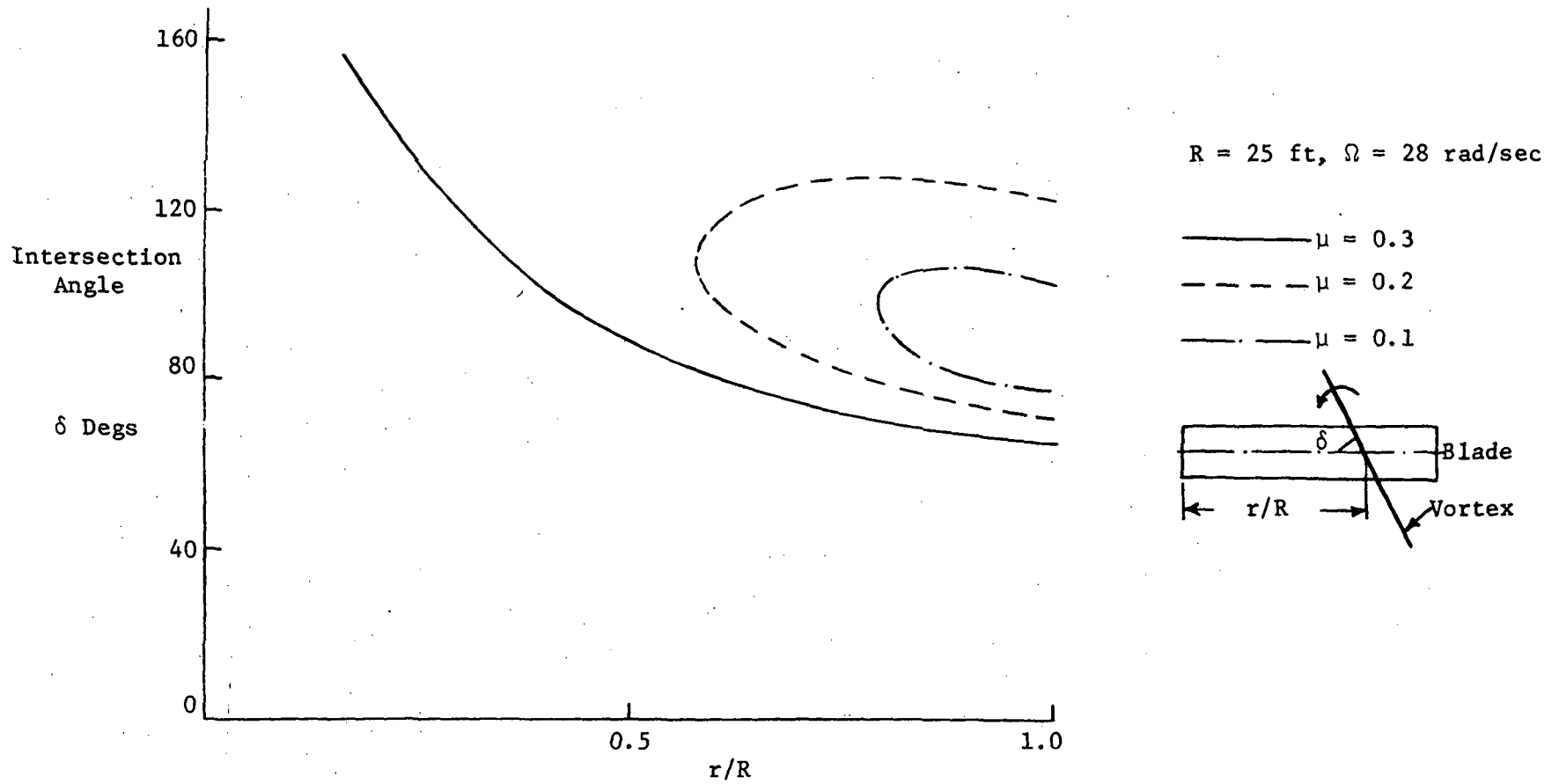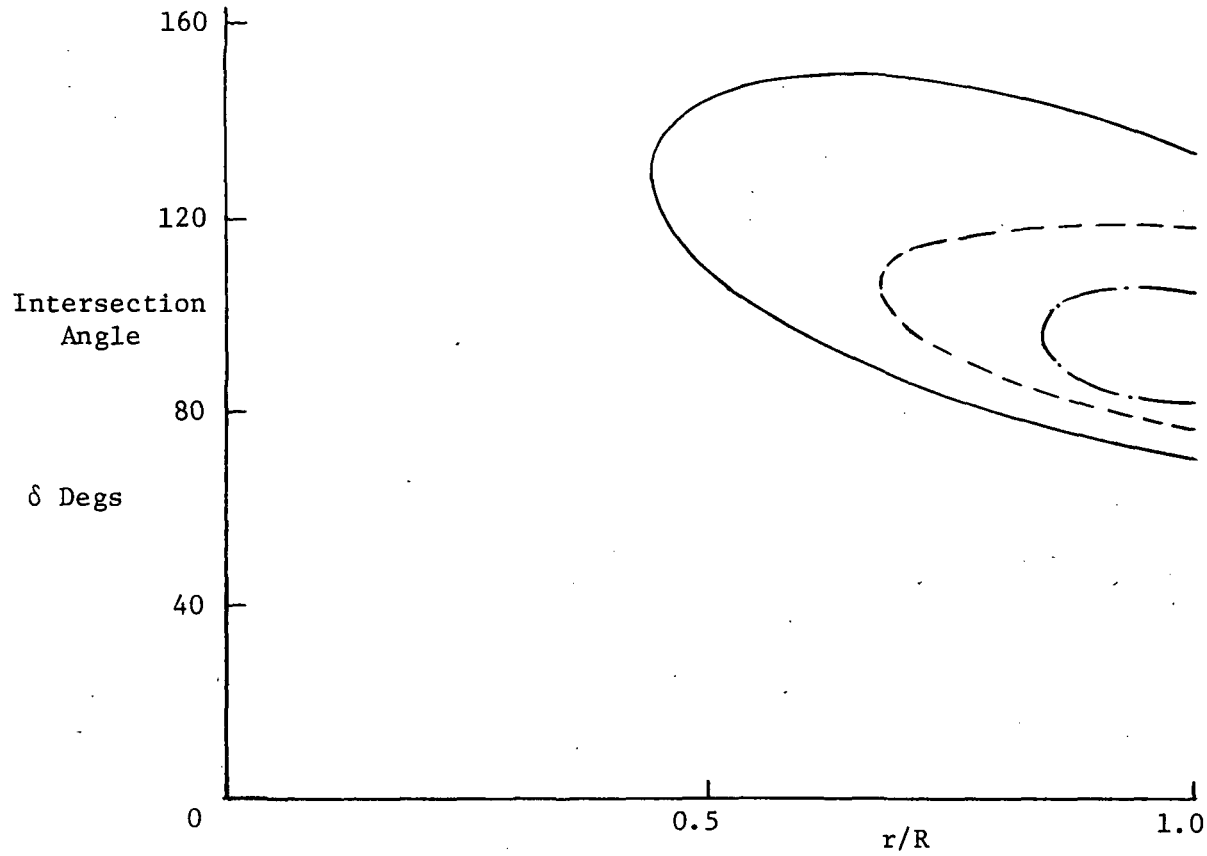for a Two Bladed Rotor.

126

Figure 63. Angle of Intersection and Radial Location of Blade-Vortex Intersection for a Three Bladed Rotor.
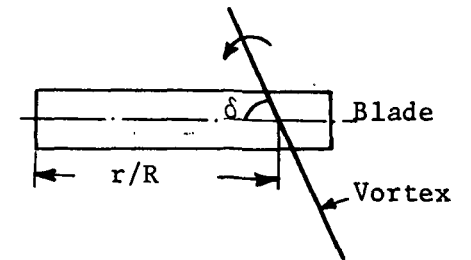
Figure 64. Angle of Intersection and Radial Location of Blade-Vortex Intersection for a Four Bladed Rotor.

Pruyn and Alexander (11) have also found that the effect of the tip vortex was large when the angle between the vortex and the blade was small. These figures provide a rapid means for determining the blade radial locations for blade-vortex intersections. Generalized charts of the form shown in these figures could be developed to cover the complete range of number of blades and advance ratios.